

AD-A197 917

AFOSR-TR- 88 - 0690

(2)

SC5418.FR

SC5418.FR

DTIC FILE COPY

Copy No. 3

INTEGRATION OF STATISTICAL AND PHYSICAL MODELS OF SHORT FATIGUE CRACK GROWTH

FINAL REPORT FOR THE PERIOD
January 15, 1985 through April 14, 1988

CONTRACT NO. F49620-85-C-0034

Prepared for

AFOSR/NA
Directorate of Aerospace Sciences
Building 410
Bolling AFB, DC 20332

B. Cox and W. Morris
Principal Investigators

DTIC
SELECTED
AUG 15 1988
CH

JUNE 1988

Approved for public release; distribution unlimited



Rockwell International
Science Center

UNCLASSIFIED

SECURITY CLASSIFICATION OF THIS PAGE

REPORT DOCUMENTATION PAGE				FORM APPROVED OMB No. 0704-0188	
1a. REPORT SECURITY CLASSIFICATION UNCLASSIFIED			1b. RESTRICTIVE MARKINGS		
2a. SECURITY CLASSIFICATION AUTHORITY			3. DISTRIBUTION/AVAILABILITY OF REPORT Approved for public release; distribution unlimited		
2b. CLASSIFICATION/DOWNGRADING SCHEDULE					
4. PERFORMING ORGANIZATION REPORT NUMBER(S) SC5418.FR			5. MONITORING ORGANIZATION REPORT NUMBER(S) AFOSR-TR- 88-0690		
6a. NAME OF PERFORMING ORGANIZATION ROCKWELL INTERNATIONAL Science Center		6b. OFFICE SYMBOL (If Applicable)	7a. NAME OF MONITORING ORGANIZATION AFOSR		
6c. ADDRESS (City, State, and ZIP Code) 1049 Camino Dos Rios Thousand Oaks, CA 91360		7b. ADDRESS (City, State and ZIP Code) Same as 8c.			
8a. NAME OF FUNDING/SPONSORING ORGANIZATION AFOSR/NA Directorate of Aerospace Sciences		8b. OFFICE SYMBOL (If Applicable) NA	9. PROCUREMENT INSTRUMENT IDENTIFICATION NUMBER CONTRACT NO. F49620-85-C-0034		
8c. ADDRESS (City, State and ZIP Code) Building 410 Bolling AFB, DC 20332		10. SOURCE OF FUNDING NOS.	PROGRAM ELEMENT NO. 611004	PROJECT NO. 2302	TASK NO. B2
			WORK UNIT ACCESSION NO.		
11. TITLE (Include Security Classification) INTEGRATION OF STATISTICAL AND PHYSICAL MODELS OF SHORT FATIGUE CRACK GROWTH (u)					
12. PERSONAL AUTHOR(S) Cox, B.N., and Morris, W.L.					
13a. TYPE OF REPORT Final Report		13b. TIME COVERED FROM 01/15/85 TO 04/14/88		14. DATE OF REPORT (Year Month Day) 1988, JUNE	
				15. PAGE COUNT 138	
16. SUPPLEMENTARY NOTATION					
17. COSATI CODES			18. SUBJECT TERMS (Continue on reverse if necessary and identify by block number)		
FIELD	GROUP	SUB-GROUP			
19. ABSTRACT (Continue on reverse if necessary and identify by block number) <p>The probabilistic analysis of the propagation of small fatigue cracks has been investigated. Monte Carlo simulations have been formulated that can embrace nearly all details of the micromechanics of small crack growth. They calculate the propagation of the entire, irregular crack front as it passes through a random microstructure. The simulations illuminate both the mechanics and the statistics of small crack growth. A computationally efficient probabilistic model has also been formulated as the basis of lifetime prediction in field application. The probabilistic model is sufficiently flexible to allow incorporation of the physical aspects of propagation that have been shown in the Monte Carlo simulations to be necessary for accurate predictions. In particular, the probabilistic model begins with the premise that two independent variables, for example but not necessarily the crack length and the crack shape, are required to account for the observed statistics of growth. (u) ←</p>					
20. DISTRIBUTION/AVAILABILITY OF ABSTRACT UNCLASSIFIED/UNLIMITED <input checked="" type="checkbox"/> SAME AS RPT. <input type="checkbox"/> DTIC USERS <input checked="" type="checkbox"/>			21. ABSTRACT SECURITY CLASSIFICATION UNCLASSIFIED		
22a. NAME OF RESPONSIBLE INDIVIDUAL George Haritos			22b. TELEPHONE NUMBER (Include Area Code) (202) 767-0463		22c. OFFICE SYMBOL NA

DD FORM 1473, JUN 86

Previous editions are obsolete.

UNCLASSIFIED

SECURITY CLASSIFICATION OF THIS PAGE

UNCLASSIFIED

SECURITY CLASSIFICATION OF THIS PAGE

UNCLASSIFIED

SECURITY CLASSIFICATION OF THIS PAGE



Rockwell International
Science Center

SC5418.FR

1.0 INTRODUCTION

This is the final report on the program "Integration of Statistical and Physical Models of Short Fatigue Crack Growth". It reviews progress of the entire period of the contract from January 15, 1985 through April 14, 1988.

The report consists primarily of: 1) a summary that draws attention to significant achievements; 2) an account of various avenues of future research and applications; and 3) copies of articles published under the program.



Accession For	
NTIS GRA&I	<input checked="checked" type="checkbox"/>
PTN TAB	<input type="checkbox"/>
Unannounced	<input type="checkbox"/>
Justification	
By	
Distribution/	
Availability Codes	
Avail and/or	
List	Special
A-1	

2.0 SIGNIFICANT ACHIEVEMENTS

The purpose of this program was to explore the possibility of constructing physically based probabilistic models of small* fatigue crack growth. The degree of detail and explicitness in which the underlying physics of crack propagation are represented in such a model can be chosen with great variety.¹⁻⁵ In general, the more physical detail the model embraces, the greater its potential for accuracy,^{1,2} provided the underlying physics are correct. When less physical detail is incorporated, more reliance is placed on merely fitting parametric curves or models to statistical data.³⁻⁵ While the potential accuracy is inferior in the latter case, the models are more easily implemented and apply equally to a wider class of materials and the necessity for painstaking laboratory studies is reduced.

One general conclusion reached in this program concerns the optimal level of detail for a probabilistic model of small fatigue crack growth. It has been shown that, for accurate prediction of fluctuations in crack velocity and remaining lifetime, a probabilistic model should possess at least two dimensions. If a model is couched in terms of only one independent variable, which has traditionally been the crack length, then it is impossible to avoid significant errors in statistical predictions. This necessitates an overly conservative implementation. While this conclusion has been based in the present work on physically based analyses of crack growth,^{1,2,6,7} it is important to note that it can also be reached by purely statistical analyses of long crack data.⁸ The importance of a second independent variable is also implicit in the early data analysis of Lin and Yang,⁹ and the more recent work of Bogdanoff and Kozin.¹⁰ The importance of our own contribution is that 1) the multidimensional nature of fatigue crack growth has been shown more irrefutably than ever, especially in the small crack regime, and 2) this fundamental maxim has been associated directly with the underlying mechanics of crack growth.

The association with the underlying mechanics rests on our being able to account for the fluctuations in crack velocity (and hence lifetime) observed under uni-

* A 'small' crack is herein one whose spatial dimensions are all of the same order of magnitude as the grain size. See the Second Annual Report, page 1, for remarks on the distinction between small and short cracks.



SC5418.FR

form cyclic loading in terms of the randomness of the microstructure. This was achieved only in Monte Carlo simulations, in which the irregular shape of the crack front is calculated in detail. The distributions of surface crack velocities, dc/dN , and the remaining lifetimes of surface-breaking cracks were shown to depend strongly on fluctuations in both the gross crack shape, e.g., the aspect ratio $a/2c$ (depth/surface length) and local irregularities in shape, especially retardation of the surface tips relative to the subsurface crack front. Now that the road to understanding these relationships is clear, it is quite feasible to incorporate them in a mathematically simpler and computationally more efficient probabilistic model than the Monte Carlo simulations. One such model was formulated in the program's first year. In addition to the crack length $2c$, that model possesses a second independent random variable, the growth control variable u . The variable u can be interpreted as befits any particular application, and probability transition matrices can be constructed to describe its stochastic evolution accordingly. In one application already presented, it was defined to represent the average grain size in the neighborhood of the crack tip,⁶ a choice appropriate to describing the statistics of roughness-induced closure. The variable u could also be defined to represent the evolving shape of the crack. The calculation of probability transition matrices to define the statistics of the evolution of the crack shape would not be trivial, but it could be done in principle by analyzing the statistics of shape predicted by the Monte Carlo simulations. This is one of the most appealing items for future research.

In the course of developing accurate descriptions of stochastic crack growth, it became evident that analyzing the experimental statistics of small cracks is an important but sadly overlooked way of elucidating the mechanics of their growth. The statistics of crack shape are in particular the most direct way available of comparing the equality of laws governing the growth of surface and subsurface segments of the crack front.^{1,7} For example, the degree of irregularity of the crack and its dependence on crack length are quite sensitive to the strength of microstructural influences. The statistics of the aspect ratio reveal much about the isotropy of the mechanics of growth.

3.0 OUTLOOK

This program has the virtue of having posed but left unanswered many questions that did not exist and could not have been foreseen before it began. In this section, these and other outstanding problems are reviewed and sensible approaches to solving them are outlined.

The greatest challenge now facing those desiring to understand the mechanics of small cracks is to measure various of their statistics, especially of their shape. The statistics of crack shape have been shown to bear directly on fundamental questions such as the equality or inequality of surface and subsurface mechanics, and the origin of certain features of the distribution of crack velocities, especially the high velocity tail, which is of prime engineering importance. Of course, measurements of crack shape are difficult and laborious, but they are feasible, even for small cracks. Both striations, as left by intermittent underloads or overloads, and destructive sectioning have been successful in the past. Measurement of crack shape ought also to be very illuminating in studying the effect of overloads. For small cracks, one would conjecture that overloads will affect different segments of the crack front to different degrees, depending on the sizes of the grains in which they lie and their proximity to the free surface. The Monte Carlo simulations will then allow analysis of the ensuing effects on the shape of the crack front for any hypothetical laws: and comparison with experimental statistics will then permit those laws to be tested and parameters in them to be evaluated.

As to the statistics of the surface velocity, dc/dN , this program has highlighted the inadequacy of the common form of their presentation in the literature. One generally finds surface crack growth data presented as plots of dc/dN vs ΔK , where ΔK has been calculated from the assumption that the crack is a smooth semi-ellipse. Now ΔK for experiments at constant stress amplitude is effectively a measure of $2c$. Therefore, the statistics of dc/dN embodied in such a plot are those of cracks of given length. It would be far more enlightening to know the distribution of dc/dN for all cracks after a given number of cycles.⁷ Tables of $2c$ vs N would convey much more information to retrospective analysts, especially concerning the statistics of deceleration and arrest. Yet, even in reports of large statistical studies, such tables do not appear. This must be rectified in future publications.



SC5418.FR

Another inadequacy of experimental reporting concerns the frequent and uncritical use of surface replicas to study small cracks. Replicas are a practical and perhaps necessary way of recording the history of a crack while it is too small to be easily detected. However, their use leads to uncontrolled censoring of small crack statistics. The cracks whose histories are included in the final data are those whose lengths at the time the last replica is made exceed the minimum for easy detection. This normally means that only relatively fast growing cracks are analyzed, which can obviously have a severe effect on statistical averages. When such small crack data are compared to long crack data at the same nominal ΔK , it is often observed that they appear to have higher dc/dN . But it is just possible that they actually have the same average dc/dN as long cracks, but a much wider variance. If only the faster small cracks in such a broad distribution are included in the data, they will create the illusion that their average velocity exceeds that of the average long crack. Realistic modeling such as the Monte Carlo simulations will enable this question to be answered. If it turns out that censoring accounts for much of the difference between small and long cracks, then hypotheses such as that small cracks grow faster because they suffer no plasticity induced closure would be thrown into doubt. The following conjecture ought then to be tested: that the mechanics of small cracks are in fact the same as those of long cracks, with the principal distinction being just that the random microstructure influences small cracks more strongly, because they span fewer grains, and therefore causes more scatter in dc/dN .

The prominent role of crack shape in determining the statistics of dc/dN and remaining lifetime suggests that shape will serve as an excellent quantity to be associated with the random variable u in the probabilistic model of Ref. 2. This association is facilitated by the existence of the Monte Carlo simulations, which provide some obvious means of calculating a priori the probability transition matrices required in Ref. 2. This simple demonstration will be undertaken and written up for publication as homework in the next few months.

If random microstructure is indeed the source of fluctuations in small crack growth rates, then this should be borne out in correlation lengths for the covariance of dc/dN , crack irregularity, fluctuations in aspect ratio etc. Experimental verification of this, which requires records of $2c$ vs N for many cracks, would go far towards validating physically based probabilistic models of growth. Indeed, whether a physically based model of statistical growth is accurate is equivalent to the question of the accuracy of

SC5418.FR

the higher moments it predicts. Correlation lengths are one very important property of the higher moments. If there are insufficient data to measure them, then acceptance of a physically based model is an act of faith.



3.0 REFERENCES

1. B.N. Cox and W.L. Morris, "Monte Carlo Simulations of the Growth of Small Fatigue Cracks," Engng Fracture Mech., in press.
2. B.N. Cox and W.L. Morris, "A Probabilistic Model of Short Fatigue Crack Growth," Fatigue Fracture Engng Mater. Struct. 10, 419-28 (1987).
3. J.L. Bogdanoff and F. Kozin, Probabilistic Models of Cumulative Damage, John Wiley & Sons, NY (1985).
4. K.P. Oh, "A Diffusion Model for Fatigue Crack Growth," Proc. Roy. Soc. Lond. A367, 47-58 (1979).
5. K. Sobczyk, "On the Markovian Models for Fatigue Accumulation," J. Mécanique Théorique et Appliquée, Numéro Spécial, 147-60 (1982).
6. B.N. Cox and W.L. Morris, "Model-Based Statistical Analysis of Short Fatigue Cracks Growth in Ti 6Al-2Sn-4Zr-6Mo," Fatigue Fracture Engng Mater. Struct. 10, 429-46 (1987).
7. B.N. Cox, "Inductions from Monte Carlo Simulations of Small Fatigue Cracks," submitted to Engng Fracture Mech.
8. J.L. Bogdanoff and F. Kozin, "Probabilistic Models in Fatigue Crack Growth: Results and Speculations," J.N. Engng and Design, in press.
9. Y.K. Lin and J.N. Yang, "On Statistical Moments of Fatigue Crack Propagation," Engng Fracture Mech. 18, 243-56 (1983).
10. J.L. Bogdanoff and F. Kozin, "Probabilistic Models of Fatigue Crack Growth - II," Engng Fracture Mech. 20, 255-70 (1984).
11. J.C. Newman, Jr. and P. Edwards. AGARD Report on Short Crack Growth Behavior in an Aluminum Alloy - An AGARD Cooperative Test Program.

4.0 STATEMENT OF WORK

First Year

1. Incorporate models of microstructural short crack growth phenomena into a stochastic damage growth model.
2. Compare model structures of various levels of complexity against synthetic data bases generated principally by Monte Carlo methods.

Second Year

3. Address the formulation and characterization of compound physical/statistical models which account for load history and cyclic stress amplitude.
4. Integrate crack coalescence and stress overload effects into the models.

Third Year

5. Develop a strategy for choosing the most advantageous formulation for a statistical model in a given situation and specify a process of calibration that will optimize predictions of remaining lifetime.
6. Evaluate the performance of predictions made under a range in extremes of predictive requirements.



5.0 PERSONNEL

Dr. Brian N. Cox - Ph.D. in Physics, Monash University (Australia), 1976.

Thesis Title - "A Spherical Cell Model of Metals"

Dr. Winfred L. Morris - Ph.D. in Physics, Northwestern University, 1968

Thesis Title - "The Nucleation of Gold on Muscovite Mica"

6.0 PUBLICATIONS UNDER THIS CONTRACT

B.N. Cox and W.L. Morris, "A Probabilistic Model of Short Fatigue Crack Growth," Fatigue Fracture Engng Mater. Struct. 10, 419-28 (1987).

B.N. Cox and W.L. Morris, "Model-Based Statistical Analysis of Short Fatigue Cracks Growth in Ti 6Al-2Sn-4Zr-6Mo," Fatigue Fracture Engng Mater. Struct. 10, 429-46 (1987).

B.N. Cox and W.L. Morris, "The Statistics of the Shape of Small Fatigue Cracks," in Proc. "Fatigue '87," 3rd Int. Conf. on Fatigue and Fatigue Thresholds, ed., R.O. Ritchie and E.A. Starke, Jr., Charlottesville, VA, June-July 1987, Vol. 1, pp. 241-50.

B.N. Cox and W.L. Morris, "Monte Carlo Simulations of Small Fatigue Crack Growth," Engng Fracture Mech., in press.

B.N. Cox, "Inductions from Monte Carlo Simulations of Small Fatigue Cracks," submitted to Engng Fracture Mech.

B.N. Cox, "The Role of Crack Shape in Probabilistic Models of Small Fatigue Crack Growth," in preparation, probably for submission to Fatigue Fracture Engng Mater. Struct.



Rockwell International
Science Center

SC5418.FR

7.0 INTERACTIONS AND MEETINGS

In the third year of the program, an invited paper entitled "The Influence of Crack Shape on the Statistics of Small Fatigue Crack Growth" was presented before the Small Cracks Task Group at the April meeting of ASTM in Reno, NV.

SC5418.FR

8.0 COPIES OF PUBLICATIONS

A PROBABILISTIC MODEL OF SHORT FATIGUE CRACK GROWTH

B. N. COX and W. L. MORRIS

Rockwell International Science Center, 1049 Camino Dos Rios, Thousand Oaks, CA 91360, U.S.A.

(Received in final form 24 June 1987)

Abstract—A probabilistic model is presented that draws a direct link between stochastic microstructure and the statistics of measured growth rates. The model is formulated as a semi-Markov process. The underlying Markov process describes the evolution of a growth control variable as an explicit function of crack length. The growth control variable is open to a variety of interpretations, depending on the mechanisms known to control growth in any given application. Elapsed fatigue cycles and the distribution of times to failure are calculated by invoking an empirical or postulated law of growth rate. This law is either a deterministic or probabilistic relationship between the growth control variable and the crack velocity. It may, and usually does, contain parameters that are evaluated by calibration against available statistical data. This process guarantees a high level of robustness of the model's predictions. The computational generality of the formulation facilitates the treatment of spectral loading.

NOMENCLATURE

- a = Crack length, or some other measure of crack size
- δ = Kronecker delta function
- E = Operator generating expectation value
- $F_u^{(k)}$ = The cumulative probability distribution of u at the discrete crack length a_k
- λ^\pm = Forward and backward correlation lengths
- $h_{ij}^{(k)}(n)$ = Holding time: probability that nN_g cycles elapse when the crack length increases from a_{k-1} to a_k and u goes from u_i to u_j
- μ_2 = Second moment of the crack velocity
- N = Number of elapsed fatigue cycles
- N_g = Number of cycles in each interval of discrete time grid
- $\phi_{ij}^{(k)}(k|n)$ = Probability that u has the value u_j upon its k th transition after nN_g cycles given that it acquired the value u_i upon the k th transition at time zero
- $\pi^{(m)}$ = The probability mass function for u at crack length a_m
- $P^{(m)}$ = The probability transition matrix for u , when the crack grows from length a_{m-1} to length a_m
- ρ_c = Covariance function
- σ = Amplitude of the external cyclic stress
- σ_u = The root mean square deviation of u
- u = The growth control variable
- $v(a, u)$ = The relationship between da/dN ($\equiv v$) and u .

INTRODUCTION

A century of experimental research into fatigue crack growth has demonstrated that fatigue cracks grow in an inherently stochastic manner. There are always large fluctuations, sometimes over an order of magnitude or more, in macroscopic observables such as the instantaneous crack velocity, da/dN , and the cycles to failure. Yet before the last decade there were very few attempts to analyze quantitatively the relationship between these fluctuations and the intrinsic variability of the various material characteristics, such as local grain size, yield stress, and crystal orientation, that control the mechanics of growth. The attention of fundamental theories was usually restricted to the law of average growth rate, and its dependence on stress level, average grain size, environment, etc.

The scatter in quantities of engineering importance, usually the time to failure, is still conventionally treated by fitting *ad hoc* some convenient, analytic density function. The limits of safety are demarked by a safety curve some number of standard deviations on the conservative side of the average. The required number of standard deviations is established by rules of thumb and experience.

More recently, significant efforts have been made to match more sophisticated and flexible statistical models to experimental data. They include formulations in terms of diffusion equations[1,2] and conservation equations for probability densities[3], Monte Carlo simulations[4,5]; Markov chains[7-10]; birth processes[13]; point processes[14]; and stochastic differential equations[2,6,11]. But the variety in mathematical formulation does not constitute the most important division between these various approaches. From a functional point of view, most of them may instead be considered to fall into two categories.

In the first, more numerous category, the models begin with the least generality necessary to reproduce the average and variance of engineering growth rate data (e.g. Refs [1, 2, 6, 7, 14, 15]). In some cases, the sophistication has then been gradually increased as the relevance of further details of the statistical data, such as the covariance of crack velocities measured at different lengths, has been recognized[12]. These models usually purport to have some ability to calculate the effects of changes in stress level, even to the case of spectral loading, but in a way that is based on simplistic growth rate laws. Such approaches are probably valid accounts of the statistics of cracks that grow according to linear elastic fracture mechanics. However, they are probably inaccurate and certainly physically unrealistic when applied to the propagation of short fatigue cracks. In many circumstances, short crack propagation constitutes most of the fatigue lifetime.

The second category of probabilistic models has attempted to address this shortcoming by building explicitly upon detailed knowledge of the micromechanics of short crack growth. For example, in certain heavily studied aluminum alloys, deterministic laws have been established that describe the dependence of growth rate on the immediate microstructural environment of the tips of surface fatigue cracks. The microstructure is itself stochastic, and it has been shown in Monte Carlo simulations[5] and by a kinetic model[3] that the fluctuations observed in growth rate data can be directly traced to fluctuations in the grains being traversed. These models have been and will continue to be extremely useful in connecting raw growth data with micromechanical theories. However, they incorporate the laws of dependence of velocity upon microstructure in a very explicit way. They can only be applied when those laws have been carefully established by extensive and painstaking experimental observations on the microscopic scale. Such experiments have always been done in a controlled laboratory environment, and because of the time that they take, have by necessity concentrated on the prevalent mechanism under just those restricted conditions. It is not practicable to repeat them in an exhaustive set of tests for all possible loads and environments. Therefore, models operating on such a detailed level can never be robust enough for engineering application. One could never be sure that the failure of a part in field service would always be by the mechanism or mechanisms studied so thoroughly in the controlled laboratory tests.

In short, there exists an important gap between the accomplishments of these two main categories of probabilistic models. This present work has the aim of bridging the gap, by constructing robust probabilistic models that nevertheless, by their very forms, retain the essential core of our knowledge of the mechanics of short crack growth.

A small amount of prior work has sown the seeds of the approach to be followed here. Lin and Yang[6] introduced the important idea of seeking a correlation length in statistical crack growth data. This correlation length is a measure of the typical distance over which the material factors controlling growth rate change. It may be a function of crack length, and it is an intrinsic material

property. Identifying such a correlation length, relating it to micromechanical theories of crack growth, and investigating its dependence on crack length, are important aims of the present work. Ghonem and Provan[13] explored the point of view that a crack front advances through a stochastic environment with a distribution of material properties bearing on different segments of it at any time. Although they did not themselves consider how this might lead to the definition of a correlation length, it clearly may. Such models also lead to predictions of the dependence of the scatter in measured crack velocities upon crack length. This functional dependence, which is much more easily measured than that of the correlation length, will also be an object of study here.

The present work has the goal of continuing such efforts to link the statistics of measured crack growth rates and micromechanical models of fatigue crack growth. Attention is focussed especially on the role of the randomness of the microstructure that determines the growth of short fatigue cracks. To this end, a new, very flexible computer-based probabilistic model has been formulated on physical principles. In this model, the evolution of a growth control variable, u , is described by a finite Markov chain. (This choice of formulation was inspired by the demonstration by Bogdanoff and co-workers[7-12] of the power and flexibility of finite Markov chains in fatigue problems.) The control variable is some measure of the local microstructural environment of the crack tip or front, rather than the crack's length itself, and its evolution is described as a function of the crack's length, rather than elapsed cycles. The elapsed cycles are calculated as an additive process or holding time associated with the Markov chain, according to an empirical law relating crack velocity to crack length and the control variable. (This structure is known as a semi-Markov process or embedded Markov chain.) Because of the physical nature of the problem, the Markov chain is nonhomogeneous (the statistics of the evolution of u are functions of the crack length), which is an important generality. This and other generalizations make necessary carefully chosen numerical algorithms.

The model will be useful both as a research tool and as a means of generating engineering predictions. In the former role, it allows the assessment of the probabilistic implications of a great variety of possible geometrical or mechanical models of crack growth. This is because of the broad interpretations that it is possible to associate with the growth control variable. For engineering applications, calibration procedures can be devised that ensure a high degree of robustness, while preserving the advantage of the knowledge acquired during research of the functional form of the statistical fluctuations, and their dependence on stress level and loading history.

The formulation itself, the arguments leading to it, and computational methods are described in this paper. An example of the application of the model, to the analysis of short crack growth data for Ti 6Al-2Sn-4Zr-6Mo, is presented in a companion paper[16] (henceforth referred to as II). There it will be seen how the model allows the deduction of micromechanical information from the magnitude and functional form of the scatter observed in gross crack growth data. The ability of the model to treat stochastic loading is reviewed here, as well as other aspects of its generality including its adequacy for studying intermittent short crack growth.

OUTLINE OF THE PROBABILISTIC MODEL

In this section, the outline of the new, probabilistic model is presented. It is described at first with the highest degree of generality. Specific, illustrative Markov chain models, laws of growth, and interpretations of the basic variables are presented in II.

The growth control variable u

The model examines the evolution of a discretized variable, u , ($i = 1, \dots, n$), that is governed by a nonhomogeneous discrete Markov process. The variable u is *not* the crack length, and this is the

point at which the present model departs from previous probabilistic models based on Markov chains[7-10]. Instead, u is to be interpreted as a measure of some local, physical property of the material that varies stochastically and controls the rate of crack growth at each point. For example, u might be related to the local flow stress, which governs the crack growth rate by determining the spatial size and intensity of the plastic zone; or it might be some microstructural length scale, such as grain size, that determines the magnitude of roughness induced closure. The latter example is taken up as the illustration of the method in II.

Because u represents a stochastic material property (so that its spatial variation rather than its variation in time is stochastic), it is convenient and useful on physical grounds to consider its evolution as an explicit function of crack length rather than elapsed fatigue cycles. This is another major departure of the new model from previous work[7-10]. The evolution is defined by a nonconstant sequence of probability transition matrices $\mathbf{P}^{(m)}$ ($m = 0, 1, \dots$), whose elements are to be calculated a priori from certain geometrical and probabilistic calculations of the rate of change of the environment of the crack front. The superscript m refers to the m th value a_m of the discretized crack length. (The precise meaning of 'crack length' depends on the application. For example, for a surface-breaking crack it might refer to the surface length, depth, or total area.) The element $P_{ij}^{(m)}$ of $\mathbf{P}^{(m)}$ is the probability that the discretized variable u has the value u_j when the crack length is a_m , given that it had the value u_i when the crack length was a_{m-1} . The assumed Markovian property of the model is that $P_{ij}^{(m)}$ does not depend on the history of the crack prior to its reaching length a_{m-1} . The calculation of the elements $P_{ij}^{(m)}$ and the reasonableness of the Markovian assumption will be illustrated in II for a simplistic model of crack growth dominated by roughness induced closure, and in subsequent work for other kinds of growth. In general, the calculation of the $P_{ij}^{(m)}$ may involve certain empirical parameters to be established by comparing the output of the model with crack growth data.

For computational efficiency, it is important to choose the discrete values of u with some care. For physical reasons, the second moment μ_u of u often decreases significantly as the crack length a increases. In other words, there tends to be less scatter in crack velocity, measured as a fraction of the average velocity, for longer cracks than for shorter cracks. Therefore, it is often very helpful to choose a different grid $\{u_i^{(m)}\}$ for each crack length a_m . Furthermore, it is usually advantageous to choose a nonlinear distribution for each set $\{u_i^{(m)}\}$, with a higher density of points near the average value. Note that these choices, while being directed by physical considerations, are nevertheless merely questions of numerical methods. For sufficiently dense grids, the output of the model does not depend on their details.

The choice of the discrete values of the crack length a should also be guided by physical considerations. For example, the memory that a crack has of its velocity at any particular length a_1 may persist for less time (or increase in length) as a_1 increases. To allow the model to calculate accurately such persistence of memory will in such cases require $\{a_m\}$ to be a finer mesh at longer crack lengths than at small lengths. Whether or not the lengths a_m can then be chosen arbitrarily depends on the model available for calculating the transition matrices $\mathbf{P}^{(m)}$. The details of the choice of $\{a_m\}$ can usually be made immaterial apart from considerations of computational efficiency.

The law of crack growth

The model requires that the rate of growth be specified as a function of the external cyclic stress amplitude, σ , and the growth control variable u . This information is to be provided as a subroutine that returns the number of cycles δN required to grow from one crack length, a_1 , to another, a_2 , given a value of σ and the prevailing value of u . The function $\delta N(a_1, a_2, u, \sigma)$ clearly contains much of our knowledge of the mechanics of crack growth. Its form can depend very strongly on the type

of material being modelled, the loading and environmental conditions, and the crack length itself. $\delta N(a_1, a_2, u, \sigma)$ may or may not contain empirical parameters to be evaluated by comparison of the model's output with growth data. If the mechanisms known to affect growth are believed to operate exclusively, then any empirical parameter in $\delta N(a_1, a_2, u, \sigma)$ can be evaluated at the outset from deterministic observation of the growth of single cracks. On the other hand, if a robust treatment is required for a material possessing other, unknown mechanisms influencing growth, then some parameters can be varied to fit the model against the statistics of growth data taken under field conditions. In such cases, one still retains the advantage of a model whose form is optimally constructed to illuminate the known physical significance of trends in the statistics.

Characteristics of the Markov chain

The probabilities $\pi_i^{(m)}$ that the growth control variable u has the value u_i at crack length a_m may be considered to form a vector (a probability mass function)

$$\pi^{(m)} = (\pi_1^{(m)}, \pi_2^{(m)}, \dots, \pi_M^{(m)}), \quad (1)$$

where M is the number of discrete values of u . It is convenient to make M independent of m , so that square transition matrices of constant rank can be defined. Then

$$\pi^{(m)} = \prod_{i \leq m} \pi^{(0)} \mathbf{P}^{(i)}. \quad (2)$$

Given an initial distribution $\pi^{(0)}$ of u , equation (2) embodies the entire history of its evolution. From it, one can calculate the mean and moments of u at any length. The mean $Eu^{(k)}$ and root mean square deviation $\sigma_u^{(k)}$ of u at crack length a_k are given by

$$Eu^{(k)} = \sum_j \pi_j^{(k)} u_j^{(k)} \quad (3)$$

and

$$\sigma_u^{(k)} = \sqrt{\sum_j \pi_j^{(k)} (u_j^{(k)})^2 - (Eu^{(k)})^2}. \quad (4)$$

A discontinuous cumulative probability distribution for u at length a_k is given by

$$F_u^{(k)}(u_j^{(k)}) = \sum_{i \leq j} \pi_i^{(k)}. \quad (5)$$

Given a reasonably dense grid $\{u_j^{(k)}\}$, a numerically smoothed, continuous analog, $\tilde{F}_u^{(k)}(u)$, can be readily constructed. The latter quantity can be used to generate the distribution of crack velocities at the length a_k , which information is used in model validation. From equation (2) may also be calculated the covariance between the values of u at two different lengths. The covariance will be observed to decay with increasing separation of the two lengths in an approximately exponential way. This allows the definition of a characteristic correlation length, which is related to some intrinsic length scale of the material.

The crack velocity da/dN

Since the crack velocity da/dN is a known or postulated function of u , equation (2) may also be used to calculate the evolution of da/dN . Once again, its distribution, moments, covariance, and a correlation length can be deduced. Since da/dN (or, equivalently, a itself) is an experimentally accessible function of N , these calculated properties can usually be compared directly with data.

Suppose that there is a deterministic relation

$$\frac{da}{dN} = v(a, u) \quad (6)$$

between the crack velocity (henceforth called v for brevity) and the damage control variable u . (The following statements are readily generalized to the case where the connection between u and v is probabilistic. Such generality is avoided here solely for ease of explanation.) Then the average value of v at crack length a_k is

$$Et^{(k)} = \sum_i v(a_k, u_i) \pi_i^{(k)}. \quad (7)$$

It is useful to define the function

$$\mu_i(k, k') \equiv E(v^{(k)} v^{(k')}) = \sum_{ij} v(a_k, u_i) v(a_{k'}, u_j) \pi_i^{(k)} \pi_j^{(k')}. \quad (8)$$

When $k = k'$, the root mean square deviation of v at the crack length a_k is given by

$$\sigma_i^{(k)} = \sqrt{\mu_i(k, k') - (Et^{(k)})^2}. \quad (9)$$

From $\mu_i(k, k')$ can also be constructed the correlation function (or covariance)

$$\rho_i(k, k') \equiv \frac{E\{(v^{(k)} - Et^{(k)})(v^{(k')} - Et^{(k')})\}}{\sqrt{E\{(v^{(k)})^2 - (Et^{(k)})^2\} \cdot E\{(v^{(k')})^2 - (Et^{(k')})^2\}}} = \frac{\mu_i(k, k') - Et^{(k)} \cdot Et^{(k')}}{\sigma_i^{(k)} \cdot \sigma_i^{(k')}}. \quad (10)$$

This function must always have a value in the interval $[-1, 1]$. It gives a simple, quantitative measure of the memory a crack has when it reaches length a_k of the velocity it had when it was of the lesser length $a_{k'}$. It bears on the fundamental engineering question: if a crack is growing faster (slower) than average now, for how long will it continue to grow faster (slower) than average?

The correlation function will almost always decay monotonically with increasing $|a_k - a_{k'}|$. It turns out (although it might not have for a nonhomogeneous Markov chain) that the decay is generally very nearly exponential in both directions. For given a_k , it is useful to define forward and backward correlation lengths $\lambda^+(k)$ and $\lambda^-(k)$ according to

$$\rho_i^{(k, k')} = \rho^{-(a_k - a_{k'}) \lambda^+(k)} \quad a_k > a_{k'}$$

and

$$\rho_i^{(k, k')} = e^{-(a_k - a_{k'}) \lambda^-(k)} \quad a_k < a_{k'}. \quad (11)$$

These correlation lengths reflect some intrinsic length scale of the material. Further discussion of them appears in II.

Elapsed fatigue life

The number of cycles elapsed when a crack has reached length a_m may be written

$$N_m = \sum_{i \leq m} \delta N^{(i)}, \quad (12)$$

where $\delta N^{(i)}$ is the number of cycles taken to go from length a_{i-1} to length a_i . N_m may be considered to be an additive process defined on the underlying Markov chain $\{\mathbf{P}^{(i)}\}$ describing the evolution of u , and its distribution can be calculated in principle using integral transformation methods [17].

However, when analytical approximations are unavailable or inappropriate, as is the case here, integral transform methods pose special difficulties arising from the instability of procedures to invert the Laplace transform [18,19]. Therefore, a different approach is followed here, better suited to numerical work.

The Markov chain $\{P^{(m)}\}$ is viewed as embedded in a discrete "time" space. By "time" is meant elapsed fatigue cycles, not real time, and this should be understood implicitly hereafter wherever the word "time" is used without quotation marks. It is convenient and appropriate to make the time grid uniform, and it must be dense relative to physically significant numbers of cycles, a point that will be taken up again below. Such a model is usually referred to as a discrete-time semi-Markov process. The solution of it given here is analogous to the systems of recursive equations discussed by Howard [20].

Consider the fundamental question of the length to which a crack has grown after nN_g cycles, where N_g is the number of cycles in each interval of the discrete time space. This length is determined by the number of transitions made in the evolution of the variable u , since each such transition corresponds to the growth of the crack from one discrete length to the next. Define $\phi_{ij}^{(k)}(k|n)$ to be the probability that the control variable acquires the value $u_j^{(k)}$ upon its k th transition after exactly nN_g cycles, given that it acquired the value $u_i^{(k')}$ upon the k' th transition at time zero. (By including dependence of $\phi_{ij}^{(k)}(k|n)$ upon k' , no generality is lost by considering this k' th transition to have occurred at time zero, or, in other words, considering the dependence of $\phi_{ij}^{(k)}(k|n)$ on an incremental time nN_g only.) Define $h_{ij}^{(k)}(n)$ to be the probability that nN_g cycles elapsed between the $(k-1)$ th and k th transitions of u , given that u went from the value $u_i^{(k-1)}$ to the value $u_j^{(k)}$. The probability mass function $h_{ij}^{(k)}(n)$ is often called a holding time, and it is clearly derived from the quantity $\delta N(a_1, a_2, u, \sigma)$. If the stress σ is a random variable, then its distribution will be comprised in $h_{ij}^{(k)}(n)$. $h_{ij}^{(k)}(n)$ may also depend in a probabilistic rather than deterministic way upon the initial value $u_i^{(k-1)}$ and final value $u_j^{(k)}$ of u . If the stress σ can take only one value and $\delta N(a_1, a_2, u, \sigma)$ is a deterministic function of u , then $h_{ij}^{(k)}(n)$ must represent a delta function. Since the time space is discrete, it is necessary in this case to spread the mass in $h_{ij}^{(k)}(n)$ over several grid points, to avoid computational errors. This imposes an obvious lower bound on the chosen density of grid points (i.e. the chosen value of N_g).

The recursive relation used to evaluate $\phi_{ij}^{(k)}(k|n)$ is

$$\phi_{ij}^{(k)}(k|n) = P_{ij}^{(k+1)} \delta(k - k' - 1) h_{ij}^{(k+1)}(n) + \sum_{m=1}^{n-1} \sum_{l=1}^M P_{ij}^{(k)} \phi_{il}^{(k-1)}(k-1|m) h_{ij}^{(k)}(n-m) \quad (13)$$

where

$$\phi_{ij}^{(k)}(k|n) = \begin{cases} 0 & \text{if } k' > k \\ \delta(n) & \text{if } k' = k, \end{cases}$$

and $\delta(n)$ is the Kronecker delta function. All required information concerning elapsed cycles and crack lengths is constructed from equation (4), together with the initial condition $\pi^{(0)}$.

Consider, for example, some key probabilities and conditional probabilities. Let $[N(a_k) = n]$ be the event that the crack reaches the k th discrete value of length after nN_g cycles. Then the unconditional probability of this event is given by

$$\text{Prob} \{N(a_k) = n\} = \sum_j \phi_{ij}^{(1)}(k|n). \quad (14)$$

Let $[u(a_k) = u_j^{(k)}]$ be the event that the growth control variable u has the discrete value $u_j^{(k)}$ when the crack's length is a_k . Then the conditional probability, that $[N(a_k) = n]$ given that $[u(a_k) = u_j^{(k)}]$, is given by

$$\text{Prob} \{N(a_k) = n | u(a_k) = u_j^{(k)}\} = \sum_i \phi_{ij}^{(1)}(k | n) \pi_i^{(0)}. \quad (15)$$

In analogous notation,

$$\text{Prob} \{N(a_k) = n | u(a_0) = u_i^{(0)}\} = \sum_j \phi_{ji}^{(1)}(k | n); \quad (16)$$

and

$$\text{Prob} \{N(a_k) = n | N(a_k) = n'\} = \sum_i \left[\sum_j \phi_{ji}^{(k)}(k | n - n') \right] \frac{\sum_j \phi_{ji}^{(1)}(k' | n') \pi_j^{(0)}}{\sum_{j'} \phi_{j'i}^{(1)}(k' | n') \pi_{j'}^{(0)}}. \quad (17)$$

If $[a(n) = a_k]$ is the event that the crack length after nN_g cycles is a_k , then

$$\text{Prob} \{N(a_k) = n | a(n') = a_k\} = \sum_{i=1}^n \sum_{j|p} \phi_{ji}^{(k)}(k | n - i) \phi_{pj}^{(1)}(k' | i) \pi_p^{(0)}. \quad (18)$$

The last two expressions are particularly important, since they address the problem of predicting remaining fatigue lifetime given an inspection. If, during the inspection, the damage control variable u can also be measured, even if with some uncertainty, then this additional condition can be readily included, and can have a pronounced effect on the predicted remaining lifetime. One has:

$$\text{Prob} \{N(a_k) = n | N(a_k) = n' \& u(a_k) = u_i\} = \sum_j \phi_{ij}^{(k)}(k | n - n'). \quad (19)$$

Examples of the application of equations (14)–(19) appear in II.

SPECTRUM LOADING

One of the chief reasons for setting up the models as described above is that the growth rate law, including its stress dependence, appears explicitly. Therefore, as long as the growth rate law [embodied in $h_y^{(k)}(n)$] is known correctly, the model can be applied immediately to cyclic loads of any constant amplitude. The treatment of spectral loads is also greatly facilitated, as will be shown in this section.

The load spectra to be treated can be divided into three broad classes: stochastic loading (reversals fluctuating in magnitude rapidly compared to measurable increments of crack length); block loading (blocks of constant amplitude or blocks of stochastic loading); and spectra containing spike overloads. Stochastic loading may be treated by a simple generalization of the model for constant loading. For a given set of statistical parameters (mean, variance, etc.) defining the stochastic loading, the holding times will be no longer deterministic but distributed according to some density function. If the stochastic load fluctuations rapidly during a growth increment, and contains no isolated overloads, then load sequence effects will be averaged out, and the probability mass function $h_y^{(k)}(n)$ is easily calculable.

Block loading requires the creation of a separate Markov chain for each block, convolved together to form a single model. Suppose the block loading consists of a sequence of blocks of

length N_i cycles and stress level σ_i ($i = 1, 2, \dots$). Consider the probability $\text{Prob}\{a(n_j) = a_k\}$ that a crack has length a_k after n_j cycles, where

$$n_j = \sum_i N_i. \quad (20)$$

This may be written in terms of the distribution of lengths at the end of the preceding block:

$$\text{Prob}\{a(n_j) = a_k\} = \sum_{i=0}^k \text{Prob}\{a(n_j) = a_k | a(n_{j-1}) = a_{k-i}\} \text{Prob}\{a(n_{j-1}) = a_{k-i}\}. \quad (21)$$

Equation (21) is a recursive relation that requires the conditional probabilities $\text{Prob}\{a(n_j) = a_k | a(n_{j-1}) = a_{k-i}\}$ and some initial density $\text{Prob}\{a(0) = a_k\}$. The conditional probabilities are calculated from the analysis of a single block, as described above, and conveniently stored in an upper triangular matrix. The product of these matrices gives the required distribution of lengths after j blocks. Such a computation is probably feasible for tens of blocks, which is adequate for comparison with the usual experimental data. Note that each block may itself consist of stochastic loading, in the sense of the preceding paragraph, rather than uniform loading.

Spike overloads may be treated by carrying the Markov chain simulation to a certain time (not crack length), changing the model parameters (e.g. dependence of $\Delta N_j(n)$ upon u_i and u_j) to correspond to microscopic understanding of the change induced in the growth laws, and restarting the model with appropriate convolution over length. This procedure is feasible for only a few overloads. However, if the overloads are very frequent, then their load sequence effects become unimportant, and one returns to the case of the rapidly varying stochastic load.

CONCLUSIONS

A probabilistic model has been formulated that draws a direct link between micromechanical models of short fatigue crack growth and the statistics of measured growth rates. The model has the structure of an embedded Markov chain or semi-Markov process. The Markov chain describes the evolution of a damage control variable as an explicit function of crack length. The damage control variable is open to a variety of interpretations, depending on the mechanisms known to control growth in any given application. Elapsed fatigue cycles and the distribution of times to failure are calculated by invoking an empirical or postulated law of growth rate. This law may, and usually does, contain parameters that are evaluated by calibration against available statistical data. This process guarantees a high level of robustness of the model's predictions.

The model is useful both as a research tool and as a method of making accurate predictions in engineering field conditions. Its usefulness as a research tool is demonstrated in II, where it is applied to the analysis of laboratory data for short surface fatigue crack growth in Ti 6Al-2Sn-4Zr-6Mo. It is shown there how model-based analysis of the scatter in growth data can lead to verification of geometrical aspects of the mechanisms believed to control crack growth at the microscopic level. The usefulness of the model in predicting remaining lifetime in engineering field applications has yet to be studied in detail. However, an illustration will be given in II of the importance of knowledge of the growth control variable, or, equivalently, the instantaneous crack velocity. Such information can have a dramatic effect on estimates of remaining lifetime.

Although the model is valid for both long and short fatigue cracks, it is with the latter that the greatest advantages lie over previous statistical models. In most materials, the widest fluctuations in crack velocity are found in the short crack regime. The mechanisms generating those fluctuations are varied, and depend strongly on the microstructural geometry of the crack's environment. A

model whose formulation reflects the statistics of that geometry has the best chance of reproducing accurately the statistics of short crack growth. In many circumstances, the period of short crack growth constitutes most of the entire fatigue lifetime of a material.

On the other hand, if the model is applied to analyzing fluctuations in crack velocity, da/dN , over very short changes in crack length, a , then, in certain materials, it will fail. In these materials, visible surface crack tips are observed to be temporarily arrested when they encounter grain boundaries. If da/dN is recorded as a function of a , it exhibits large variations as the crack crosses grains, and then falls to zero for some time when the crack reaches a grain boundary. Such a velocity history cannot be reproduced by a model with the structure of the present one. It requires explicit separation of propagating and temporarily arrested crack tips[3]. If this is not done, as it is not in this paper, then it is impossible to describe future propagation of a temporarily arrested crack. In the formulation of this paper, for example, once a crack has stopped it can never contribute to failure, because it never reaches the next discrete value of crack length. This is incorrect, because cracks stopped temporarily can indeed subsequently propagate to failure. To avoid this difficulty, it is necessary to average crack velocities over gauge lengths of at least one grain width, so that temporary arrest produces small, but non-zero velocities. It remains an open question whether such a procedure generates a sufficiently accurate statistical model when grain boundary blockage occurs.

Acknowledgement—Research sponsored by the Air Force Office of Scientific Research (AFSC) under Contract F49620-85-C-0034. The United States Government is authorized to reproduce and distribute reprints for governmental purposes notwithstanding any copyright notation hereon.

REFERENCES

1. Oh K. P. (1979) A diffusion model for fatigue crack growth. *Proc. R. Soc. Lond.* **A367**, 47–58.
2. Sobczyk K. (1982) On the Markovian models for fatigue accumulation. *J. Mec. Theor. Appl.* Numero Special, pp. 147–160.
3. Cox B. N., Pardee W. J. and Morris W. L. (1987) A statistical model of intermittent short fatigue crack growth. *Fatigue Fract. Engng Mater. Struct.* **9**, 435–455.
4. Itagaki H. and Shinozuka M. (1972) Application of the Monte Carlo technique to fatigue-failure analysis under random loading. In *Probabilistic Aspects of Fatigue*, ASTM STP 511, pp. 168–184.
5. Morris W. L., James M. R. and Buck O. (1980) Remaining fatigue lifetime prediction for retirement-for-cause in aluminum alloys. In *Proc. TMS Fall Meeting*, Pittsburgh, pp. 389–399.
6. Lin Y. K. and Yang J. N. (1983) On statistical moments of fatigue crack propagation. *Engng Fract. Mech.* **18**, 243–256.
7. Bogdanoff J. L. (1978) A new cumulative damage model. Part 1. *J. appl. Mech.* **45**, 246–250.
8. Bogdanoff J. L. and Krieger W. (1978) A new cumulative damage model. Part 2. *J. appl. Mech.* **45**, 251–257.
9. Bogdanoff J. L. (1978) A new cumulative damage model. Part 3. *J. appl. Mech.* **45**, 733–739.
10. Bogdanoff J. L. (1980) A new cumulative damage model. Part 4. *J. appl. Mech.* **47**, 40–44.
11. Kozin F. and Bogdanoff J. L. (1981) A critical analysis of some probabilistic models of fatigue crack growth. *Engng Fract. Mech.* **14**, 59–89.
12. Bogdanoff J. L. and Kozin F. (1984) Probabilistic models of fatigue crack growth—II. *Engng Fract. Mech.* **20**, 255–270.
13. Ghonem H. and Provan J. W. (1980) Micromechanics theory of fatigue crack initiation and propagation. *Engng Fract. Mech.* **13**, 963–977.
14. Arone R. (1981) A statistical model for fatigue fracture under constant amplitude cyclic loading. *Engng Fract. Mech.* **14**, 189–194.
15. Virkler D. A., Hillberry B. M. and Goel P. K. (1979) The statistical nature of fatigue crack propagation. *J. Engng Mater. Tech. Trans. ASME* **101**, 148–153.
16. Cox B. N. and Morris W. L. (1986) Model-based statistical analysis of short fatigue crack growth in Ti 6Al-4Sn-2Zr-6Mo. *Fatigue Fract. Engng Mater. Struct.* **10**(6). In press.
17. Cox D. R. and Miller H. D. (1965) *The Theory of Stochastic Processes*, Methner, London.
18. Bellman R. E., Kalaba R. E. and Lockett J. A. (1966) *Numerical Inversion of the Laplace Transform*, American Elsevier, New York.
19. Krylov V. I. and Skoblya N. S. (1969) *Handbook of Numerical Inversion of Laplace Transforms*, Israel Program for Scientific Translations, Jerusalem.
20. Howard R. A. (1970) *Dynamic Probabilistic Systems*, Wiley, New York.

MODEL-BASED STATISTICAL ANALYSIS OF SHORT FATIGUE CRACK GROWTH IN Ti 6Al-2Sn-4Zr-6Mo

B. N. COX and W. L. MORRIS

Rockwell International Corporation, 1049 Camino Dos Rios, Thousand Oaks, CA 91360, U.S.A.

(Received in final form 24 June 1987)

Abstract—The framework of a new probabilistic model of short fatigue crack growth was laid down in the preceding paper. In this paper, the model is used to analyze growth rate statistics for surface fatigue cracks in Ti 6Al-2Sn-4Zr-6Mo. Specific models are proposed for the evolution of the stochastic growth control variable, which appears subsequently as an independent variable in a parametric law for the growth rate. Comparison with data shows that for cracks of length 10–250 μm in Ti 6-2-4-6, fluctuations in the instantaneous rate of propagation of each surface crack tip depend only on the visible surface microstructure in the tip's immediate neighborhood. They are not influenced by the microstructural environment of the subsurface crack front. Furthermore, they probably depend only on the sizes of at most the three grains nearest the crack tip, i.e. those within about 30 μm of it.

NOMENCLATURE

- A, z, β = Parameters in growth law
 $2c$ = The surface length of a part-through crack
 D = The distance between deflections of a crack
 E = Operator indicating expectation value
 $F_k^{(u)}$ = The cumulative probability distribution for u at the k th discrete value of crack length
 ΔK = Stress intensity range
 $\lambda, \bar{\lambda}$ = Forward and backward correlation lengths
 N = Elapsed fatigue cycles
 N_d = Number of data pairs ($2c, V$)
 N_k = Number of data pairs allocated to bin k ($\sum_k N_k = N_d$)
 n = Number of deflections upon which the instantaneous value of dc/dN depends
 $\pi^{(m)}$ = Probability mass function for u at the m th discrete value of crack length in the Markov chain
 $P^{(m)}$ = Probability transition matrix for u for the passage from the m -1th to the m th discrete value of crack length in the Markov chain
 p = Number of bins into which crack velocity data are divided
 $\phi_j(D)$ = Probability density for D in Model j ($j \equiv 1$ or 2)
 ρ_i = Covariance function for dc/dN
 σ = Amplitude of cyclic load
 σ_u = Root mean square deviation of u
 σ_v = Root mean square deviation of $2dc/dN$
 S = Cramer-von Mises test function
 u = Growth control variable
 $t(c, u)$ = Known or postulated relationship between $2dc/dN$ and u
 V_i = Datum value of crack velocity
 y_i = Random variable associated with datum pair ($2c_i, V_i$)
 Ω_k = k th bin of crack velocities
 cpd = Cumulative probability distribution
 PTM = Probability transition matrix
 rmsd = root mean square deviation

INTRODUCTION

In this paper, information about the mechanisms controlling short crack growth in Ti 6Al-2Sn-4Zr-6Mo is deduced from certain statistics of growth rate data. The statistical analysis is based upon probabilistic models of the changes in the microstructure encountered by an advancing crack front. The framework of the analysis was laid down in the preceding paper [1].

Emphasis in the analysis is placed on the information content of the deviance and covariance of the crack velocity data, and how these statistics depend on crack length. It is assumed that the stochastic nature of the microstructural environment of the crack is the source of the scatter in the growth data.

The link between stochastic microstructure and stochastic crack growth has long been widely acknowledged for cracks whose total size is comparable to the grain size, as is the case here. However, the statistics of growth data have not been used before to deduce information about the mechanisms controlling growth. The conventional approach to determining the mechanisms of short fatigue crack growth is deterministic. The dependence of crack growth on microstructure is determined by examining individual cracks and the environment through which they propagate in great detail. Fluctuations in the observed rate of growth of such a crack are directly associated with known, measurable attributes of either the crack itself (e.g. its opening displacement) or the surrounding material (e.g. the sizes of the grains near the crack front, or the proximity to the crack front of grain boundaries).

The end product of such a conventional investigation is usually a record of crack velocity $2c \frac{dN}{dc}$ vs crack length, $2c$ (or some related variable such as ΔK), for each of a few individual cracks. Each significant feature on each of these records corresponds to a specific observation of some detail of the crack or the surrounding microstructure. It is understood, usually tacitly, that the observed link between the microstructure and the growth rate implies that the latter is stochastic because the former is.

When a growth law is required, it is usually constructed in terms of the average of $dc \frac{dN}{dc}$ as a function of c (or ΔK); and perhaps some average measure of the microstructure, e.g. the average grain size. Rarely is an account attempted of the micromechanical origins of the magnitude of the scatter in the observed growth rates, or its dependence on crack length and stress level, or the covariance between the velocities of a given crack at two different lengths.

In some recently published work, Cox *et al.* [2], analyzed certain statistics of short fatigue crack growth in Al 2219-T851 under constant amplitude loading. In this alloy, cracks stop temporarily at grain boundaries, and they are strongly influenced by plasticity-induced closure as they propagate across grains. These phenomena have been described by deterministic laws whose functional form was established by observations on single cracks [3]. In Ref. [2], these laws were shown to provide a satisfactory bridge between the measured distribution of grain sizes and several observed statistics of crack growth. That work also demonstrated a way of verifying quantitatively the values of certain parameters that were less accurately evaluated by the preceding deterministic study of individual cracks [3]. However, offsetting these achievements were certain important limitations. The theory is restricted to surface cracks whose growth is determined solely by the microstructure visible on the surface. It was developed for the treatment of uniform loading only. And it is not robust, in that the parameters embedded in it cannot always be calibrated against growth rate data if the mechanisms controlling growth are very different to those assumed, including temporary arrest at grain boundaries.

A more flexible probabilistic model has now been proposed in Ref. [1]. There was introduced the concept of a stochastic growth control variable, u , that evolves according to a finite,

nonhomogeneous, discrete Markov chain. The evolution of u is described explicitly as a function of crack length rather than elapsed fatigue cycles. This reflects the premise that fluctuations in the crack growth rate are controlled predominantly by the local material properties sampled by the crack front rather than factors that depend explicitly on time or the elapsed fatigue history. The law of crack growth is to be provided as a parametric function of the stress level, the crack length, and u . The fatigue cycles required to reach a given length are calculated as an additive process defined on the Markov chain. The reader is referred to Ref. [1] for a full explanation of these features and the treatment of stochastic loading. The principal advantage of this new model is that it can remain accurate even if the mechanics of growth in a given material are incompletely understood.

The data analyzed in this paper consist of records of the visible surface lengths, $2c$, of 63 part-through cracks in Ti 6Al-2Sn-4Zr-6Mo taken at a few intervals in the fatigue life [4]. From these data, values of the crack velocity, $2dc/dN$, are deduced, and the distribution of dc/dN is examined for cracks of all lengths. Specific models are proposed for generating the probability transition matrices (PTM's) governing the evolution of the growth control variable, u . The ability of these models to account for the magnitude of the scatter in dc/dN and its length dependence is tested.

This application illustrates the power of the probabilistic model of Ref. [1] as a research tool when applied to the analysis of laboratory data. At the same time, the calibrated model allows the most accurate available predictions of engineering quantities such as remaining fatigue lifetime. An important statistical quantity for such applications is the correlation length, which measures the rate of decay of the covariance between the velocities of a crack at two different lengths. Predicted values of the correlation length and the best estimates of experimental values are presented. It is shown that experimental information about the correlation length discriminates between the models proposed for the evolution of u , allowing one to deduce the number of grains near each visible crack tip that influence the instantaneous rate of growth.

THE GROWTH CONTROL VARIABLE, u , IN Ti 6Al-2Sn-4Zr-6Mo

In this section, specific models will be proposed to describe the stochastic evolution of a growth control variable appropriate to short surface cracks in Ti 6Al-2Sn-4Zr-6Mo. These models are simplistic, but still of sufficient quality to allow the inference of important information from the available crack growth data. They also serve to illustrate the implementation of the overall probabilistic model of Ref. [1]. Repeated reference will be made to quantities defined therein. An introduction to the theory of stochastic processes on which Ref. [1] and this paper are based can be found in Refs [5] and [6].

The greatest proportion of lifetime in smooth fatigue bars of Ti 6-2-4-6 is spent growing the fatal crack to a length of 1000 μm . Over the range of crack lengths 50-200 μm , the dominant mechanism controlling growth is believed to be roughness-induced closure [4]. With the guidance of this physical background, probabilistic models were created of a growth control variable, u , that measures roughness-induced closure. PTM's $P^{(m)}$ were constructed to describe its evolution. These were then combined with a law of crack growth rate deduced from laboratory measurements on individual cracks [4].

In fact, the validity of the procedure used to construct the PTM's does not turn on the assumption that roughness-induced closure is the dominant factor controlling growth. This interpretation of the mechanics of crack growth in this particular material is instead used principally as a motivation for constructing a model of the stated form. It will be seen below that

other interpretations of the control variable would lead to the same conclusions, because the control variable simply describes a geometrical characteristic of the material at the crack front. The relationship between u and the crack velocity is ultimately calibrated against data.

In this application, particular emphasis was given to the question of whether the fluctuations observed in dc/dN for visible surface cracks are associated with one or two dimensional geometrical aspects of the crack front. Two distinct algorithms for constructing the PTM's were devised, one assuming that only the geometry of the visible surface grains affects fluctuations in each visible crack tip's velocity; and the other assuming that the visible crack tips are controlled by an average of the sizes of the grains along the entire crack front. It will be seen below that only the former case is consistent with the experimental data.

Geometrical considerations suggest that the local magnitude of roughness-induced closure is related to the sizes of the grains immediately neighboring the crack tip [7]. In this paper, it is assumed that this relationship is a simple proportionality. Although this may be a crude assumption, it is to be remembered that the goal is to describe the rate at which the roughness-induced closure fluctuates as the crack grows. This stochastic process is not very sensitive to the details of the relationship in question.

Recall from Ref. [1] that the PTM's refer to propagation of a crack over a discrete set of lengths $\{2c_m\}$ ($m = 1, 2, \dots$). (The notation $2c$ is used for crack length in this paper, instead of a as in Ref. [1], because here crack length refers specifically to the surface length of a partial through crack.) At each length, the damage control variable u is represented by a finite, discrete grid $\{u_i^{(m)}\}$, ($i = 1, \dots, M$), which is not necessarily the same at each length $2c_m$.

Model 1—a model using only the visible surface geometry

In the first algorithm, the growth rate $2dc/dN$ was taken to be governed by the average distance between the last n deflections ($n = 1, 2, \dots$) of the crack as it is seen on the surface. This average distance between deflections was then identified with the growth rate control variable, u . The elements of the PTM's $P^{(m)}$ state the probability of going from one degree of closure to another when the surface length of the crack increases from $2c_{m-1}$ to $2c_m$.

The discrete lengths $2c_m$ ($m = 1, \dots$) were set so that the interval between successive values equals the increase in length required for the crack to suffer one more deflection on average. Thus,

$$2c_k - 2c_{k-1} = \bar{D}, \quad (1)$$

where \bar{D} is the average of the distance, D between deflections. In fact, D is a random variable, distributed according to a measurable density $\phi_1(D)$. Treating u for the moment as a continuous variable, if it had the value $u^{(k-1)}$ at length $2c_{k-1}$, and the next deflection occurs after an interval D , then the new value of u may be approximated by

$$u^{(k)} = \frac{(n-1)u^{(k-1)} + D}{n}. \quad (2)$$

For the discrete variables $u_i^{(k-1)}$ and $u_j^{(k)}$, the corresponding element $P_{ij}^{(k)}$ was then calculated by asking what probability there is that the value of D in equation (2) will be such that, if $u^{(k-1)}$ falls between $(u_i^{(k-1)} + u_{i-1}^{(k-1)})/2$ and $(u_i^{(k-1)} + u_{i+1}^{(k-1)})/2$, then $u^{(k)}$ falls between $(u_{j-1}^{(k)} + u_j^{(k)})/2$ and $(u_j^{(k)} + u_{j+1}^{(k)})/2$. This was calculated by invoking the empirical density $\phi_1(D)$.

To measure the density $\phi_1(D)$, straight lines were drawn on a micrograph of the Ti 6-2-4-6 specimen. The distribution of intervals on the lines that were demarked by the grain boundaries of both the α and β phases was then counted. The resulting cumulative probability distribution (cpd) is bimodal, because the β phase grains are much bigger than the α phase grains (see the

stepped curve of Fig. 1). It was represented by a smoothed, numerically defined function, which is also shown in Fig. 1. Note that as $\phi_1(D)$ is defined, the crack is assumed to be deflected at all grain boundaries, whether they be between two α phase grains, two β phase grains, or one grain of each phase. In Model 2, a slightly different assumption will be made, in the interests of getting the most stringent assessment possible of the relative merits of the two models.

Note that the heuristic arguments leading to equation (2), including the relationship equation (1), are unaffected by the fact that $2dc/dN$ is the sum of the speeds of two visible crack tips, not just the speed of one. In counting the frequency of deflections, the model is the same whether one counts deflections suffered by one tip when the other is fixed, or by both tips propagating together. The averaging over n deflections might be carried out equally over the neighborhood of one tip or over the neighborhoods of each of a pair of tips. In the latter case, the last n deflections suffered by the crack comprise, on average, the last $n/2$ deflections suffered by each of its tips. Thus, if the net velocity of a pair of tips is being modelled (as for the data analyzed below), then n ought to be divided equally between the two tips: in other words, each tip is influenced by the nearest $n/2$ grains.

Model 2—a model that averages over the entire crack front

A different point of view, which can be neither preferred nor dismissed *a priori*, is that the visible crack tips advance with fluctuations that depend on geometrical roughness factors averaged along the entire, approximately semicircular crack front (see Fig. 2). For this case, the discrete lengths $2c_m$ ($m = 1, 2, \dots$) were set so that the intervals between them equal the increase in length required for the crack front to envelop one more grain of average area; i.e.

$$\pi((2c_k)^2 - (2c_{k-1})^2) = \bar{D}^2, \quad (3)$$

where now the random variable D refers to the width of a grain. To give Model 2 the best chance of reproducing the statistics of the data, the relevant widths were taken to be those of the β phase grains only. In other words, the crack was assumed to be deflected at the edges of the β phase grains only. This assumption maximizes the deviance predicted for dc/dN at any crack length, but it will be seen to be still irreconcilably less than that observed. The distribution $\phi_2(D)$ of the random variable D in Model 2 was taken to be a Weibull distribution of mode $D = 30 \mu\text{m}$ and half-width

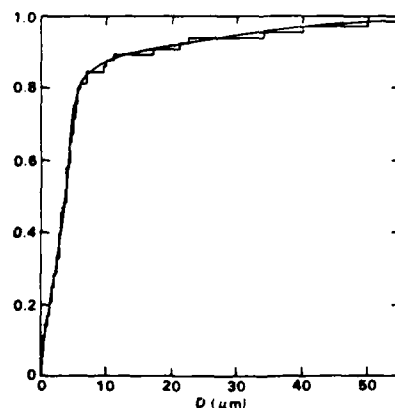


Fig. 1. The cumulative probability distribution used in Model 1 for the distance between successive crack deflections in the Ti 6-2-4-6 specimen.

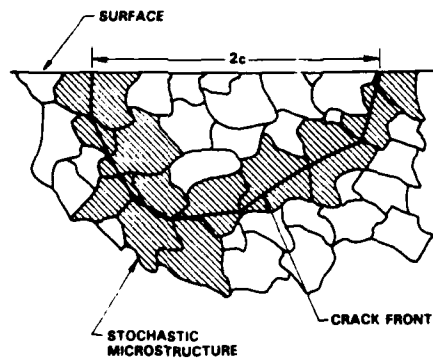


Fig. 2. A schematic illustration of the interaction of the front of a surface breaking crack with a stochastic microstructure.

40 μm (the upper arm of the cpd in Fig. 1). Because the features of the model being tested are not sensitive to the higher moments of $\phi_2(D)$, this estimate of it is quite adequate. Equation (2) was thus replaced by

$$u^{(k)} = \frac{2\pi c_{k-1} + D}{\frac{2\pi c_{k-1}}{u^{(k-1)}} + 1} \quad (4)$$

In this expression, the numerator approximates the length of the crack front when the grain of diameter D is incorporated. The denominator is proportional to the new number of grains along the crack front. Thus, $u^{(k)}$ refers to the average diameter of the grains lying on the crack front itself. It excludes grains lying in the crack's wake (see Fig. 2), a possibility allowed in Model 1. This again maximizes the deviance of u , and, therefore, the predicted scatter in dc/dN . The elements $P_{ij}^{(k)}$ were found from equation (4) in the way prescribed after equation (2).

The above algorithms for evaluating the PTM's $P^{(m)}$ are obviously crude, but they generate models that reproduce many of the observed statistics of short crack growth in Ti 6-2-4-6. Model

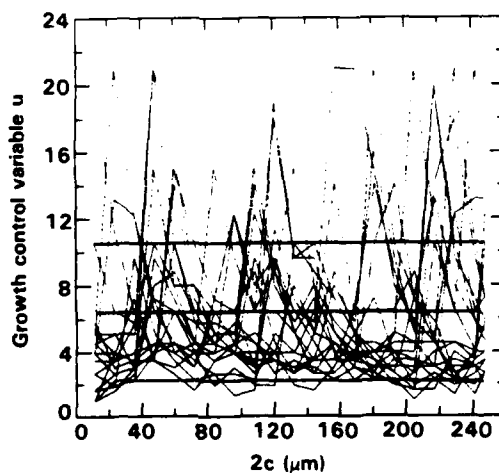


Fig. 3. Monte Carlo simulations of the evolution of u according to Model 1 ($n = 3$).

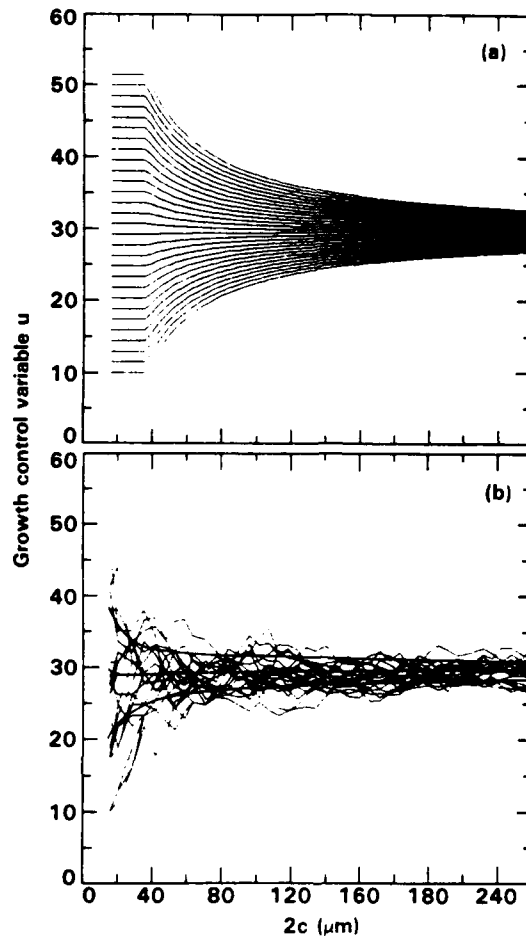


Fig. 4. (a) The grid used for the damage control variable u in Model 2. (b) Monte Carlo simulations of the evolution of u according to Model 2.

2 allows, albeit in an unrigorous and heuristic way, the important possibility that the crack's memory of its rate of growth may become shorter as the crack grows longer. This could, of course, be deduced from the crack data themselves, by calculating the appropriate correlation lengths. But what has been achieved is the association of such observations with physical causes. This enhances the prospects of making accurate probabilistic predictions for load sequences and materials for which only sparse statistical data or no data at all are available.

Evolution of the growth control variable u

The discrete grid used for the variable u in Model 1 was independent of crack length. The grid used in Model 2 is illustrated in Fig. 4(a). In Figs 3 and 4(b) are presented sets of member functions (simulated histories of u for individual cracks) generated by Monte Carlo calculations. The initial value of u was set equal to the size of a single grain, chosen randomly according to the empirical density $\phi_1(D)$ or $\phi_2(D)$. Subsequent values of u were found with weight given by the PTM's $P^{(m)}$.

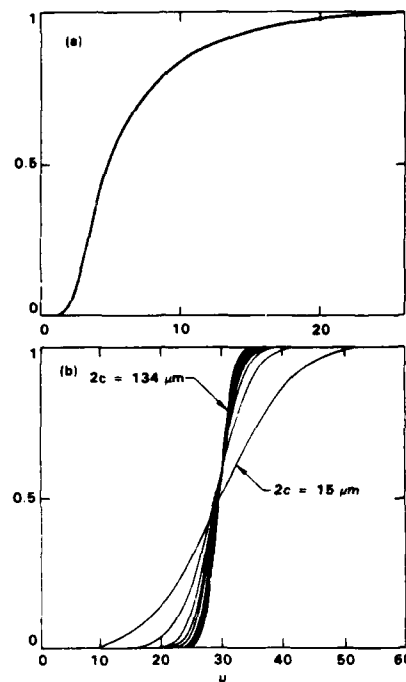


Fig. 5. Cumulative probability distributions for u in (a) Model 1 ($n = 3$); and (b) Model 2.

The discreteness of the grids in both crack length $2c$ and growth control variable u is apparent in these figures, but it can be proven to have an acceptably small influence on the predictions of the models.

The Monte Carlo calculations are easily made, illustrate basic trends quickly, and can be used to verify subsequent probabilistic calculations. However, they are not themselves an adequate solution, principally because they are an extremely inefficient way of calculating conditional probabilities such as those in equations (15)–(19) of Ref. [1]. To calculate conditional probabilities, one must sift out only those member functions for which the condition is satisfied. If the condition is a rare event, as may be expected to be the case with the fatal flaw in an engineering application, then a huge number of member functions must be calculated before good enough statistics are obtained.

Superimposed on Figs 3 and 4(b) are the average value $Eu^{(k)}$ of u and $Eu^{(k)} \pm \sigma_u^{(k)}$, where $\sigma_u^{(k)}$ is the root mean square deviation (rmsd) of u calculated at crack length $2c_k$ according to Eqs. (3) and (4) of Ref. [1]. In Fig. 5, continuous cpd's of u are shown, calculated from the discontinuous cpd given by equation (5) of Ref. [1]. For Model 1 [Fig. 5(a)], the cpd is representative of any crack length, $2c$ (after a brief, unimportant transient region, $2c \leq 20 \mu\text{m}$), because this model is homogeneous. For Model 2, the cpd for u becomes progressively narrower with increasing crack length. It is shown in Fig. 5(b) for equally spaced crack lengths lying between 15 and $134 \mu\text{m}$, as marked. Note that the cpd's for u at all crack lengths constitute a useful summary of the stochastic model proposed for whatever mechanism is believed to control the growth rate, dc/dn . When combined with a law relating dc/dn to u , they lead immediately to cpd's for dc/dn . In the present

TABLE 1
VISIBLE CRACK LENGTHS $2c$ (μm) IN Ti 6-2-4-6 AFTER VARIOUS NUMBERS OF
CYCLES OF FULLY REVERSED CYCLIC LOADING AT ± 700 MPa

CRACK NUMBER	500C CYCLES	800C CYCLES	950C CYCLES	1100C CYCLES	1250C CYCLES	CRACK NUMBER	500C CYCLES	800C CYCLES	950C CYCLES	1100C CYCLES	1250C CYCLES
1	25	65	92	140	200	33		58	68	111	128
2		50	72	108	161	34	24	33	36	49	52
3		35	68	119	156	35				27	39
4		29	50	89	114	36	46	98	115	158	200
5		19	46	55	80	37	48	88	148	191	251
6	23	42	64	88	138	38		25	26	47	61
7		29	45	75	110	39		16	20	21	25
8		17	19	25	40	40				13	26
9		28	53	75	100	41	26	35	43	53	65
10				58	81	42	21	32	44	69	8
11	20	39	57	82	107	43	22	31	44	64	71
12		16	16	17	19	44	25	47	62	88	101
13	21	26	27	29	38	45				35	40
14	31	62	102	149	210	46	18	32	41	50	75
15	24	41	69	98	S	47	16	21	32	S	
16		34	45	55	S	48			21	22	28
17		40	58	80	S	49	22	24	28	39	50
18	23	38	53	70	S	50			33	38	50
19	32	105	170	237	C	51	20	26	26	42	53
20	22	49	70	S		52				21	40
21		30	46	73	S	53	25	25	25	29	37
22	21	44	75	111	S	54	21	37	52	75	109
23	25	43	75	128	S	55		23	23	28	36
24	17	38	64	140	C	56				33	38
25		33	51	67	S	57				18	25
26	10	21	33	44	52	58				23	23
27		32	50	63	S	59				59	87
28	21	69	116	183	C	60				23	25
29		27	48	66	S	61				46	55
30				53	67	62				27	34
31		12	14	16	19	63				42	59
32		49	68	73	95						

S INDICATES THAT A CRACK HAS BECOME SHADOWED BY ANOTHER SO THAT IT NO LONGER EXPERIENCES THE APPLIED LOAD

C INDICATES THAT A CRACK HAS COALESCED WITH ANOTHER

application. the model validation consists of optimizing this law, which is done in the following section.

ANALYSIS OF THE Ti 6-2-4-6 DATA

For the present investigation, the original data [8], which had been gathered by experimental methods described in Ref. [4], were analyzed afresh. The data used are shown in Table 1. They consist of the surface lengths of 63 cracks measured on the same Ti 6-2-4-6 specimen (yield strength, 1140 MPa; Young's modulus, 140 GPa) at the stated intervals in the fatigue life. The original experiment was conducted with a polished cantilever specimen loaded in flexure. The observed cracks were initiated naturally and grown at ± 700 MPa. The lengths were measured by direct optical microscopy. The measurements were made when the specimen was loaded, to minimize any part of the crack that might be overlooked for not being open. The lengths are probably accurate to within a micron or so. For some cracks, poor definition of the crack tip might allow an error of several microns.

To simplify model validation, the data were reduced to the form shown in Fig. 6. The values of $2d_i/dN$ plotted there were obtained by simply dividing a measured increment in length by the corresponding increment in elapsed cycles. The result of each such calculation was associated with the average crack length between the first and second measurements. Since the cracks usually grew tens of microns between measurements, the errors in average velocity arising from errors in length are usually small. The scatter observed in crack velocities is caused by fluctuations in the material.

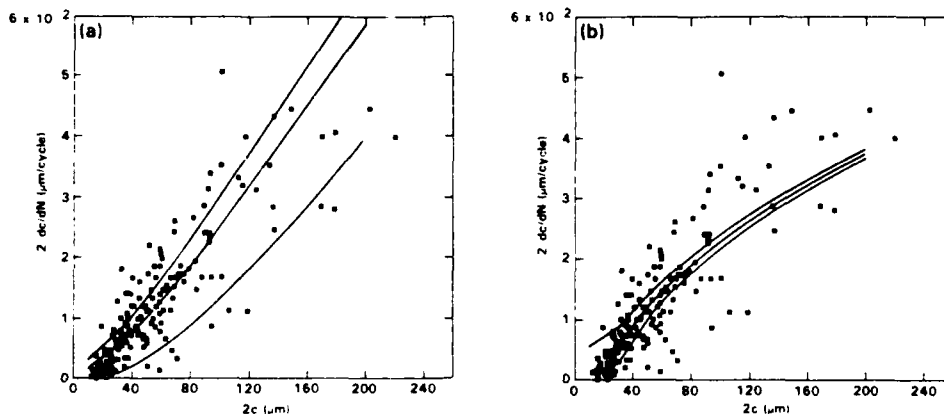


Fig. 6. The crack growth data of Ref. [8] for Ti 6-2-4-6. The three curves represent the velocity corresponding to the average value of u and two bounds that should encompass 70% of the data calculated using (a) Model 1 ($n = 3$); and (b) Model 2.

No provision was made in the data analysis for any quasi-static change in average material properties during fatigue. The number of elapsed cycles in the neighborhood of which a pair $(2c, 2dc/dN)$ had been calculated was dropped from further consideration. This is equivalent to assuming that dc/dN may be a function of crack length and the control variable u , but not of elapsed cycles N directly. This assumption follows the earlier nonprobabilistic study of Ti 6-2-4-6 [4]. In later applications of the probabilistic model of Ref. [1], the generalization that dc/dN might depend explicitly on N will be considered.

Model validation—the distribution of velocities

In the present example of short crack growth in Ti 6-2-4-6, where the dominant closure source is fracture surface roughness, the form of the law of crack growth is [4]

$$2 \frac{dc}{dN} \equiv v(c, u) = A [-\alpha u + 1.12 \sigma_{\max} \sqrt{2c}]^6, \quad (5)$$

where A is conveniently expressed in $\mu\text{m}\cdot\text{cycle}$; u is the growth control variable appearing as a continuous variable; and σ_{\max} is the applied fully-reversed cyclic load amplitude. In the original derivation of this law, the variable u represented the measured crack opening displacement at zero load. The law was established by fitting crack opening data for a moderately large number of individual cracks growing through grains whose sizes were individually measured and recorded. In fact, the measured CTOD's [4] have an approximately constant average for cracks of length $\geq 100 \mu\text{m}$, but fall away for shorter cracks, and must vanish at zero crack length. Since the velocity data continue to show considerable scatter (see Fig. 6) for even the shortest cracks, it may well be that fracture surface roughness is not the only growth control mechanism, especially for cracks of length $\leq 50 \mu\text{m}$. However, since only the shortest cracks would be strongly affected, equation (5) as it stands will suffice here.

The variable u is, of course, a random variable, whose distribution at any crack length is given by equation (5) of Ref. [1]. That equation defines the cpd $F_u^{(k)}(u_i^{(k)})$ in terms of the discrete variables $u_i^{(k)}$ defined at crack length $2c_k$. For the following model validation, $\tilde{F}_u(u|c)$, a cpd for the continuous variable u at any crack length $2c$, was generated by a numerical smoothing algorithm and interpolation over $\{2c_k\}$. $\tilde{F}_u(u|c)$ is determined almost entirely by the PTM's $\mathbf{P}^{(m)}$, which in

the present application are prescribed by Model 1 or Model 2. It is not strongly influenced by the assumed initial distribution $\pi^{(0)}$. (General note: in other applications, this may not always be the case.) Equation (5) may be regarded as a deterministic, one-to-one relationship between u and v at fixed crack length, $2c$. It possesses the inverse relationship

$$u = u(v, c), \quad (6)$$

which expresses u as a strictly monotonically decreasing function of v . The cpd for crack velocities, $\tilde{F}_v(v|c)$, may therefore be written

$$\tilde{F}_v(v|c) = 1 - \tilde{F}_u(u(v, c)|c). \quad (7)$$

The validation procedure consists of finding the parameters A , β , and α in equation (5) that cause $\tilde{F}_v(v|c)$ to resemble most closely the experimental distributions of $2dc/dN$ at all crack lengths given the model-based distributions $\tilde{F}_u(u|c)$.

There are various ways this optimization task can be carried out. In this work, a modification of a method considered by Fertig [9] was employed. Given values of the parameters A , β , and α , equation (6) implies a value, u_i , of the growth control variable for each experimental data pair $(2c_i, V_i)$. Let there be N_d such data pairs and implied values u_i . With each value u_i may be associated the random variable

$$y_i = \tilde{F}_u(u_i|c_i). \quad (8)$$

For a valid model and an infinite data set, y_i must be uniformly distributed over the interval $[0, 1]$. The optimum values of the parameters A , β , and α may be found in principle by minimizing the Cramer-von Mises test function

$$S = \sum_i \left[y_i - \frac{i}{N_d + 1} \right]^2, \quad (9)$$

with the y_i previously sorted into ascending order. For the given, finite data set, a modification of this procedure was used to avoid finding spurious, local minima of $S(A, \beta, \alpha)$ with the available minimization algorithm. The data $\{(2c_i, V_i)\}$ were divided amongst p equal subsets, Ω_k , in such a way that

$$2c_i < 2c_{j'} \text{ if } i \in \Omega_k, \quad j \in \Omega_{k'}, \text{ and } k < k'. \quad (10)$$

TABLE 2
OPTIMAL PARAMETERS, A , β , AND α AND CORRELATION
LENGTH λ^* FOR VARIANTS OF MODEL 1

n (SEE NOTE 1)	A ($\mu\text{m}/\text{CYCLE}$) $\times 10^3$	β	α (SEE NOTE 2)	λ^* (μm)
1	0.540	2.02	0.359	< 10
3	0.562	2.05	0.304	14
10	0.516	2.16	0.377	60

NOTE 1: THE INSTANTANEOUS VALUE OF da/dN IS ASSUMED TO BE CONTROLLED BY THE AVERAGE OF THE DISTANCES BETWEEN THE LAST n DEFLECTIONS SUFFERED BY THE VISIBLE SURFACE CRACK

NOTE 2: THE VALUES GIVEN FOR α ARE OBTAINED WHEN u IS EXPRESSED IN μm AND $\sigma_{\text{MAX}}\sqrt{2c}$ IN $\text{MPa}\cdot\text{m}^{1/2}$ IN EQ. (5).

The corresponding y_i of equation (8) were ordered within each subset, and the minimization was carried out for the sum

$$S = \sum_k \left\{ \sum_{i \in \Omega_k} \left[y_i - \frac{i}{N_k + 1} \right]^2 \right\}, \quad (11)$$

where N_k is the number of data points in Ω_k . The resulting values of A , β , and α were found to be essentially independent of p for $2 \leq p \leq 5$.

The results of the procedure for optimization are summarized for Model 1 in Table 2. The three cases $n = 1$, 3, and 10 are shown. There are some differences in the corresponding parameters A , β , and α , but not enough to distinguish between the merits of the three cases. In Fig. 6(a), the three functions, $v(c, Eu)$, $v(c, u^+)$, and $v(c, u^-)$, have been superimposed (solid lines) on the data for the case $n = 3$. u^\pm are the values of u defined by

$$\tilde{F}_u(u^+ | c) = 0.85$$

and

$$\tilde{F}_u(u^- | c) = 0.15, \quad (12)$$

so that the outer curves should contain 70% of the data points. The equivalent curves for $n = 1$ and $n = 10$ show no significant differences to the case $n = 3$. One cannot discriminate between the merits of these three cases by their ability to reproduce the average scatter $2dc/dN$.

On the other hand, Model 2 is clearly incorrect. In Fig. 6(b), the same curves, $v(c, Eu)$, $v(c, u^+)$, and $v(c, u^-)$ are plotted against the data using the optimized parameters of Model 2 and the corresponding distributions \tilde{F}_u . While the predicted average growth is acceptable, given the thinness of the data at lengths $> 100 \mu\text{m}$, the scatter in $2dc/dN$ is clearly not reproduced. To highlight this failure, the rmsd found experimentally in $2dc/dN$ has been compared in Fig. 7 with the rmsd calculated according to Model 1 ($n = 3$) and Model 2. The experimental values were estimated as follows. The data $(2c_i, V_i)$ were grouped into ten bins b_j centered around lengths $2c_j$. The rmsd

$$\sigma_i(c_j) = \sqrt{\frac{1}{N_{j \text{ in } b}} \sum \left[\frac{V_i - v(c_j, Eu)}{v(c_j, Eu)} \right]^2} \quad (13)$$

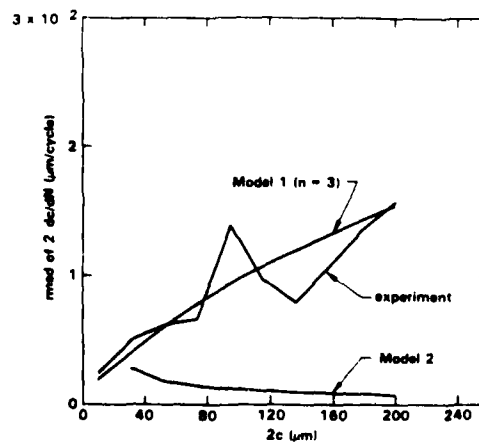


Fig. 7. Irregular curve: the rmsd of the velocity data of Fig. 5, calculated according to equation (13). Smooth curves: the rmsd of the crack velocity calculated using Model 1 ($n = 3$) or Model 2, as marked.

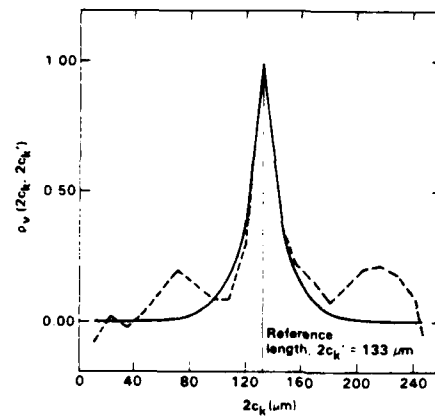


Fig. 8. An example of the covariance function $\rho_c(2c, 2c')$.

was then evaluated, with the sum being restricted to the data for which $2c_i$ falls in b_j , which is satisfied for N_j points. Note that the predicted rmsd's for $n = 1$ and $n = 10$ in Model 1 are virtually the same as that shown for $n = 3$.

Inspection of the data shown in Fig. 6 suggests that a threshold for growth may exist for cracks less than $10 \mu m$ at the stress level used in the experiment. The data for dc/dN perhaps tend to zero to the right of the origin, even though the shortest cracks observed were still propagating. This possibility was investigated by subtracting a constant threshold stress intensity factor from the bracketed terms on the right hand side of equation (5). The velocity $v(c, u)$ was then set to zero if the sum of the bracketed terms was negative. It was found that the average velocity dipped as expected for $2c \leq 20 \mu m$, without any conclusive effect on the measure S [equation (11)] of the goodness of fit. All other conclusions in this paper were unaffected by this small threshold.

Covariance and correlation lengths

The covariance function $\rho_c(k, k')$ (defined by equation (10) of Ref. [1], with $2c$ replacing a) gives a simple, quantitative measure of the memory a crack has when it reaches length $2c_k$ of the velocity

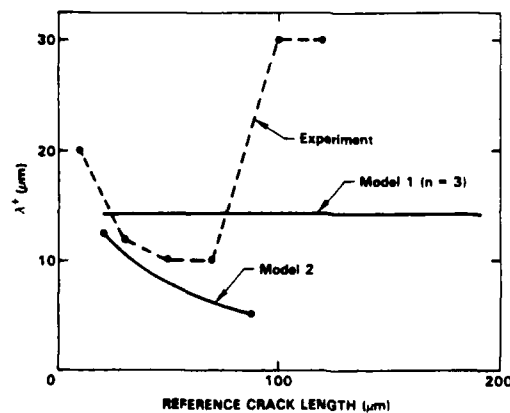


Fig. 9. The forward correlation length λ^+ as a function of the reference length, for Model 1 ($n = 3$), Model 2, and from experimental data, as marked.

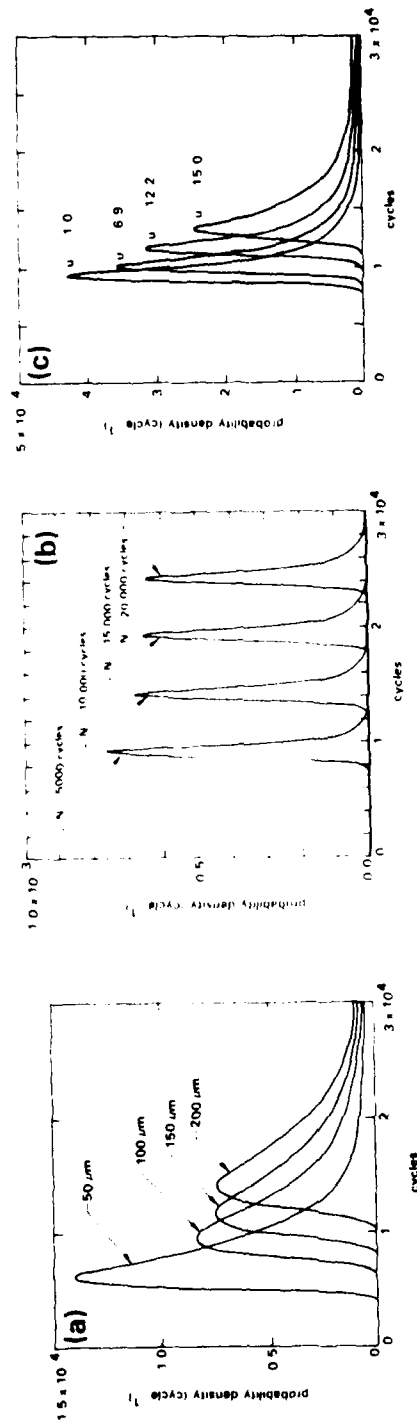


Fig. 10. (a) The probability density per cycle for the cycles taken to reach a given crack length, for the four lengths marked. These calculations are for Model I ($n = 3$); (b) the probability density per cycle for the cycles taken to grow to length 200 μm , given that the crack length was 100 μm after N cycles, for four values of N as marked; and (c) the probability density per cycle for the cycles taken to grow to length 200 μm , given that the crack length was 100 μm after 10,000 cycles and the growth control variable had the value marked.

it had (or will have) at length $2c_k$. Given the optimum values of the parameters A , β , and α in the growth law equation (5), $\rho_i(k, k')$ has been calculated as a function of $2c_k$, with $2c_k$ held constant at various values. An example of one of these calculations, for $2c_k = 133 \mu\text{m}$, is shown in Fig. 8 (solid line). It is superimposed on the analogous quantity calculated from 100 Monte Carlo simulations (dashed line). The covariance shows the expected, approximately exponential decay in both directions with increasing $|2c_k - 2c_{k'}|$. This decay may be well characterized by the correlation lengths λ^+ and λ^- defined by equation (11) of Ref. [1].

From its definition in equation (2), it is evident that Model 1 is homogeneous: the PTM's do not depend on crack length, $2c$. It follows that, in Model 1, the correlation lengths λ^+ and λ^- are asymptotically constant and equal as $2c$ increases, following an initial transient region that depends on the initial distribution $\pi^{(0)}$ assumed for u . The constant value they tend to depends strongly on n in equation (2). If $n = 1$, inspection of equation (2) shows that the values of u , and hence of dc/dN , at successive crack lengths $2c_k$ and $2c_{k+1}$ are uncorrelated, i.e. $\rho_i(c_k, c_k) = 0$ when $k \neq k'$. For $n \geq 2$, λ^+ and λ^- increase approximately linearly with n . Some representative values appear in Table 2. The strong dependence of λ^\pm upon n opens the possibility that the optimum value of n can be deduced from comparison with correlation lengths calculated from the experimental data.

The correlation lengths λ^+ and λ^- predicted from Model 2 depend on crack length. Numerical calculations show that they are approximately equal and decay monotonically with increasing $2c$. Although Model 2 has been discounted because of its inability to reproduce the scatter in dc/dN , λ^+ is shown in Fig. 9 as a function of crack length to exemplify a feature of a nonhomogeneous Markov process.

The experimental counterpart of $\rho_i(k, k')$, the covariance of the velocities of an observed crack at two different lengths, was analyzed as follows. With the same definitions of grid points $2c'_i$ and bins b_i that were used in equation (13), the experimental covariance was calculated from the data as

$$\rho_i(c'_j, c'_i) = \frac{1}{N_{ii}} \sum_p^{\text{bin } h} \sum_q^{\text{bin } h} \frac{[V_p - v(c'_j, \bar{u}(c'_j))][V_q - v(c'_i, \bar{u}(c'_i))]}{\sigma_i(c'_j) \cdot \sigma_i(c'_i)} \eta(p, q). \quad (14)$$

The function η takes the value unity if the observations p and q were of the same crack, and zero otherwise; and $\eta = 1$ for N_{ii} pairs (p, q) . In calculating the denominator of equation (14), only data contributing to the numerator are to be used. The correlation lengths $\lambda^+(c'_i)$ and $\lambda^-(c'_i)$ may be deduced from $\rho_i(c'_j, c'_i)$ by fitting an exponential function to the values obtained when c'_i is held constant and c'_j is varied. The fitted exponential function has the form

$$\rho_i(c'_j, c'_i) \approx e^{-(2c_j - 2c_i)/\lambda^\pm}. \quad (15)$$

The quality of this calculation of experimental values for λ^\pm is limited by the number of data points $(2c_i, V_i)$ available for each crack and the total number of cracks observed. In the data set considered here, there are insufficient data for $2c_i > 100 \mu\text{m}$ to make a reliable estimate of λ^\pm in that regime. The values deduced for λ^\pm are also affected strongly by the frequency at which measurements of $2c$, and elapsed cycles are made. Table 1 shows that cracks had generally grown at least $10 \mu\text{m}$ between measurements if they were relatively short ($2c < 100 \mu\text{m}$), and at least $30 \mu\text{m}$ if they were relatively long ($2c > 100 \mu\text{m}$). These minimum intervals of growth are clearly lower bounds to the deducible correlation lengths. In other words, equation (14) must give a correlation length of at least $10 \mu\text{m}$ for $2c < 100 \mu\text{m}$, even if the true correlation length of the underlying control variable u is less than that. The only way to decide whether that might be the case is to make measurements more frequently.

With these limitations acknowledged, experimental values for λ^+ were calculated according to

equations (14) and (15), and are presented in Fig. 9. Because few observations were available for the same crack over more than two or three bins, the fitting of the function in equation (15) was restricted to the first one or two bins adjacent to the reference bin. The first four experimental values for λ^+ (for $2c < 100 \mu\text{m}$) should be considered accurate to within $20 \mu\text{m}$. The results for $2c \geq 100 \mu\text{m}$ may be considerably more in error. Note especially that the latter are not accurate enough to imply an upward trend in λ^+ .

In spite of these uncertainties, it is still possible to draw at least a weak conclusion about the relative merits of the cases $n = 1, 3$, and 10 in Model 1. The case $n = 3$ generates a correlation length λ^+ of about $14 \mu\text{m}$ (Table 2 and Fig. 9), which is consistent with the experimental values. The case $n = 10$ generates a correlation length $\lambda^+ \approx 60 \mu\text{m}$, which is inconsistent with experiment. The case $n = 1$ generates $\lambda^+ < 10 \mu\text{m}$, but this cannot be ruled out because of the lower bound to the experimental λ^+ enforced by the frequency of the original measurements. In summary, it can be concluded that agreement is obtained when $n \leq 5$. In other words, fluctuations in the instantaneous value of dc/dN are controlled by the average size of at most the three $(n/2)$ grains nearest to each crack tip.

CALCULATION OF REMAINING LIFETIME

In this section, examples are presented of the calculation of remaining fatigue lifetime, using the calibrated Model 1 ($n = 3$).

The probability that a crack will grow to a given length after some number of fatigue cycles is illustrated for several lengths in Fig. 10(a). These calculations (following equation (14) of Ref. [1]) are of the cycles to grow to a given length, given that the crack had the length $2c_0$ at time zero. Therefore, the distributions shown are of times of propagation. These are not necessarily the total elapsed cycles, since there may be a significant number of cycles required to generate a crack of length $2c_0$. This initiation phase has not been considered here.

The conditional probability, that a crack will reach length $2c_k$ after N cycles given that it reached length $2c'_k$ after N' cycles, is more significant, because it does not depend on the value $2c_0$ of the first discrete crack length. It is shown in Fig. 10(b) (calculated according to equation (17) of Ref. [1]) for the case $2c'_k = 100 \mu\text{m}$, $2c_k = 200 \mu\text{m}$, and various values of N' . Note that, in this case, where $2c_k - 2c'_k \gg \lambda^+$ and the Markov process is homogeneous, there is very little dependence of $N - N'$ on N' . The four densities shown very nearly coincide if the origin for each is shifted to N' . This is not the case if additional information is available at $2c'_k$, namely the value there of the growth control variable, or, equivalently, the instantaneous velocity $2dc/dN$. Figure 10(c) shows the probability that a crack will reach length $2c_k$ after N cycles given that it reached length $2c'_k$ after N' cycles and had the value u_i of u . The number $N - N'$ of additional cycles to failure depends strongly on the conditional value u_i . This effect can be very important in calculating remaining lifetime given an NDE measurement that enables estimation of u .

DISCUSSION

The models for the growth control variable u were chosen to be consistent with earlier work [4] that had suggested that, for this range of crack lengths, roughness-induced closure is the dominant source of fluctuations in the growth rate, $2dc/dN$. However, since u measures a geometrical aspect of the material, viz., the average size of grains near the crack front, the models have much broader applicability. For example, it is known that, in certain aluminum alloys, fluctuations in dc/dN are dominated by local plasticity, and the local plasticity in each grain depends very strongly on its

size [10]. Models similar to Models 1 and 2, with u reinterpreted as a measure of plastic strain, might well be appropriate for such materials. The differences in the models for the evolution of u for that application and the present application would be mainly semantic. However, a growth law [equation (5)] of different form would probably be appropriate for the calibration of the model against data.

For Ti 6-2-4-6, the best model found for the evolution of the damage control variable, u , was homogeneous (Model 1), i.e. the PTM's $P^{(m)}$ were independent of crack length. There are many materials for which short crack growth will not be described so simply. In general, there will be a transition at some length from very small cracks whose velocity is determined by material properties along the entire crack front (as in Model 2) to larger cracks whose surface velocity fluctuates according to Model 1. In the Ti 6-2-4-6 data analysed here, this transition has evidently already occurred before the velocity data become significant, i.e. at some length less than $50 \mu\text{m}$, the equivalent of just a few grains. In the very small crack regime, the correlation length might be expected to decrease with crack length, as it does in Model 2.

On the other hand, when fluctuations in the growth rate are dominated by meanderings in the crack front or by the aspect ratio of a semielliptic crack, the correlation length might increase with crack length. The effective stress intensity factor averaged over the crack front depends on the details of the crack shape [11-14]. Fluctuations in ΔK will persist as long as fluctuations in the crack shape persist. If the fluctuations in shape scale with the crack size, rather than some characteristic material length, then fluctuations in K will persist longer for larger cracks. To examine such possibilities, it is essential that nonhomogeneous Markov processes (e.g. Model 2) can be treated. This is an important feature of the approach presented in Ref. [1].

For the Ti 6-2-4-6 specimens considered here, such shape effects were not evident over the range of lengths in which the data fall. Crack planes were exposed by brittle fracture at liquid nitrogen temperature, leaving the fatigue crack front distinctly outlined. The fatigue cracks were all observed to be approximately semielliptical, with an aspect ratio of ~ 0.4 . Departures of the crack front from a simple, smooth curve will be more pronounced when the crack is smaller relative to the grain size, or if other inhomogeneities of larger period remain from manufacture.

The conclusions reached do not depend strongly on the correctness of the deterministic law, equation (5), derived in previous work [4] and used here to relate dc/dN to u . Of course, if this law had taken a different functional form, then different optimal values of the parameters A , β , and α (or their substitutes) would have been deduced. But various parametric laws could have been concocted that would have accounted equally well for the observed statistics. The literature abounds with demonstrations that it is possible to fit in various ways the average of dc/dN , which is the quantity usually reported. However, physically unrealistic functions of u [e.g. raising u to a power very different from unity inside the brackets in equation (5)] would be eliminated by their inability to reproduce the higher moments of the distribution of dc/dN at each value of $2c$. The statistical test given in equation (9) is a convenient, quantitative measure of the success of any model in this regard.

CONCLUSIONS

The model-based statistical analysis of the data for Ti 6-2-4-6 over the range of surface crack lengths $10\text{--}250 \mu\text{m}$ has shown that:

- (1) In the regime studied, fluctuations in the instantaneous velocity of the visible crack tips depend only on the geometry of the visible, surface microstructure; and

- (2) Fluctuations in the instantaneous velocity are probably influenced by at most the three grains nearest each crack tip, or those within $\sim 30 \mu\text{m}$ of it.

These conclusions demonstrate the value of analyzing the statistics of growth rate data as a way of inferring micromechanical information and checking the validity of micromechanical models. This potentially fruitful approach has been generally ignored in the past, even when statistically significant data have been available. The model presented in Ref. [1] provides a powerful, flexible vehicle for such studies.

The fact that the model is only weakly dependent on the correctness of the rationale used to derive it guarantees robustness of any ensuing statistical predictions. This is the key to the model's potentially accurate performance as a method of predicting remaining lifetime in an engineering environment. Indeed, this was originally intended to be and remains the model's primary function. In this paper, the calibration of the model against growth rate data has been demonstrated. The relationship between dc/dN and u becomes fully defined by the optimization of the parameters in it. The conditional probabilities concerning remaining lifetime that were defined in Ref. [1] can then be computed easily and economically. Examples have been presented of the kinds of output available.

Acknowledgements—Research sponsored by the Air Force Office of Scientific Research (AFSC) under Contract No. F49620-85-C-0034. The United States Government is authorized to reproduce or distribute reprints for governmental purpose notwithstanding any copyright notation hereon. The authors are indebted to Dr Ken Fertig for his frequent, friendly advice on statistical analysis.

REFERENCES

1. Cox B. N. and Morris W. L. (1986) A probabilistic model of short fatigue crack growth. *Fatigue Fract. Engng Mater. Struct.* **10**, 419–428.
2. Cox B. N., Pardee W. J. and Morris W. L. (1987) A statistical model of intermittent short crack growth. *Fatigue Fract. Engng Mater. Struct.* **9**, 435–455.
3. Morris W. L., James M. R. and Buck O. (1981) Growth rate models for short surface cracks in Al 2219-T851. *Met. Trans.* **A14**, 57–64.
4. James M. R. and Morris W. L. (1983) Effect of fracture surface roughness on growth of short fatigue cracks. *Met. Trans.* **A14**, 153–155.
5. Howard R. A. (1970) *Dynamic Probabilistic Systems*. Wiley, New York.
6. Papoulis A. (1965) *Probability, Random Variables, and Stochastic Processes*. McGraw-Hill, New York.
7. Suresh S. (1985) Fatigue crack deflection and fracture surface contact: micromechanical models. *Met. Trans.* **A16**, 249–260.
8. Unpublished data of James M. R. and Morris W. L.
9. Fertig K. W. (1981) Asymptotic power of von Mises goodness-of-fit statistics when parameters are estimated. Rockwell International Science Center Technical Report No. SC TR-81-9.
10. Morris W. L., Cox B. N. and James M. R. (1987) Microplastic deformation of Al 2219-T851. *Acta Met.* **35**, 1055–1065.
11. Smith F. W. and Sorensen D. R. (1976) The semi-elliptical surface crack—a solution by alternating method. *Int. J. Fract.* **12**, 47–57.
12. Ruiz C. and Epstein J. (1985) On the variation of the stress intensity factor along the front of a surface flaw. *Int. J. Fract.* **28**, 231–238.
13. Rice J. R. (1985) First-order variation in elastic fields due to variation in location of a planar crack front. *J. appl. Mech.* **52**, 571–579.
14. Cox B. N. and Morris W. L. (1987) Statistics of the shape of small fatigue cracks. In *Fatigue '87, Proc 3rd Int. Conf. on Fatigue and Fatigue Thresholds*, Charlottesville, Va.

THE STATISTICS OF THE SHAPE OF SMALL FATIGUE CRACKS

B.N. Cox* and W.L. Morris*

This paper presents Monte Carlo simulations of the growth of small fatigue cracks through stochastic microstructures. The simulations are based on canonical formulae for the stress intensity factor around an irregular crack front, and laws of crack growth extracted from prior experiments or theories to describe the influence of the microstructural environment. The simulations allow the convenient examination of the statistics of crack shape, which may be compared with easily obtained experimental data. The magnitude and persistence of fluctuations in crack shape may be used to test postulated laws of growth. The physical insight available from the Monte Carlo simulations will ultimately permit more accurate predictions of fatigue lifetime.

INTRODUCTION

Small fatigue cracks having no dimension greater than a few grain diameters are subject to large stochastic variations in the driving force acting at different points along the crack front. Therefore, the crack front does not remain smooth, but shows irregularities which may be large or small depending on the strength of the stochastic factors generating them. In this paper, Monte Carlo simulations of the growth of such irregular cracks are presented. The Monte Carlo simulations can be used to validate postulated laws of crack growth by comparison with observations of crack shape; and to illuminate the sources of various statistical properties of small cracks, which may allow more accurate predictions of fatigue lifetime.

For small cracks, the stochastic variations in the driving force originate in the stochastic nature of the microstructure encountered by the advancing crack front. The rate of advance of a segment of the crack front can be influenced by several mechan-

*Rockwell International Science Center, 1049 Camino Dos Rios, Thousand Oaks, CA 91360

isms whose impact depends on the size, orientation, and mechanical properties of the grains in the immediate vicinity. The mechanisms include temporary arrest at grain boundaries, deceleration caused by back stress or by fracture surface roughness, acceleration caused by enhanced local plasticity, and fluctuations in the local stress field caused by elastic inhomogeneity and anisotropy. The Monte Carlo simulations allow the consideration of one or all of these mechanisms, as long as a corresponding law is available to express their influence on the growth rate of each segment of the crack front.

The tendency of the stochastic microstructure to make the crack front irregular is balanced by the dependence of the stress intensity factor on crack shape. For example, for an embedded irregular plane crack, the mode I stress intensity factor, K_I , is generally reduced on protrusions and enhanced on retarded segments, so that, in the absence of microstructural fluctuations, the crack always tends to be circular. For a surface breaking crack under mode I loading, the equilibrium shape is approximately a smooth semi-ellipse of aspect ratio 0.4. For the Monte Carlo simulations, a simple algorithm has been derived to estimate K_I for either an embedded or surface breaking plane crack of any shape.

STOCHASTIC MICROSTRUCTURES

A single instance of a stochastic microstructure is generated as follows. Nucleation sites of a prescribed average density are placed on the plane of the crack in a Poisson process (i.e., with no correlation in their locations) by invoking a pseudo-random number generator. The grain boundaries are then determined by the Wigner-Seitz construction, which defines each grain as the area bounded by the perpendicular bisectors of the lines joining that grain's nucleation site to the nucleation sites of all its contiguous neighbors. Nonequiaxed grain structures are generated by rescaling one of the axes. The locations of the vertices and the total area of each grain are stored until the next microstructure is generated.

To enable convenient reference to the information contained in a given microstructure, a discrete square grid is defined on the plane of the crack. Each point on this grid is then associated with the number of the grain containing it and with other measures of the local microstructure. For example, for modeling crack growth in Al alloys, an appropriate measure upon which plasticity-induced closure depends is the distance from the grid point to the next grain boundary measured along the line emanating from the center of the crack. Other characteristics, such as grain orientation, might be preferred for other materials.

APPROXIMATE, FAST ALGORITHM FOR K_I

The feasibility of the Monte Carlo simulations depends critically on being able to estimate K_I very quickly for plane cracks of arbitrary shape. Exact calculation of K_I would be prohibitively slow and, therefore, simple approximations to K_I have been derived. The approximations are based on estimates, $K_I(P)$, of K_I at the zenith, P, of a protrusion and $K_I(Q)$ at the nadir, Q, of a retarded segment. Both the protrusion and the retarded segment considered have the square-shouldered geometry shown in Figure 1. A combination of analytical and numerical work has led to the following expressions for $K_I(P)$ and $K_I(Q)$:

$$K_I(P) = 2\sigma_\infty \sqrt{t/\pi} \cdot \frac{2}{\pi} \tan^{-1} \left| \frac{3 + s/t}{1 - s/t} \tan \frac{\alpha}{2} \right|, \quad (1)$$

and

$$K_I(Q) = 2\sigma_\infty \sqrt{s/\pi} / \frac{2}{\pi} \tan^{-1} \left| \frac{3 + s/t}{1 - s/t} \tan \frac{\alpha}{2} \right|, \quad (2)$$

where s , t and α are defined in Figure 1. The identification of α for a smooth rather than square-shouldered protrusion or retarded region is subjective and, therefore, the term $\alpha/2$ in Equations (1) and (2) was replaced by $\pi/2 \cdot \alpha/\alpha_0$, with the parameter α_0 evaluated by calibration against K_I for elliptical cracks.

For crack fronts of arbitrary profile, the half-width α of a protrusion or retarded segment was defined as half the angle between the points on either side of the extrema at which the radius of the crack was equal to its average radius (Figure 2a). The value of K_I between the zenith of a protrusion and the nadir of a retarded segment is then written simply as

$$K_I(\theta) = [(r(\theta) - s)K_I(P) + (t - r(\theta))K_I(Q)]/(t - s), \quad (3)$$

where $r(\theta)$ is the radius of any point and s and t are defined in Figure 2a. The exact results for an elliptical crack with $s = t$ can be fitted perfectly by Equation (3) by adjusting α_0 . With this value of α_0 (viz., $\alpha_0 = 0.201$) retained for all cases, the agreement with other known solutions is as illustrated in Figure 3. Even for protrusions and retarded segments of significant magnitude ($s/t = 0.5$), the approximation is always accurate to within a few percent. Most importantly for the present application, it gives fair estimates of the dependence of K_I on α and of the relative magnitudes at extrema on the same crack. These are

FATIGUE 87

the properties essential to balancing the tendency of $K_I(\theta)$ to make a crack regular against the disrupting effects of the microstructure. Note that $K_I(Q)$ is correctly predicted to diverge and $K_I(P)$ to vanish as $a \rightarrow 0$. This implies that very sharp irregularities of the crack front are unlikely to be found.

K_I on Surface Breaking Cracks

Convenient algorithms for estimating K_I around semi-elliptical surface cracks have been given by Newman and Raju (2,3). If $2c$ is the crack's length on the surface, and a its depth, then for $2c \geq a$,

$$K_I(\phi) = \sigma \sqrt{\frac{\pi a}{E(k)}} F\left(\frac{a}{c}, \phi\right) \quad (4)$$

where E is the elliptic integral of the second kind, $k^2 = 1 - a^2/c^2$, and F is a polynomial in a/c and c/a and a simple trigonometric function of ϕ , the parametric angle of the ellipse.

To account for departures of the crack front from the semi-elliptical shape, Equation (4) was combined with Equation (3) by the following ansatz. The center of mass and the moments of inertia I_x and I_y of an irregular crack were found, and taken to define the center and semi-axes ($c = 2\sqrt{I_x}$ and $a = 2\sqrt{I_y}$) of a smoothed semi-elliptical crack. The x axis was rescaled by the factor a/c , so that the fitted semi-elliptical crack would become a semi-circular crack, and the mirror image was added (Figure 2(b)) to generate an entire irregular, approximately circular crack. Equation (3) was then used to generate values of $K_I(\theta)$ around this scaled crack, normalized to $K_I(a) = 2\sigma_\infty\sqrt{a/r}$. These normalized values of $K_I(\theta)$ represent the relative acceleration and retardation of local protrusions and retarded segments. These values were then multiplied by the results of Equation (4) for the semi-elliptical crack of semi-axes c and a , to account for gross shape and size effects.

MONTE CARLO SIMULATIONS

A Monte Carlo simulation begins by generating a random, two-dimensional pattern of grains lying in the plane of growth. A small crack is introduced, spanning a few grains or perhaps just one. The crack front is divided into discrete segments, which increase in number as the crack grows, so that they remain small relative to the microstructure. The position of the crack front is updated at regular intervals according to the laws governing

FATIGUE 87

the growth of each segment, which embody the dependence of the growth rate on the details of the surrounding microstructure. The advance of the crack front is always assumed to be in the direction of the normal to it at any point. If a newly calculated crack front possesses unphysical loops or overlapping spurs, these are eliminated by deleting the offending segments.

CLOSURE-INDUCED SHAPE EFFECTS IN AL 7075-T6

A typical simulation of a surface crack is shown in Figure 4. The grain structure there corresponds to that exposed on a plane cut normal to the rolling direction and normal to the surface of a rolled sheet of Al 7075-T6. The average grain length normal to the rolling direction is ~ 120 μm , and the average depth normal to the surface is ~ 20 μm . After a brief crystallographic phase immediately following initiation, small fatigue cracks in such specimens grow in a transgranular noncrystallographic mode. Plasticity-induced closure causes them to slow down upon reaching each grain boundary and accelerate as each grain is being traversed (Zurek et al (4)). Observations on just the visible surface outlines of individual cracks have led to laws relating the rate of advance of each surface tip to its distance, z , from the next grain boundary. In the simulations shown here, the same law has been assumed to prevail all around the crack front, with z always measured along a line radiating from the original center of the crack. The law has the form

$$\frac{dw}{dN} = A\Delta K^2 (1 - bz/2\bar{r})^2 H(1 - bz/2\bar{r}) \quad (5)$$

where w refers to displacement of the crack front along the normal direction, \bar{r} is the average radius of the crack, and b is a parameter whose value for visible surface crack tips in Al 7075-T6 is ~ 0.5. H is the Heaviside step function, and its presence signifies the possibility of part or all of the crack front being arrested by closure. Small cracks in Al alloys are also arrested temporarily by grain boundaries, but this effect is relatively weak in large-grained specimens and it has been ignored here. (Note, however, that grain boundary arrest is readily treated in the simulations, and it will be a principal subject of future studies.)

The simulation shown in Figure 4 exhibits some important general characteristics of small crack growth. When the crack is small relative to the microstructure (less than or equal to a few grains), the crack front can be highly irregular. Parts of it may be arrested by closure (or grain boundary blockage), and the aspect ratio, i.e., the ratio of the average depth to the surface

FATIGUE 87

length, fluctuates widely from crack to crack and as the crack grows.

Some statistics of the aspect ratio, defined to be $a/2c$, where $a = 2\sqrt{I_x}$ and $c = 2\sqrt{I_y}$, are shown in Figure 5 as functions of the average crack radius, defined as $\bar{r} = \sqrt{ac}$. Both experimental and theoretical data in Figure 5 were calculated from observations or simulations of many cracks: 16 experimental cracks and 100 simulations. The experimental data were obtained by splitting open specimens after various fatigue exposures and measuring the outline of the fatigue crack front. One striking feature of the experimental data is that many cracks show $a/2c > 0.5$ at $50 \mu\text{m} \leq \bar{r} \leq 100 \mu\text{m}$. This characteristic is reproduced in the simulation (continuous curves of Figure 5), and can be traced to the fact that the grains are highly nonequiaxed. Values of z tend to be much smaller for those segments of the crack front propagating down into the specimen, and Equation (5) then implies that $a/2c$ will be augmented. The agreement between the experimental data and the simulations, both in average and deviation, supports the hypothesis that the law of growth obtained from surface observations is also valid for segments of the crack growing down into the bulk.

When the crack spans more than a few grains, the relative strength of microstructural factors decreases, and in the simulations the crack front is restored to its smooth equilibrium configuration, with aspect ratio ~ 0.4 , by the variation of $K_I(\theta)$ according to Equations (1)-(4). For very small cracks, $a/2c$ is found experimentally to be ~ 0.2 . This was mimicked in the simulations by assuming that initiation (e.g., by fracture of stringers of particles or by persistent slip bands forming microcracks) generates relatively long, shallow cracks, about $90 \mu\text{m} \times 4 \mu\text{m}$. Such an assumption is, of course, testable by appropriate experiments. For the largest cracks, the experimental values of $a/2c$ in Figure 5 fall below 0.4 because the cracks were grown in bending.

OTHER STATISTICS OF THE SHAPE OF SMALL CRACKS

There are many other statistical properties of small cracks that can be conveniently studied by Monte Carlo simulations. These include: (1) the degree of irregularity of the crack front; (2) the covariance between the rates of advance of different segments of the crack front; (3) the persistence of fluctuations in the degree of irregularity or the aspect ratio; (4) the relationships between either the aspect ratio or the degree of irregularity and the rate of growth averaged around the crack front; and (5) the correlation between the visible surface crack velocity and the velocity of the invisible subsurface crack.

FATIGUE 87

CONCLUSIONS

Statistical data for small cracks can be directly related to the stochastic nature of the microstructure by appropriate laws of growth. Monte Carlo simulations present a powerful and flexible method of exploring this relationship.

Comparison of the simulations with experimental data allows existing laws of growth to be tested and optimized. This process both illuminates the physical mechanisms controlling growth, and forms the basis for accurate, calibrated models for predicting fatigue lifetime. The utility of the experimental data available for comparison with the simulations does not depend on being able to measure the actual pattern of grains through which each individual crack grows.

The simulations offer a powerful and convenient way of investigating whether the laws of growth for subsurface portions of a crack are the same as those deduced for growth of the visible surface crack tips. They give immediate insight into the question of whether fluctuations seen in the velocity of surface crack tips are generated by local surface phenomena or can be attributed to stochastic variations in the subsurface crack shape and growth rate.

Acknowledgements

The authors are grateful to D.C. Lim for her assistance with the computer programming. The research was sponsored by the Air Force Office of Scientific Research (AFSC) under Contract No. F49620-85-C-0034. The United States Government is authorized to reproduce or distribute reprints for governmental purposes notwithstanding any copyright notation hereon.

REFERENCES

1. Mastrojannis, E.N., Keer, L.M. and Mura, T., *Int. J. Fract.*, 15, 1979, pp. 247-58.
2. Newman, J.C., Jr and Raju, I.S., *Eng. Fract. Mech.* 15, 1981, pp. 185-92.
3. Newman, J.C., Jr. and Raju, I.S., NASA Technical Memorandum 85793, April 1984.
4. Zurek, A.K., James, M.R., and Morris, W.L., *"Met. Trans. A"* 14, 1983, pp. 1697-1705.

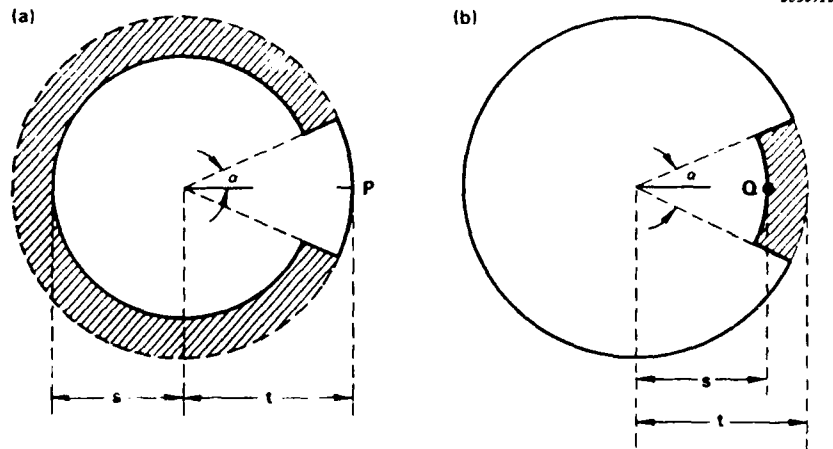


Figure 1. The geometries of (a) the protrusion and (b) the retarded segment used to estimate K_I at the extrema of an irregular plane embedded crack.

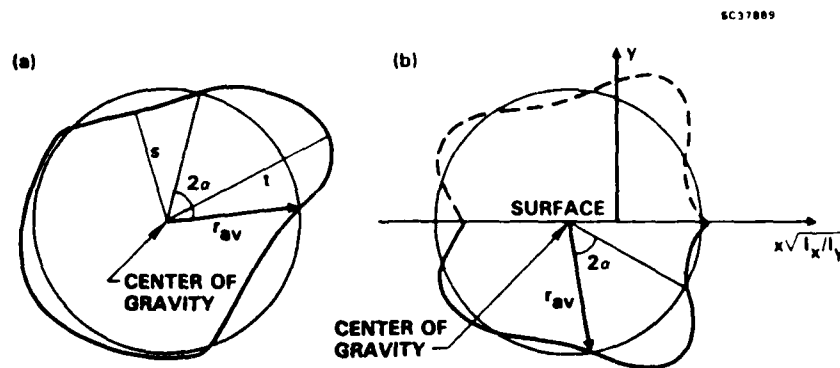


Figure 2. Illustrating the procedures used to define protrusions and retarded segments on an irregular crack for the purpose of invoking Equations (1)-(3).

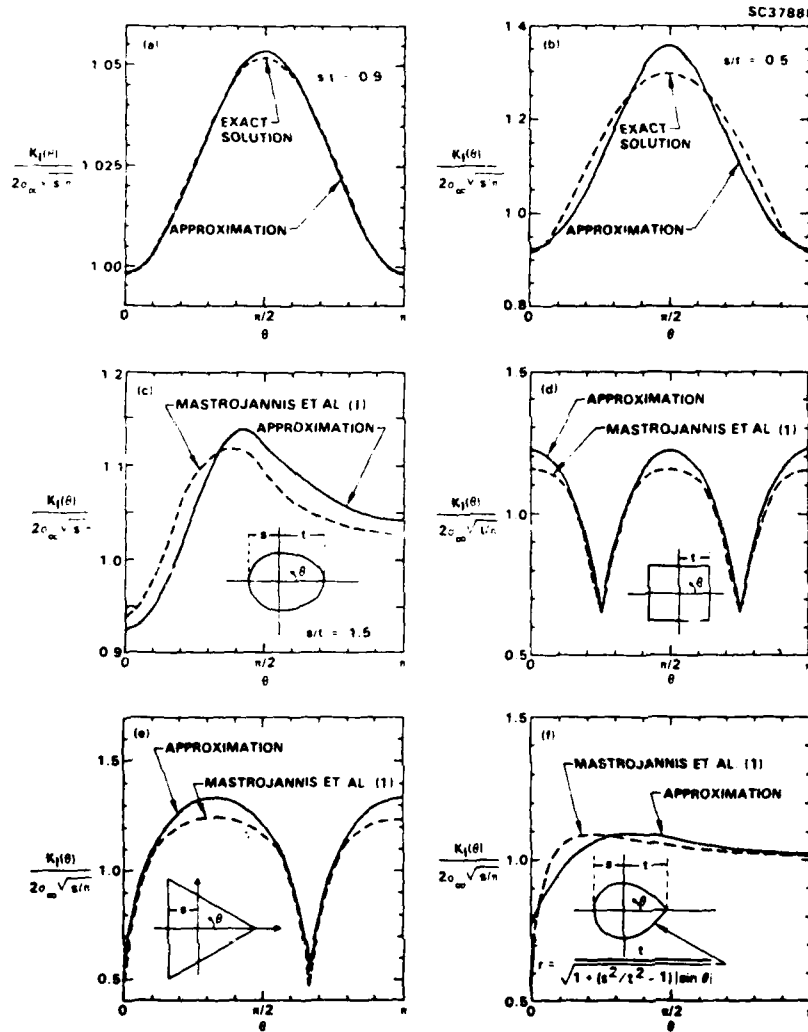


Figure 3. Testing the algorithm Equations (1)-(3) against known solutions for embedded irregular cracks. (a) and (b) are for ellipses with semi-axes as marked. The shapes of the cracks in (c)-(f) are shown in insets.

FATIGUE 87

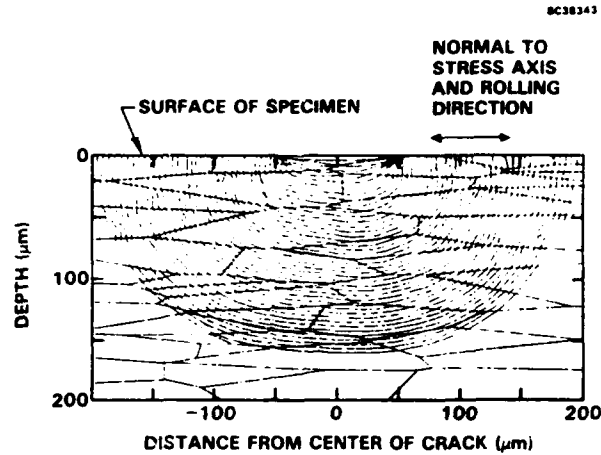


Figure 4. A simulation of the growth of a surface crack in AL 7075-T6. The position of the crack front is recorded at approximately equal intervals in crack size \sqrt{ac} , rather than in cycles.

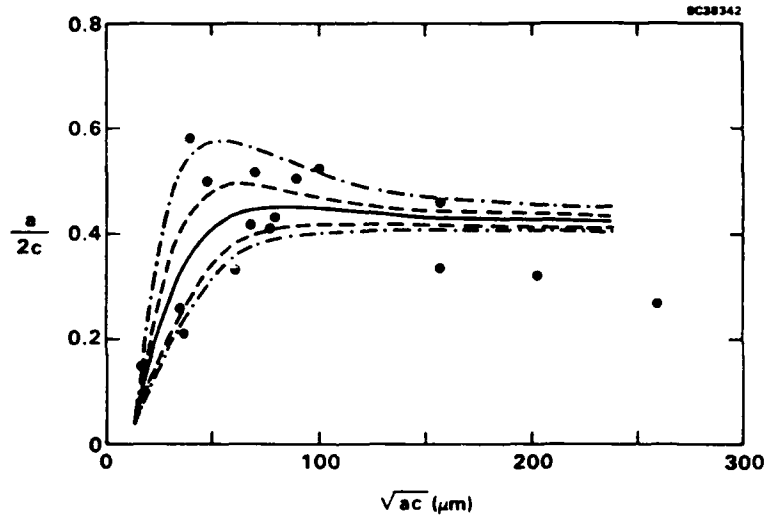


Figure 5. Aspect ratios of small cracks in Al 7075-T6 as a function of the crack size \sqrt{ac} . The data (circles) were taken at a stress amplitude of 408 MPa. The curves show the distribution of $a/2c$ found in simulations of 100 cracks. The solid curve shows the average of $a/2c$ in the simulations. The dashed curves should contain 70%, and the chain-dot curves 95%, of the data.

MONTE CARLO SIMULATIONS OF THE GROWTH OF SMALL FATIGUE CRACKS

B.N. Cox and W.L. Morris
Rockwell International Science Center
1049 Camino Dos Rios
Thousand Oaks, CA 91360

ABSTRACT

In this paper are presented Monte Carlo simulations of small, plane embedded or surface-breaking fatigue cracks propagating under Mode I cyclic loading through stochastic microstructures. Unlike most prior statistical models of surface-breaking fatigue cracks, which study only the behavior of the visible surface tips of the crack, the simulations calculate the advance of the entire crack front. The rate of growth of any segment of the crack front is determined by empirical or postulated laws that quantify the influence of its immediate microstructural environment. To make feasible the generation of many simulations at reasonable computational expense, approximate, simple algorithms have been derived for estimating the Mode I stress intensity factor around a plane, embedded or surface-breaking crack of any shape.

The computational procedures used to carry out the simulations are defined. The potential of the simulations for analyzing experimental measurements of fluctuations in crack shape and velocity is explored. The dependence on crack length and the variance of the aspect ratios of small surface-breaking cracks in Al 7075-T6 are accounted for successfully by the effects of microstructure-dependent plasticity-induced closure. Various other statistics of crack shape and velocity that can be predicted by the simulations and compared to experiment are considered. Laws describing the mechanics of crack growth both at and below the surface can be inferred from such comparisons.

1. INTRODUCTION

Over the last decade, it has become clear that small cracks are distinguished from large cracks by, among other things, the fact that they are small relative to the microstructure. This not only can destroy similitude with large cracks under the scaling relationship of linear elastic fracture mechanics (LEFM), but it can also make small cracks susceptible to extreme fluctuations in their growth rates. In many alloys, including aluminum alloys [1-3], large-grained nickel-based superalloys [4], steels [5-7], and titanium alloys [8], small cracks are temporarily arrested by grain boundaries. The duration of the arrest depends on stress level, crack length, and the size of the next grain [9]. Plastic strains induced ahead of the crack tip are usually much larger for small cracks than for large cracks at the same applied stress intensity factor [10]. When the crack is no larger than a few grains, the plastic zone is constrained by the nearest grain boundaries [11], causing closure stresses and backstresses to depend on grain size and the location of the crack front. Other factors determining the growth rate that involve the stochastic microstructure include roughness-induced closure, crack deflection, and variations in stress fields due to the anisotropy and random orientation of neighboring grains.

It follows from these considerations that the statistics of the growth rates of small fatigue cracks are intimately linked to those of the microstructure. In recognition of this, several probabilistic models of small fatigue crack growth have been formulated based on more or less explicit laws relating growth rates to microscopic variables [12-14]. However, these models have either been too simplistic for critical examination of the assumed role of the microstructure [15], or they have been restricted to modeling the statistics of only the visible, surface tips of surface-breaking cracks [12-14]. The validity of the latter models rests on the assumption that fluctuations in subsurface crack growth are either uncorrelated with or wholly determined by those observed on the surface. This thesis is probably valid whenever cracks span more than a few grains [16]. In such cases, fatigue lifetime prediction is greatly simplified, since surface observations alone, in conjunction with stress analysis accounting for the extrinsic effects of part shape and stress state, will provide sufficient basis for a probabilistic model. However, for cracks smaller than a few grains, the situation is generally more complicated. As might be expected from the strong influence of the stochastic microstructure, the shapes

of such small cracks are often highly irregular. Significant departures from semi-elliptical shapes and large variance in aspect ratios have been reported for small cracks in aluminum alloys [17,22], steels [18,19], nickel-based superalloys [20], and titanium alloys [8,21,22]. In such cases, it must be expected that the growth rates of surface tips and subsurface segments of the crack front are strongly but not necessarily perfectly correlated. Furthermore, the velocity of the surface crack tips will depend on generally unobserved fluctuations in the shape of the subsurface crack. To study the statistics of cracks in this regime, one must model the crack as a two-dimensional entity. By far the most convenient format for such work is Monte Carlo simulations, which are the subject of this paper.

As well as establishing the basis for accurate remaining lifetime predictions, the Monte Carlo simulations can also serve as a powerful tool for interpreting experimental measurements, especially of crack shape. Variations in crack shape are a direct reflection of the influence of the microstructure ~~in~~ crack growth. By comparing the statistics of crack shape predicted by simulations with those measured experimentally, the first direct evidence can be acquired for determining whether the subsurface crack front is governed by the same mechanisms as the surface crack tips. This question has been largely avoided in the past. In this paper, analysis of the statistics of the aspect ratios of small cracks in Al 7075-T6 will be used to provide just such information. on

2. STATE VARIABLES FOR THE SIMULATIONS

Several mechanisms related to microstructure can cause small crack propagation to depart from the predictions of LEFM or, in other words, destroy similitude with the propagation of large cracks when the growth rate is plotted as a function of the range ΔK of the applied stress intensity factor, K_I . The mechanisms include temporary arrest at grain boundaries, deceleration caused by back stress or fracture surface roughness, acceleration caused by enhanced local plasticity, and fluctuations in the local stress field caused by elastic inhomogeneity and anisotropy. In each case, the strength of the effect of these mechanisms depends on the size, orientation, and mechanical properties of the grains in the immediate vicinity of the crack front. This knowledge is based exclusively on observations of fluctuations in dc/dN for the visible surface tips of small

cracks, together with detailed records of the surface microstructure through which the crack tips are propagating. However, it is reasonable to begin by hypothesizing that the same or at least similar mechanisms are also affecting the propagation of subsurface segments of the crack front, with the pertinent microstructural factors being the size, orientation, and mechanical properties of invisible, subsurface grains. In that case, the microstructure-based modifications to the crack driving force will fluctuate around the crack front in concert with fluctuations in the microstructure. The stochastic microstructure will thus cause fluctuations in the local rate of advance of different segments of the crack front, and the crack front must become irregular. It is the purpose of the Monte Carlo simulations to quantify such irregularity, and relate it directly to laws of growth hypothesized or determined empirically to represent the effects of the microstructure.

In this first exposition of the Monte Carlo simulations, it will be assumed that the driving force acting at each point on the crack front can always be expressed in terms of a local effective Mode I stress intensity factor, K_I^{eff} , or its range, ΔK_I^{eff} , the applied cyclic stress amplitude, σ^a , the size and shape of the crack, and various parameters describing the immediate microstructural environment of the point. Since stress level and crack size may appear as independent variables, it is not necessary that similitude exist between small and large cracks under scaling at constant ΔK_I^{eff} . In other words, it is not assumed that there exists any definition of ΔK_I^{eff} that will lead to small and large crack data being correlated in some variant of LEFM. Nevertheless, it is convenient to express the laws of growth and especially the effects of irregular crack shape and some of the effects of stochastic microstructure in terms of the variable K_I .

The tendency of the stochastic microstructure to make the crack front irregular is balanced by the dependence of K_I on crack shape. For example, for an embedded irregular plane crack, K_I is generally reduced on protrusions and enhanced on retarded segments, so that, in the absence of microstructural fluctuations, the crack always tends to be circular. For a surface-breaking crack under mode I loading, the equilibrium shape is approximately a smooth semiellipse of aspect ratio 0.4.

The degree of irregularity expected for any small crack will therefore be determined by the relative strengths of the disordering microstructural effects and the

smoothing shape dependence of K_I . Since K_I can be calculated, the laws purporting to describe microstructural effects can be tested by measuring the degree of irregularity. Note that as the small crack grows into a large crack, the role of the microstructure diminishes, and the crack will generally be driven by K_I to be smooth.

3. APPROXIMATE, FAST ALGORITHM FOR K_I

The feasibility of the Monte Carlo simulations depends critically on being able to estimate K_I very quickly for plane cracks of arbitrary shape. Exact calculation of K_I would be prohibitively slow and, therefore, simple approximations to K_I have been derived.

The estimation of K_I is based on the assumption that K_I is determined solely by the external stress and the locus of the crack front. The possibility of generalizing the estimates to treat the effects on K_I of residual stresses, fracture surface roughness, or crack deflections is discussed in Section 7.

3.1 Approximation for K_I Around an Embedded Crack

The approximation for K_I around an embedded, plane crack is based on estimates $K_I^P(\alpha)$ of K_I at the zenith, P, of a protrusion, and $K_I^Q(\alpha)$ at the nadir, Q, of a retarded segment, where α is the half-angle subtended by either feature at the center of the crack. Both the protrusion and the retarded segment considered have the square-shouldered geometry shown in Fig. 1. The uniform applied tensile stress has the value σ_∞ .

3.1.1 $K_I^P(\alpha)$ at the Zenith of a Protrusion

$K_I^P(\alpha)$ was estimated by calculating the reduction from $K_I^t = 2\sigma_\infty\sqrt{t/\pi}$ for a circular crack of radius t generated by closing most of the crack down to radius s (see Fig. 1a). The normal surface tractions required to close the part of the crack shaded in that figure were approximated by the stress field that exists outside a loaded crack of radius s , given analytically by Sneddon [23]. The estimate of K_I^P is then obtained by integrating over the shaded area the product of Sneddon's stress field and the Green's function for the penny crack in a homogeneous, isotropic material obtained by Smith et al [24]. Thus,

$$K_I^P(\alpha) = 2\sigma_\infty \sqrt{t/\pi} - \int_{s/t}^1 \frac{4\sigma_z(r)}{(\pi t)^{3/2} \sqrt{1-\rho^2}} \left\{ \tan^{-1} \left[\frac{1+\rho}{1-\rho} \tan\left(\pi - \frac{\alpha}{2}\right) \right] - \tan^{-1} \left[\frac{1+\rho}{1-\rho} \tan \frac{\alpha}{2} \right] \right\} t^2 \rho d\rho, \quad (1)$$

where $\rho = s/t$ and

$$\sigma_z(r) = \frac{2\sigma_\infty}{\pi} \left[\sin^{-1} \frac{s}{t} - \frac{s}{\sqrt{r^2 - s^2}} \right]. \quad (2)$$

When $\alpha = 0$, this expression is exact. Equation (1) then yields zero for all values of s and t , since, when the crack is closed between s and t , there is no longer a singularity at $r = t$. When $\alpha > 0$, $\sigma_z(r)$ of Eq. (2) is in fact insufficient to close the crack at any point for which $r < t$. This can be seen by observing that, if the remanent crack opening displacement were exactly zero over some subspace of ($s < r < t$, $\alpha < \theta < 2\pi - \alpha$) (where θ is the angular variable defined in Fig. 1) and nonzero elsewhere, then some derivative of the nonnegative displacement field must have a discontinuity for $s < r < t$. This is impossible because all the derivatives of the field $\sigma_z(r)$ of Eq. (2) are continuous over $s < r < t$. Nevertheless, the results given below show that the displacement is probably small except near $\theta = \alpha$ (the edge of the protrusion), and therefore the approximation should be reasonable.

Normalized to $2\sigma_\infty \sqrt{t/\pi}$, K_I^P is independent of t . Because of the singularity in the integrand of Eq. (1) at $\rho = 1$, which arises from the Green's function, it is not an adequate approximation to replace $\sigma_z(r)$ of Eq. (2) by the asymptotic form $A(r-s)^{-1/2}$, even for $s \approx t$. The integral of Eq. (1) may be evaluated conveniently by cubic spline integration after removing the singularities at $\rho = s/t$ and $\rho = 1$ by the substitution $\sin^2 u = \frac{\rho - s/t}{1 - s/t}$.

$K_I^P(\alpha)/(2\sigma_\infty \sqrt{t/\pi})$ is shown in Fig. 2. It is significantly reduced from unity only at small α (tens of degrees), even when $s = 0$. Further calculations show that 80% of the reduction is generated by the surface forces applied within $\pi/3$ of the protrusion for

all values of s/t and $\alpha \leq \pi/2$. In other words, the protrusion is only weakly influenced by the more distant periphery of the crack.

Numerical calculations show that $K_I^P(\alpha)$ evaluated according to Eq. (1) is well approximated for $s/t > 0.5$ by

$$K_I^P(\alpha) \approx 2\sigma_\infty \sqrt{t/\pi} \cdot \frac{2}{\pi} \tan^{-1} \left[\frac{3 + s/t}{1 - s/t} \tan \frac{\alpha}{2} \right] \quad (3)$$

3.1.2 $K_I^Q(\alpha)$ at the Nadir of a Retarded Segment

A similar argument was used to estimate K_I^Q . The surface tractions required to close down the fracture surfaces of a loaded crack over the area shaded in Fig. 1b can be related by an integral equation [25] to the normal displacement of the original penny crack of radius t . If the required stress field is assumed to be independent of the polar angle θ , which is a fair approximation when evaluating $K_I^Q(\alpha)$ at the center of the retarded segment, then the integral equation is one-dimensional and easily solved numerically as follows.

The normal displacement along $\theta = 0$ of a penny crack of radius t subjected to surface tractions $\sigma_z(r)$ over $-\alpha \leq \theta \leq \alpha$ is given by

$$u(x) = \frac{4(1-\nu^2)}{\pi E} \int_x^t \frac{1}{c'^2 \sqrt{1-x^2/c'^2}} \int_0^{c'} \frac{\sigma_z(r) h(x/c', r/c', \alpha) r dr}{\sqrt{1-r^2/c'^2}} dc' \quad (4)$$

where ν is Poisson's ratio, E is Young's modulus, and

$$h(p, q, \alpha) \equiv \frac{1-p^2}{2\pi^2} \int_0^{2\pi} \frac{\tan^{-1} \left[\frac{1+q}{1-q} \tan \frac{\alpha-\theta}{2} \right] - \tan^{-1} \left[\frac{1+q}{1-q} \tan \frac{-\alpha-\theta}{2} \right]}{1-2p \cos(\theta-\alpha) + p^2} d\theta \quad (5)$$

The function h is readily computed, stored, and evaluated subsequently by interpolation, since $0 \leq h \leq 1$.

If $u(x)$ in Eq. (4) is made equal to the opening displacement of the original penny crack under load σ_∞ , i.e. [28],

$$u(x) = \frac{4(1-\nu^2)\sigma_\infty}{\pi E} \sqrt{t^2 - x^2}, \quad (6)$$

and one writes $\sigma_z(r) = \Sigma_z(r)/(r-s)^{1/2}$ to introduce explicitly the singularity at Q , then Eq. (4) becomes a straightforward integral equation in $\Sigma_z(r)$; and $K_I^Q(\alpha) = \Sigma_z(s) \cdot \sqrt{2\pi}$. The integral equation is solved by guessing $\Sigma_z(r)$, and iterating by some heuristic algorithm until self-consistency is achieved. Further numerical calculations then show that, to a good approximation for $s/t \geq 0.5$,

$$K_I^Q(\alpha) = 2\sigma_\infty \sqrt{s/\pi} / \left\{ \frac{2}{\pi} \tan^{-1} \left[\frac{3+s/t}{1-s/t} \tan \frac{\alpha}{2} \right] \right\}. \quad (7)$$

3.1.3 Embedded Plane Cracks of Arbitrary Profile

For stochastic crack fronts of arbitrary profile, the identification of the parameters s , t , and α used to calculate K_I^P and K_t^Q is subjective. The approach followed was to settle upon reasonable definitions of s and t for each feature on the crack front, and then introduce a single parameter α_0 related to α , which could be varied to optimize the estimated values of K_I for a nearly circular elliptical crack. This procedure was then tested by comparison with various known solutions.

The first task in analyzing a stochastic crack front (e.g., Fig. 3a) is to identify the major protruding and retarded features. These are defined as those extrema i, j, \dots for which $|r_i - r_{i+1}| > \gamma (r_{\max} - r_{\min})$, where r_i is the radius of the crack at the i^{th} extremum measured from the center of gravity of the crack, and r_{\max} and r_{\min} are the maximum and minimum of the set $\{r_i\}$. The factor γ is set arbitrarily to 0.7: its exact value has negligible effect on the outcome of the simulations. For each protrusion thus defined, t in Eq. (3) is identified with \bar{r} and s with r_i ; and, for each retarded feature, s in Eq. (7) is identified with \bar{r} and t with r_j , where \bar{r} is the average radius of the entire crack front. (Note that this convention is slightly different to that presented in a preliminary report of this work [26].)

The half-width α of each such protrusion or retarded segment is defined as half the angle between the points on either side of the extremum in question at which the radius of the crack is equal to its average radius (Fig. 3a). Of course, square-shouldered protrusions or retarded segments, such as those on which the estimates of K_I^P and K_I^Q were based, almost never occur in natural fatigue cracks, because K_I vanishes at the apex of a square feature that leads the crack front and diverges at such points that trail the crack front. Because of this and the approximations from which Eqs. (3) and (7) were derived, the term $\alpha/2$ therein was replaced by $\pi/2 \cdot \alpha/\alpha_0$, with the parameter α_0 evaluated by calibration against K_I for nearly circular elliptical cracks. With K_I^P and K_I^Q evaluated at successive extrema according to Eqs. (3) and (7), the value of K_I at any point in between is then simply written as

$$K_I(\theta) = [(r(\theta) - s)K_I^P + (t - r(\theta))K_I^Q]/(t - s) \quad , \quad (8)$$

where $r(\theta)$ is the radius of the crack at that point, and s and t are now the radii at the extrema, as shown in Fig. 3a.

The exact results for an elliptical crack [27] with $s \approx t$ can be fitted perfectly by Eq. (8) by adjusting α_0 . With this value of α_0 retained for all cases (viz., $\alpha_0 \approx 0.402$, found by fitting to K_I for an ellipse having $s/t = 0.99$), the agreement with other known solutions is as illustrated in Fig. 4. For all the cases shown, the approximation is always accurate to within a few percent. Of course, the near agreement at the sharp points of cases (c), (d), and (e) is fortuitous, since K_I should really vanish there, and both the approximation and the numerical results of Mastrojannis et al [28] are in error in this regard. However, this is an unimportant shortcoming, because extremely sharp features are not found in natural cracks.

Most importantly for the present application, the approximation gives fair estimates of both the dependence of K_I on α and its relative magnitudes at smooth extrema on the same crack. These are the properties essential to balancing the tendency of $K_I(\theta)$ to make a crack regular against the disruptive effects of the microstructure.

Note that K_I^Q is correctly predicted to diverge and K_I^P to vanish as $\alpha \rightarrow 0$. Because of the definition of s and t for the general crack, K_I for an embedded crack will always be enhanced on retarded segments and diminished on protrusions. Thus it is assumed that, in the absence of microstructural effects, an embedded circular crack is always stable with respect to small fluctuations in its shape. This is not the case for straight cracks [29].

3.2 K_I on Surface-Breaking Cracks

Convenient algorithms have been given by Newman and Raju for estimating K_I around semielliptical surface cracks in rectangular beams of width $2b$ and depth t under remote uniform tension σ_∞ and remote bending stress S_b [30,31,32]. If $2c$ is the crack's length on the surface and a its depth, then for $2c \geq a$,

$$K_I(\phi) = (\sigma_\infty + H_S S_b) \frac{\sqrt{\pi a}}{E(k)} F\left(\frac{a}{c}, \frac{a}{t}, \frac{c}{b}, \phi\right) \quad , \quad (9)$$

where E is the complete elliptic integral of the second kind; $k^2 = 1 - a^2/c^2$; F is a polynomial in a/c , c/a , a/t , and c/b , and a simple trigonometric function of ϕ , the parametric angle of the ellipse; and H_S , the bending multiplier, is a simple algebraic function of a/t , a/c , and $\sin\phi$.

To account for departures of the crack front from the semielliptical shape, Eq. (9) was combined with Eqs. (3), (7), and (8) by the following ansatz. The center of mass and the moments of inertia I_x and I_y of an irregular crack were found, and taken to define the center and semi-axes ($c = 2\sqrt{I_y}$ and $a = 2\sqrt{I_x}$) of a smoothing semielliptical crack. (I_x was calculated for the combination of the surface-breaking crack and its mirror image.) The x axis was rescaled by the factor a/c , so that the fitted semielliptical crack would become a semicircular crack, and the mirror image was added (Fig. 3b) to generate an entire irregular, approximately circular crack. Equation (8) was then used to generate values of $K_I(\theta)$ around this scaled crack, normalized to $K_I(a) = 2\sigma_\infty\sqrt{a/\pi}$. These normalized values of $K_I(\theta)$ represent the relative acceleration and retardation of local protrusions and retarded segments. These values were then

multiplied by the results of Eq. (9) for the semielliptical crack of semi-axes c and a , to account for gross surface, aspect ratio, and size effects.

The quality of the results generated by this procedure was then tested by comparison with the essentially exact numerical solutions of Gyekenyesi and Mendelson [33] for a rectangular surface crack in a finite rectangular slab. In Ref. 33, calculations were made for a crack embedded in a slab whose depth and width in the crack plane were as shown in the insets of Fig. 5, and whose length normal to the crack plane was also finite (3.38c), whereas Newman and Raju have supplied expressions (Eq.(9)) for bars of infinite length only. With the understanding that this might detract from the fairness of the test, the comparison of the results of Ref. 33 and the present approximate algorithm is presented in Fig. 5. Despite the fact that the rectangular surface crack is an extreme shape and therefore a severe test, the agreement is reasonable except for the case of very low aspect ratio ($a/2c = 0.15$), and even there the qualitative trends are faithfully reproduced. Considering that the present algorithm will always tend correctly to Newman and Raju's standard and well tried [34] expressions (Eq.(9)) as the crack shape tends to semielliptical, and that crack fronts generated in the simulations and found naturally are generally fairly smooth and not far from semielliptical, the approximate algorithm is adequate for the purpose at hand. Note, in contrast, that K_I for the fitted semi-ellipse using Eq. (9) alone (dotted curves in Fig. 5) fails completely to follow the correct variation around the crack front.

4. THE GENERATION OF RANDOM MICROSTRUCTURES

A single instance of a stochastic microstructure is generated as follows. Nucleation sites of a prescribed average density are placed on the plane of the crack in a Poisson process (i.e., with no correlation in their locations) by invoking a pseudo-random number generator. The grain boundaries are then determined by the Wigner-Seitz construction, which defines each grain as the area bounded by the perpendicular bisectors of the lines joining that grain's nucleation site to the nucleation sites of all its contiguous neighbors. The resulting cellular structure, an example of which is shown in Fig. 6, is a set of Voronoi, Dirichlet, or Wigner-Seitz polygons. All the polygons have straight edges, at least three neighbors, and are convex. The average grain size is established by the

prescribed density of nucleation sites. There is some correlation between the sizes of adjacent grains, with large (small) grains tending to have large (small) neighbors. This correlation is often expressed in terms of the number of sides of the polygons, but it also exists for their areas. The extensive literature on random Voronoi polygons may be conveniently entered through Refs. 35-37.

There are some characteristics of Voronoi polygons that are unrealistic in the context of metal or alloy microstructures. For example, there are numerous very small grains, which would probably be subsumed in an alloy by larger neighbors during annealing, and the straight-edged polygons are unnaturally smooth, since natural grain boundaries are generally faceted, curved, and otherwise irregular. However, the dependence of the laws of crack growth on local microstructure does not usually involve such geometrical details. The laws of growth refer perhaps to the average grain size in the vicinity of a segment of the crack front, or some crude measure of local slip distances. Therefore, Voronoi polygons are, to the best of current knowledge, quite acceptable for the Monte Carlo simulations. Note that nonequiaxed grain structures can be generated simply by rescaling one of the axes.

The procedure for executing the Wigner-Seitz construction was as follows. For a given nucleation site, i , the grain enclosing it was first supposed to be the entire, usually rectangular, area A within which crack growth was going to be simulated. For every other nucleation point, j , lying within a cutoff distance, d_c , of site i , the perpendicular bisector was formed, and the question asked whether it intersected the polygon currently recorded as surrounding site i . If so, the polygon was reduced to include the appropriate interval of the bisector as a new side. This was repeated for all sites j within d_c of site i , and then for all sites i . The area A must always be chosen large enough that an embedded crack never reaches the boundary region during a simulation, because this implementation of the Wigner-Seitz method is affected by the external boundaries of A : unusually large grains are formed there. When required, a free specimen surface was formed by deleting all grains and parts of grains lying beyond a line drawn across area A , just as though the specimen had been physically cut.

To enable convenient reference to the information contained in a given microstructure, a discrete square grid was defined on the plane of the crack. Each point on

this grid was then associated with the number of the grain containing it and with other measures of the local microstructure. For example, for modeling crack growth in Al alloys, an appropriate measure upon which plasticity-induced closure depends is the distance from the grid point to the next grain boundary measured along the line emanating from the center of the crack. Other characteristics, such as grain orientation, might be preferred for other materials.

5. INITIATION AND PROPAGATION OF A CRACK FRONT

The simulation of fatigue crack initiation can be treated according to various models. Depending on the known mode of initiation and the stage of crack growth under study, one might begin with a crack spanning several grains, or extending exactly to the boundaries of just one grain, or smaller than a single grain, or even vanishingly small. For crack fronts that are not assumed to coincide initially with a grain boundary, the aspect ratio and shape remain to be prescribed. For naturally initiated cracks, it is frequently the case that initiation occurs mainly in unusually large grains. The appropriate initiation model that takes all such factors into account must be chosen for each application of the Monte Carlo simulations.

A Monte Carlo simulation begins by generating a random, two-dimensional pattern of grains lying on the plane of growth, as described in the preceding section. The initial crack is introduced according to the initiation model. The crack front after N_1 cycles (beginning with $N_1 = 0$) is represented as a sequence of straight line segments meeting at the vertices $\{(x_j, y_j)\}$. The applied cyclic mode I stress intensity factor, $\Delta K_I^{(j)}$, corresponding to the prescribed external stress range, is calculated at each vertex j according to the algorithms derived in Section 3.3. The microstructural environment of the vertex j can be found immediately by identifying the element of the square grid (see Fig. 7) in which (x_j, y_j) lies, and referring to the corresponding elements in the stored tables of microstructural parameters for the current microstructure. For a continuously varying microstructural parameter such as the distance to the next grain boundary, it is necessary for preserving accuracy in the simulations to use linear interpolation amongst values stored on the square grid to obtain the value of (x_j, y_j) . $\Delta K_I^{(j)}$ (or $K_{min}^{(j)}$ and $K_{max}^{(j)}$) and the microstructural parameters for vertex j are then

supplied to a subroutine that invokes the prescribed laws of crack growth for the given simulation. The output of that subroutine is the velocity, v_j , of the crack front at the vertex j .

The crack front after N_{i+1} cycles is found by assuming that it advances in the direction of the normal to the front at every point. At each vertex, this direction is taken to bisect the angle between the two adjacent straight segments (Fig. 7). The distance over which vertex j advances is just $v_j(N_{i+1}-N_i)$. The step length $N_{i+1}-N_i$ is chosen to be small enough that the simulation is independent of it. This entire process amounts to first-order integration of a set of coupled differential equations governing the advance of the vertices of the crack front according to the prescribed laws of growth.

The number of vertices on the crack front is chosen initially to be large enough that each segment is small relative to the scale of the microstructure. This condition is maintained as the crack grows by adding a new vertex at the midpoint of any segment that exceeds some critical length.

Because cracks tend to grow faster as they get bigger, it is usually convenient to control the maximum or average of the distances of advance, d_j , during each increment of cycles, rather than choosing $N_{i+1}-N_i$ to be constant. In this way, the spacing between successive calculated crack fronts can be kept small relative to the microstructure.

5.1 Crack Growth in the Absence of Microstructural Effects

The propagation of surface cracks growing according to the Paris law

$$v_j = A(\Delta K^{(j)})^p \quad (10)$$

in the absence of any microstructural effect is illustrated in Fig. 8. Note that memory of the initial value of the aspect ratio disappears by the time the surface length of the crack has increased two- or three-fold, and that the equilibrium shape is approximately, but not exactly or necessarily, semi-elliptical. The velocities v_s of the surface tip and v_b of the bottom of a crack whose shape has reached equilibrium at an aspect ratio $a/2c$ are related by

$$v_b/v_s = a/c \quad . \quad (11)$$

When the velocities are governed locally by the Paris law, it follows that the equilibrium aspect ratio must depend on the parameter p in Eq. (10).

The variation of the aspect ratio with increasing crack size and the dependence of the equilibrium shape on the parameter p have been studied previously by Carter et al for large cracks [34], using Newman and Raju's expression, Eq. (9), for ΔK . Carter et al assumed that the crack always remains semi-elliptical with semi-axes c and a given by half the surface length and the depth. Invoking Eq. (9) for the values of c and a so given at any stage of the growth, they calculated the progression of the surface tips and deepest part of the crack only. In fact, their approach can be extended to all other points on the crack front, by applying Eq. (9) for the same c and a and all ϕ between 0 and π , without altering the results obtained at $\phi = 0$ and $\pi/2$. The crack front resulting in a semi-infinite solid from such a calculation is illustrated in Fig. 9a, where sufficient growth has occurred for the aspect ratio $a/2c$ to have reached equilibrium. The front is clearly not semi-elliptical: the surface tips have surged in advance of the rest of the crack, and the front is mildly reentrant near $\phi = 30^\circ$ and 150° . The dashed curves in Fig. 9 show semi-ellipses with semi-axes (c, a) and $(2\sqrt{I_y}, 2\sqrt{I_x})$.

Figure 9b shows a crack front that has reached equilibrium with each point on the crack front propagating according to the Paris Law and ΔK calculated according to the algorithm of Eqs. (3), (7), (8), and (9). The protrusions at the surface tips are now reduced relative to Fig. 9a, and the reentrant areas are much shallower, but the front still departs significantly from a semi-ellipse. l.c.

5.2 Crack Growth in the Presence of Microstructural Effects

If the laws of growth imply that certain segments of the crack are merely accelerated or retarded in growth, then the simulation proceeds just as in the absence of microstructural effects, except that the crack front may, of course, be irregular. On the other hand, if the laws of growth admit arrest of the crack, then part or all of the crack front may stop growing altogether, either temporarily or permanently. The state of

being arrested must then be continually monitored as an attribute of each vertex. If all vertices are arrested, then the subroutine containing the laws of growth is interrogated to determine whether the arrest is temporary or permanent, based on the existing microstructural environment of the crack front. If arrest is temporary, the record of elapsed cycles is modified and each vertex is freed to propagate as the laws of growth allow. If arrest is total and permanent, the simulation ceases.

When microstructure influences the growth, the crack front frequently develops small, local minima in the crack radius, illustrated schematically in Fig. 10a. The algorithm of Eqs. (3), (7), and (8) for estimating K_I generates large values at the nadir of such a narrow retarded segment, because K_I^Q (Eq. (8)) diverges as the half-angle α vanishes. This causes the prediction of an unusually large advance for that part of the crack front during a finite increment in elapsed cycles, leading to the false generation of a local protrusion (Fig. 10b). The protrusion in turn generates large values of K_I on either side of it, and a distortion of the crack front similar to the original locally retarded segment occurs on the subsequent iteration (Fig. 10c). This unphysical leap-frogging, which can propagate indefinitely if unattended, can be cut short by identifying the transition from Fig. 10a to Fig. 10b and resetting the crack front along the smoothing dashed line shown in the latter. Note that if there is a persistent microstructural reason for the local change in shape of the crack front, this will still occur over several or many increments of cycles.

When the effects of the microstructure are very strong, the crack front becomes highly irregular, and certain topological quirks can arise when calculating the new position of the front according to the algorithm illustrated in Fig. 7. For example, the crack front can form extraneous closed loops by crossing over itself, or spurs where it doubles back on itself. The former phenomenon must be excised from the crack front because it quickly leads to numerical explosions in the algorithm for advancing the front; and the latter because it is beyond the scope of the algorithms for estimating K_I . All such aberrations can be readily identified by demanding that the vertices on the front always progress clockwise (or anticlockwise) around the center of mass of the crack, and deleting any that do not.

6. STATISTICS OF THE SHAPE AND GROWTH RATE OF SMALL FATIGUE CRACKS

In this section will be presented a comparison of the measured and predicted statistics of the aspect ratios of small surface cracks in Al 7075-T6, and the definitions of other statistics of shape and growth rate for which experimental data do not yet exist, but could be readily obtained.

6.1 Statistics of the Aspect Ratio

A typical simulation of a surface crack is shown in Fig. 11. The grain structure there corresponds to that exposed on a plane cut normal to the rolling direction and normal to the surface of a rolled sheet of Al 7075-T6. The average grain length normal to the rolling direction is $\sim 120 \mu\text{m}$, and the average depth normal to the surface is $\sim 20 \mu\text{m}$. After a brief crystallographic phase immediately following initiation, small fatigue cracks in such specimens grow in a transgranular noncrystallographic mode. Plasticity-induced closure causes them to slow down upon reaching each grain boundary and accelerate as each grain is being traversed [3]. Because of these growth characteristics, at some stage the crack front coincides approximately with the boundary of the grain in which the crack initiated. In the absence of more complete information about initiation, the simulations were therefore begun by assuming that the crack front coincided with the boundary of whatever surface grain contained the origin. Observations on just the visible surface outlines of individual cracks in Al 7075-T6 have led to laws relating the rate of advance of each surface tip to its distance, z , from the next grain boundary. In the simulations shown here, the same law has been assumed to prevail all around the crack front, with z always measured along a line radiating from the original center of the crack. The law has the form

$$\frac{dw}{dN} = A\Delta K^2 (1-\beta z/2\bar{r})^2 H(1-\beta z/2\bar{r}) \quad , \quad (12)$$

where w refers to displacement of the crack front along the normal direction, \bar{r} is the average radius of the crack, and β is a parameter whose value for visible surface crack tips in Al 7075-T6 is ~ 0.5 . H is the Heaviside step function, and its presence signifies

the possibility of part or all of the crack front being arrested by closure. Small cracks in Al alloys are also arrested temporarily by grain boundaries, but this effect is relatively weak in large-grained specimens and it has been ignored here. (Note, however, that grain boundary arrest is readily treated in the simulations, and it will be a principal subject of future studies.)

The simulation shown in Fig. 11 exhibits some important general characteristics of small crack growth. When the crack is small relative to the microstructure (less than or equal to a few grains), the crack front can be highly irregular. Parts of it may be arrested by closure (or grain boundary blockage), and the aspect ratio, i.e., the ratio of the average depth to the surface length, fluctuates widely from crack to crack and as the crack grows.

Some statistics of the aspect ratio, defined to be $a/2c$, where $a = 2\sqrt{\overline{I}_x}$ and $c = 2\sqrt{\overline{I}_y}$, are shown in Fig. 12 as functions of the average crack radius, defined now as $\bar{r} = \sqrt{ac}$. The continuous curves in Fig. 12 show the history of the aspect ratio for 10 simulated cracks. The points show experimental data, which were obtained by splitting open specimens after various fatigue exposures and measuring the outline of the fatigue crack front. One striking feature of the experimental data is that many cracks show $a/2c > 0.5$ at $50 \mu\text{m} \leq \bar{r} \leq 100 \mu\text{m}$. This characteristic is reproduced in the simulations and can be traced to the fact that the grains are highly nonequiaxed. Values of z tend to be much smaller for those segments of the crack front propagating down into the specimen, which are therefore less retarded by plasticity-induced closure (see Eq. (12), and $a/2c$ is augmented. The agreement between the experimental data and the simulations, both in average and deviation, supports the hypothesis that the law of growth obtained from surface observations is also valid for segments of the crack growing down into the bulk. Note, however, that other laws of growth could be proposed that might also account for these limited data. To achieve the best test of postulated laws, it will always be desirable to have other kinds of data in conjunction with data on shape; for example, a history of the velocity of various segments of the crack front, rather than just the position of the front at one time. Such data could feasibly be acquired by measuring striations.

When the crack spans more than a few grains, the relative strength of microstructural factors decreases, and in the simulations the crack front is restored to its smooth equilibrium configuration, with aspect ratio ~ 0.4 , by the variation of $K_I(\theta)$ according to Eqs. (3), (7), (8), and (9). For very small cracks, $a/2c$ is found experimentally to be ~ 0.2 , which was reproduced in the simulations by virtue of the assumption that each crack began by spanning one grain and the fact that the grains are elongated. Such an assumption is, of course, testable by appropriate experiments.

When $\sqrt{ac} > 100 \mu\text{m}$, $a/2c$ is predicted in the simulations to decrease steadily. At first this reflects the lessening of the effects of plasticity-induced closure, which favored higher values of $a/2c$, but, for $\sqrt{ac} > 200 \mu\text{m}$, $a/2c$ decreases because the fatigue was performed in bending. This fact enters the simulation through the bending multiplier H_S in Raju and Newman's expression Eq. (9). However, the experimental data available for $\sqrt{ac} > 200 \mu\text{m}$ show $a/2c$ to be still less than in the simulations. There are various plausible explanations for this discrepancy. First, the experiments were done using tapered cantilever specimens $1500 \mu\text{m}$ thick and having one fixed end, whereas Eq. (9) refers to a rectangular beam in pure bending. This difference in geometry introduces uncertainty about the rate at which the crack will be slowed down as it grows down towards the neutral plane. Second, coalescence of surface cracks is observed occasionally in Al 7075-T6, which would also lead to unusually low values of $a/2c$. Third, there may well be a hidden source of inhomogeneity in the material varying on a characteristic spatial scale greater than the grain size. For example, fluctuations in hardness or texture in crystal orientation spanning several grains may exist, causing significant fluctuations in $a/2c$ to persist for cracks many times the grain size. More experimental data would be required to test this possibility.

It is noteworthy that the histories of $a/2c$ generated by the Monte Carlo simulations depend on the parameter α_0 used in the algorithm for K_I (Eqs. (3) and (7)) only weakly for individual simulations and negligibly when averaged over many simulations. On the other hand, they depend strongly on the parameter β appearing in the closure law Eq. (12), $a/2c$ showing increasing scatter and achieving higher values for $\sqrt{ac} \approx 100 \mu\text{m}$ as β increases. Thus the statistics of shape are not vitiated by the quality of the approximation to K_I . They are influenced primarily by the geometrical

description of the stochastic microstructure as it influences the crack front through the law of growth. The best agreement with the experimental data of Fig. 12 was found by eye to be for $\beta = 0.7 \pm 0.1$. It is not surprising that this value of β should depart slightly from that determined originally by studying surface crack tips alone [3], since the present simulations account more completely for variations in the stress intensity factor and crack shape effects.

6.2 Other Statistics of the Shape and Growth of Small Cracks

There are many other statistical properties of small cracks that can be conveniently studied by Monte Carlo simulations. These include: (1) the degree of irregularity of the crack front; (2) the covariance between the rates of advance of different segments of the crack front; (3) the persistence of fluctuations in the degree of irregularity or the aspect ratio; and (4) the relationships between either the aspect ratio or the degree of irregularity and the rate of growth averaged around the crack front.

Irregularity may be defined in various ways, and the appropriate definition may depend on the physical mechanisms that generate it. One simple definition is

$$X^2 = \int (1-r(\theta)/\rho(\theta))^2 d\theta / \int d\theta \quad , \quad (13)$$

where $r(\theta)$ is the radial distance from the center of gravity of the crack to the crack front at angle θ , and $\rho(\theta)$ is the equivalent distance for the elliptical crack of semi-axes $c = 2\sqrt{I_y}$ and $a = 2\sqrt{I_x}$. The function X^2 measures the relative departure of the crack from the ellipse of best fit, averaged around the crack front. X^2 is generally expected to be largest for small cracks and become smaller as the cracks grow. This trend is illustrated in Fig. 13 for the same simulations for which $a/2c$ was presented in Fig. 12. The magnitude and rate of decay of X^2 , and the covariance between values of X^2 at different times for the same crack, are direct indicators of the strength of the stochastic microstructural factors that tend to disrupt crack growth.

The covariance between the rates of advance of different segments of the crack front (at angles θ and θ') may be defined by

$$\rho_v(\theta, \theta', \bar{r}) = \frac{E\{(v(\theta, \bar{r}) - \bar{v}(\bar{r}))(v(\theta', \bar{r}) - \bar{v}(\bar{r}))\}}{\sqrt{E\{(v(\theta, \bar{r}) - \bar{v}(\bar{r}))^2\} E\{(v(\theta', \bar{r}) - \bar{v}(\bar{r}))^2\}}} \quad (14)$$

where E denotes the expectation value for an ensemble of many cracks, and $v(\bar{r}) = E\{v(\bar{r})\}$, where $v(\bar{r})$ is the rate of growth of a crack of size $\bar{r} \equiv \sqrt{ac}$ averaged around its front. ρ_v is very important to the estimation of remaining fatigue lifetime when experimental observations are limited. For example, NDE of surface cracks generally returns no more information than the visible surface crack length, and perhaps some gross estimate, by acoustic or eddy current measurements, of the size of the invisible subsurface crack. In the small crack regime, it is then critical to know with what certainty the rate of growth of the subsurface crack can be inferred from the rate of growth of the visible crack. The covariance, $\rho_v(\theta, 0)$, obtained from the Monte Carlo simulations using models tested and calibrated by comparing that and other statistics with destructively inspected cracks, provides the answer. Note that a transition in $\rho_v(\theta, 0)$ is expected as the crack grows out of the small crack regime. The surface velocity of small cracks will be relatively strongly correlated with the velocity of subsurface segments, because the same microstructural factors may often be affecting both. For larger cracks, the microstructural environment of the surface tips is unrelated to the subsurface microstructure, and $\rho_v(\theta, 0)$ will ultimately vanish for $\theta \neq 0$.

The persistence of fluctuations in shape can be quantified by the covariance ρ_x of values of X^2 determined at different times for the same crack:

$$\rho_x(\bar{r}_1, \bar{r}_2) = \frac{E\{(X^2(\bar{r}_1) - E(X^2(\bar{r}_1)))(X^2(\bar{r}_2) - E(X^2(\bar{r}_2)))\}}{\sqrt{E\{(X^2(\bar{r}_1) - E(X^2(\bar{r}_1)))^2\} E\{(X^2(\bar{r}_2) - E(X^2(\bar{r}_2)))^2\}}} \quad (15)$$

$\rho_x(\bar{r}_1, \bar{r}_2)$ will generally decay as $\exp[-(\bar{r}_2 - \bar{r}_1)/\lambda]$, and the half-life λ , itself a function of \bar{r}_1 , is a useful measure of both the spatial wavelength of the underlying microstructural disorder and the range of influence of one part of the crack upon another.

One would generally expect the growth rate averaged around the crack front to be strongly correlated with the degree of irregularity. For example, if the role of the

microstructure is to retard the crack front locally where it lies in large grains, then a highly irregular crack in which the crack is retarded at several places would usually be propagating slower than a smoother crack front of which no segment is severely retarded. Or, conversely, if the role of the microstructure is to cause local acceleration of the front, then the more irregular cracks might be expected to be propagating faster than the average. In either case, comparison of such correlations predicted by simulations with those found by experimental (destructive) measurements of crack shape and velocity would serve as a further direct test of postulated laws of growth. For similar reasons, the average velocity and the aspect ratio can be expected to be correlated. This correlation could be especially useful for predicting remaining lifetime based on NDE measurements, since representative aspect ratios can be measured even for irregular cracks by acoustic methods.

7. SOME FEASIBLE GENERALIZATIONS AND KNOWN LIMITATIONS

The basis of the feasibility of the Monte Carlo simulations is the approximate algorithm for estimating K_I for a plane crack of arbitrary shape. In devising and applying this algorithm, it has been assumed that K_I depends only on the magnitude of the external stress and the locus of the crack front. In some cases, the effective stress intensity factor K_I^{eff} acting at each point on the crack front may be modified by further geometrical or material considerations. For example, the minimum value K_I^{min} of K_I^{eff} in any cycle can be increased locally by fracture surface roughness or debris propping open the crack front. In such a case, the required modification would pose an additional calculation, beyond the application of the algorithm developed in Section 3. For cracks propped open by the contact of point asperities, the additional variation in K_I^{eff} could be estimated using the Green's function for a penny crack with point loading on the fracture surfaces [38]. Similar estimates could be made of the effect on K_I^{eff} of closure pressure generated by residual stresses that vary from grain to grain, perhaps invoking approximations based on analytical expressions for K_I for elliptical cracks under arbitrary loading [38]. The variation in K_I caused by stochastic out-of-plane deflections of the crack front might be estimated from other pertinent calculations in the literature [39-42].

The algorithm for estimating the dependence of K_I on crack shape was derived from consideration of cases of uniform mode I loading. To deal with nonuniform loading, the shape dependence was combined in an ad hoc way with the canonical results of Raju and Newman [27,35,36] for surface-breaking semielliptical cracks in finite beams. Since Raju and Newman's expression extends to remote bending as well as uniform loading, the net algorithm ostensibly shares the same generality. However, it is probably unsound to assume that the shape dependence of K_I is still well represented when the crack reaches or crosses the neutral plane. When the crack has penetrated the neutral plane, part of it is in compression, and it would then no longer be necessarily true that protrusions would be marked by relatively low values of K_I and retarded segments by relatively large values. In the simulations and experiments reported in Section 6, the cracks never penetrated more than 20% of the way through the specimen, so that loading was never far from uniform, and the application of the algorithm ought to have been valid.

The treatment of spectrum loading in Monte Carlo simulations is very straightforward. There is no restriction on how the load might be varied as the crack grows, and it is in principle simple to intersperse periods of uniform or bounded random loading with spike overloads. For small cracks, load history effects and the response to overloads are very likely dependent on the local microstructure, which would create another mechanism by which stochastic microstructure could cause a crack to be irregular. As for other such relationships, measurements of crack shape following overloads, when analyzed by Monte Carlo simulations, would elucidate the mechanics of retardation.

Although the Monte Carlo simulations have been presented in the context of fatigue crack growth in alloys, a very similar approach is clearly applicable to stable growth under monotonic loading. For example, in granular ceramic materials, monotonic strength is often determined by the limits of stable growth of cracks that are small relative to the microstructure, experience large, stochastic variations in the net driving force acting around the crack front, and therefore grow with irregular shapes. Relatively slight modifications to the Monte Carlo code would be required to model such growth, and the mechanics of growth could be examined by analyzing the statistics of crack shape in ways analogous to those proposed here for fatigue cracks in metals.

The Monte Carlo simulations are very flexible and well divided into self-contained computational units. With minimal programming effort, it is straightforward to change the method of generating random microstructures, and this may be done with no effect on the code for crack propagation. The laws of growth can be substituted freely, and the incorporation of intermittent arrest of part or all of the front by closure or grain boundary blockage, while not reported in detail here, has already been effected. With modest, feasible embellishments, crack coalescence and growth by the formation of microcracks ahead of the crack front could also be simulated.

On the other hand, the Monte Carlo simulations are too computationally demanding to serve themselves as predictive models for remaining fatigue lifetime in engineering practice. They are inefficient for calculating remaining lifetimes conditioned on some measurement, especially if the result of the measurement is a rare event, such as the observation of an unusually large or fast-growing crack. For such applications, probabilistic models that regain computational efficiency by appropriate, physically-based simplifications would be superior [14]. The Monte Carlo simulations provide an excellent test of the validity of the various simplifying assumptions made in such models.

8. CONCLUSIONS

This paper has presented realistic Monte Carlo simulations of small fatigue cracks propagating through stochastic microstructures. The simulations are made feasible by simple algorithms for estimating the Mode I stress intensity factor K_I around an embedded or surface-breaking plane crack of any shape. By varying a single parameter (α_0), the algorithms are able to reproduce acceptably well certain known solutions for K_I for cracks of various shapes. The estimates of K_I are based on dividing an irregular crack front into a sequence of protruding and retarded segments. The algorithms embody credible representations of the dependence of K_I on the magnitude of such a feature and the half-angle it subtends.

The propagation of any segment of the crack front is governed by empirical or theoretically postulated laws of growth describing the influence of its immediate micro-

structural environment. The propagation of the entire crack front is then represented by a system of coupled differential equations, one for each vertex on a finite mesh. It has been demonstrated that first-order solution of this system of equations is sufficiently accurate and fast to enable the accumulation of statistics from hundreds of simulations at minimal cost.

The simulations have two important roles to fulfil. First, they are a potentially powerful tool for analyzing statistical short crack data, especially when the data include information about crack shape. This potential has been illustrated by an analysis of the aspect ratios of small fatigue cracks propagating in Al 7075-T6 under uniform cyclic loading. Such analysis provides the first direct means of establishing whether the mechanics of growth for subsurface segments of the crack front are identical, similar, or entirely different to those identified by observations of the surface crack tips alone. The analysis for Al 7075-T6 demonstrated that such data can be used to test the validity of putative laws describing microstructural effects in crack growth, since the statistics of the crack shape are quite sensitive to both the forms of such laws and the parameters they comprise.

The second role of the simulations is to develop bases for probabilistic models of small fatigue crack growth and remaining lifetime prediction. The simulations allow important statistics of short crack growth, such as the covariance between surface and subsurface velocities of a crack front, and spatial correlation lengths for fluctuations in growth rates, to be attributed directly to the effects of stochastic microstructure. That this is a valid depiction of the source of variance in growth rates may then be tested directly by comparing the predicted statistics of crack growth (e.g., crack shape and correlation lengths) with those found experimentally. The simulations then allow the generation of physically-based and therefore more accurate models of crack propagation, permitting, for example, accurate calculation of the possibly nonconservative effects of fluctuations in aspect ratio.

ACKNOWLEDGMENT

Research sponsored by the Air Force Office of Scientific Research (AFSC) under Contract No. F49620-85-C-0034. The United States Government is authorized to

reproduce or distribute reprints for governmental purpose notwithstanding any copyright notation hereon.

9. REFERENCES

- [1] W.L. Morris, M.R. James, and O. Buck, "Growth Rate Models for Short Surface Cracks in Al 2219-T851," Met. Trans. A 12A, 57-64 (1981).
- [2] J. Lankford, "The Growth of Small Fatigue Cracks in 7075-T6 Aluminum," Fatig. Engng. Mater. Struct. 5, 233-248 (1982).
- [3] A.K. Zurek, M.R. James, and W.L. Morris, "The Effect of Grain Size on Fatigue Growth of Short Cracks," Met. Trans. A 14A, 1697-1705 (1983).
- [4] W.J. Pardee (ed.), "Quantitative Nondestructive Evaluation (NDE) for Retirement-for-Cause," Final Report on DARPA Contract No. MDA903-80-C-0641, Rockwell International Science Center (1984).
- [5] J. Lankford, "Initiation and Early Growth of Fatigue Cracks in High Strength Steel," Engng. Fract. Mech. 9, 617-24 (1977).
- [6] K.J. Miller, H.J. Mohamed, M.W. Brown, and E.R. de los Rios, "Barriers to Short Fatigue Crack Propagation at Low Stress Amplitudes in a Banded Ferrite-Pearlite Structure," in Small Fatigue Cracks, ed. R.O. Ritchie and J. Lankford, Proc. 2nd Engng. Found. Workshop, Santa Barbara, CA, January, 1986, pp. 639-56.
- [7] E.R. de los Rios, Z. Tang, and K.J. Miller, "Short Crack Behaviour in Medium Carbon Steel," Fatigue Engng. Mater. and Struct. 7, 97-108 (1984).
- [8] L. Wagner, J.K. Gregory, A. Gysler, and G. Lütjering, "Propagation Behaviour of Short Cracks in a Ti-8.6 Al Alloy," in Small Fatigue Cracks, ed. R.O. Ritchie and J. Lankford, Proc. 2nd Engng. Found. Workshop, Santa Barbara, CA, January, 1986, pp. 117-28.
- [9] W.L. Morris, "The Noncontinuum Crack Tip Deformation Behaviour of Surface Microcracks," Met. Trans. A11, 1117-23 (1980).
- [10] K.S. Chan, J. Lankford, and D.L. Davidson, "A Comparison of Crack-Tip Field Parameters for Large and Small Fatigue Cracks," J. Engng. Mater. and Technol. 108, 206-13 (1986).

- [11] W.L. Morris, M.R. James, and A.K. Zurek, "The Extent of Crack Tip Plasticity for Short Fatigue Cracks," *Scripta Metallurgica* 19, 149-53 (1985).
- [12] W.L. Morris, M.R. James, and O. Buck, "Computer Simulation of Fatigue Crack Initiation," *Engng. Fract. Mech.* 13, 213-21 (1980).
- [13] B.N. Cox, W.J. Pardee, and W.L. Morris, "A Statistical Model of Intermittent Short Fatigue Crack Growth," to be published in *Fatigue Fract. Engng. Mater. Struct.*
- [14] B.N. Cox and W.L. Morris, "A Probabilistic Model of Short Fatigue Crack Growth," ~~submitted to~~ *Fatigue Fract. Engng. Mater. Struct.*, *in press*.
- [15] H. Ghonem and J.W. Provan, "Micromechanics Theory of Fatigue Crack Initiation and Propagation," *Engng. Fract. Mech.* 13, 963-77 (1980).
- [16] B.N. Cox and W.L. Morris, "Model-Based Statistical Analysis of Short Fatigue Crack Growth in Ti 6Al-2Sn-4Zr-6Mo," ~~submitted to~~ *Fatigue Fract. Engng. Mater. Struct.*, *in press*.
- [17] A. LeFrancois, P. Clement, and A. Pineau, "The Growth of Short Fatigue Cracks in an Aluminum Alloy in Relation with Crack Closure Effect," in *Proc. Internat. Conf. on Fatigue of Engng. Struct. and Mater.*, Sheffield, England, 15-19 September, 1985.
- [18] P. Clement, J.P. Angeli, and A. Pineau, "Short Crack Behaviour in Nodular Cast Iron," *Fatigue Engng. Mater. Struct.* 7, 251-65 (1984).
- [19] K. Tokaji, T. Ogawa, Y. Harada, and Z. Ando, "Limitations of Linear Elastic Fracture Mechanics in Respect of Small Fatigue Cracks and Microstructure," *Fatigue Fract. Engng. Mater. Struct.* 9, 1-14 (1986).
- [20] T.A. Beer, "Crack Shapes During Biaxial Fatigue," Report No. 106, Materials Engineering-Mechanical Behaviour, College of Engineering, University of Illinois at Urbana-Champaign (1984).
- [21] L. Wagner and G. Lütjering, "Microstructural Influence on Propagation Behaviour of Short Cracks in an ($\alpha + \beta$) Ti alloy," *Z. Metallkde.* 78 (1987).
- [22] R.K. Bolingbroke and J.E. King, "The Effect of Microstructure on the Surface Crack Length: Crack Depth Relationship for Short Cracks," in *Fatigue '87, Proc. 3rd Int. Conf. on Fatigue and Fatigue Thresholds*, Charlottesville, VA, 1987.

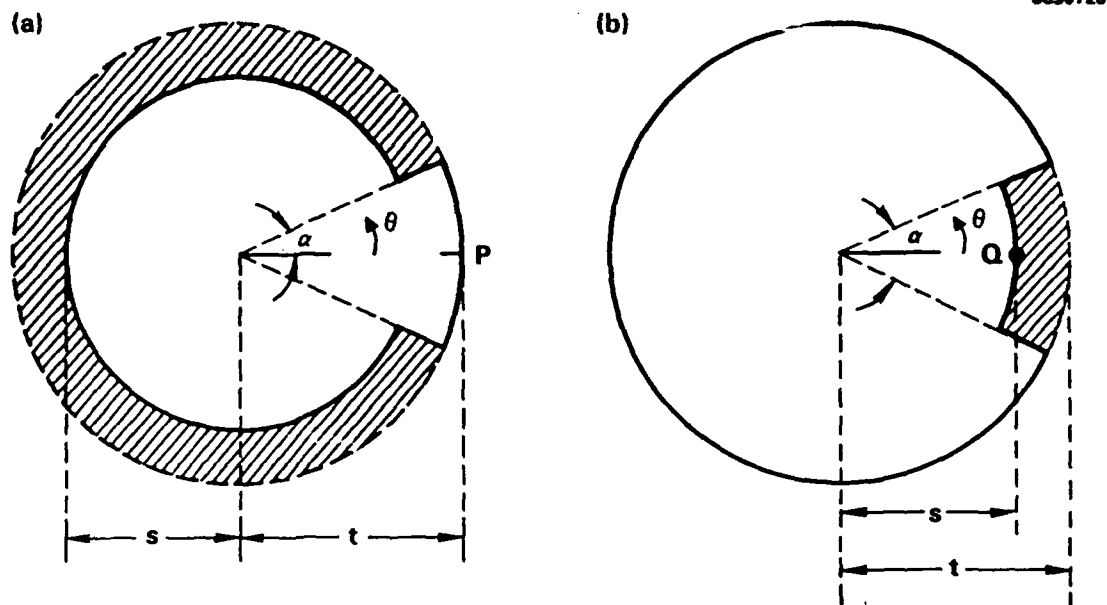
- [23] I.N. Sneddon, "The Distribution of Stress in the Neighborhood of a Crack in an Elastic Solid," Proc. Roy. Soc., Series A 187, 229-60 (1946).
- [24] F.W. Smith, A.S. Kobayashi and A.F. Emery, "Stress Intensity Factors for Penny-Shaped Cracks. Part I - Infinite Solid," J. Appl. Mech. 34, 947-52 (1967).
- [25] I.N. Sneddon and M. Lowengrub, "Crack Problems in the Classical Theory of Elasticity" (Wiley, NY), 1969.
- [26] B.N. Cox and W.L. Morris, "The Statistics of the Shape of Small Fatigue Cracks," in Fatigue '87, Proc. 3rd Int. Conf. on Fatigue and Fatigue Thresholds, Charlottesville, VA, June, 1987.
- [27] M.K. Kassir and G.C. Sih, "Three-Dimensional Stress Distribution Around an Elliptical Crack Under Arbitrary Loading," J. Appl. Mech. 33, 601-11 (1966).
- [28] E.M. Mastrojannis, L.M. Keer and T. Mura, "Stress Intensity Factor for a Plane Crack Under Normal Pressure," Int. J. Fract. 15, 247-58 (1979).
- [29] J.R. Rice, "First-Order Variation in Elastic Fields Due to Variation in Location of a Planar Crack Front," J. Appl. Mech. 52, 571-9 (1985).
- [30] I.S. Raju and J.C. Newman, Jr., "Stress-Intensity Factors for a Wide Range of Semi-Elliptical Surface Cracks in Finite-Thickness Plates," Engng. Fract. Mech. 11, 817-29 (1979).
- [31] J.C. Newman, Jr. and I.S. Raju, "An Empirical Stress-Intensity Factor Equation for the Surface Crack," Eng. Fract. Mech. 15, 185-92 (1981).
- [32] J.C. Newman, Jr. and I.S. Raju, "Stress-Intensity Factor Equations for Cracks in Three-Dimensional Finite Bodies Subjected to Tension and Bending Loads," NASA Technical Memo. 85793, April 1984.
- [33] J.P. Gyekenyesi and A. Mendelson, "Stress Analysis and Stress-Intensity Factors for Finite Geometry Solids Containing Rectangular Surface Cracks," J. Appl. Mech. 44, 442-8 (1977).
- [34] D.K. Carter, W.R. Canda, and J.R. Blind, "Surface Flaw Crack Growth in Plates of Finite Thickness," AFWAL-TR-86-4034, January, 1987.
- [35] B.N. Boots, "The Arrangement of Cells in 'Random' Networks," Metallography 15, 53-62 (1982).
- [36] D. Weaire and N. Rivier, "Soap, Cells, and Statistics - Random Patterns in Two Dimensions," Contemp. Physics 25, 59-99 (1984).

- [37] D.A. Aboav, "The Arrangement of Cells in a Net. IV," *Metallography* 18, 129-47 (1985).
- [38] M.K. Kassir and G.C. Sih, "Three Dimensional Crack Problems," in *Mechanics of Fracture*, Vol. II, ed. G.C. Sih, Noordhoff, Holland (1975).
- [39] B. Cotterell and J.R. Rice, "Slightly Curved or Kinked Cracks," *Int. J. Fract.* 16, 155-69 (1980).
- [40] S. Suresh, "Crack Deflection: Implications for the Growth of Long and Short Fatigue Cracks," *Metall. Trans. A.* 14, 237-85 (1983).
- [41] K.T. Faber and A.G. Evans, "Crack Deflection Processes - I. Theory," *Acta Metall.* 31, 565-76 (1983).

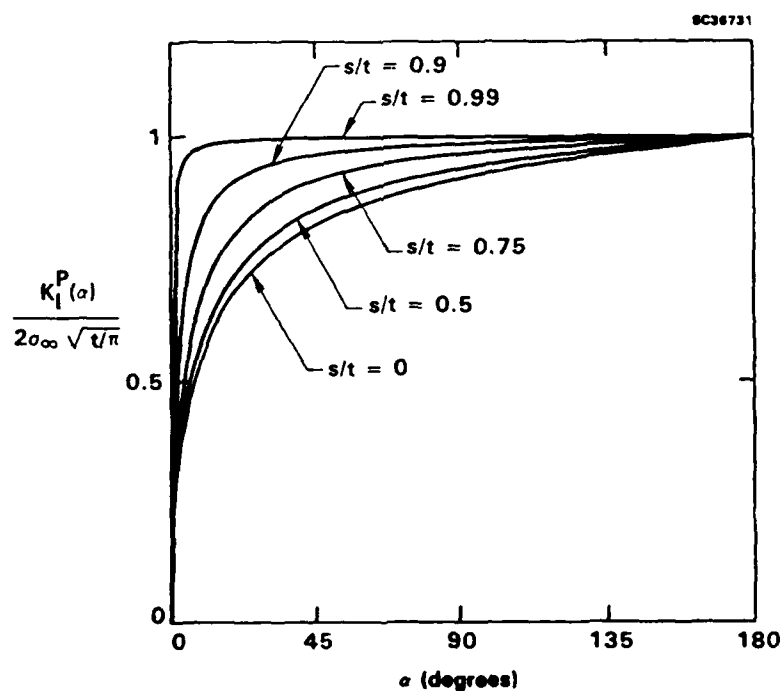
Figure Captions

1. The geometries of (a) the protrusion and (b) the retarded segment used to estimate K_{Ip} at the extrema of an irregular plane embedded crack.
2. $K_{Ip}(\alpha)$ normalized with respect to K_I for a penny crack of radius s , as a function of s/t .
3. Illustrating the procedures used to define protrusions and retarded segments on an irregular crack for the purpose of invoking Eqs. (3), (7), and (8).
4. Testing the algorithm of Eqs. (3), (7), and (8) for embedded cracks against known solutions for embedded irregular cracks: (a) is for an ellipse with semi-axes as marked; the shapes of the cracks in (b)-(e) are shown as insets. The results of Mastrojannis et al were taken from Ref. 28.
5. Testing the algorithm of Eqs. (3), (7), (8), and (9) for surface cracks against the calculations of Gyekenyesi and Mendelson [33] for rectangular cracks in finite rectangular bars. The insets show the dimensions of the cases considered. All values of K_I are normalized to \sqrt{c} , where $2c$ is the surface crack length. The curve marked 'fitted semiellipse' (dotted line) in each case shows the results of Eq. (9) for a semielliptical crack having the same moments of inertia as the rectangular crack.
6. A typical random microstructure consisting of Voronoi polygons.
7. Illustrating the algorithm for advancing the crack front. The square grid marks the discrete elements within each of which the microstructural parameters (e.g., size of the grain containing the element, or the distance of the element from the next grain boundary) are taken to be constant.
8. Propagation of surface cracks according to the Paris law in the absence of microstructural effects starting from a crack of aspect ratio (a) 0.25 and (b) 0.08. The parameter p in Eq. (10) has been assigned the value 2.
9. The equilibrium shapes of cracks propagating according to the Paris Law when (a) K_I is set at each point to the value calculated for a semiellipse whose semi-axes are calculated from the second moment of the crack; and (b) K_I is evaluated according to the algorithm of Eqs. (3), (7), (8), and (9).

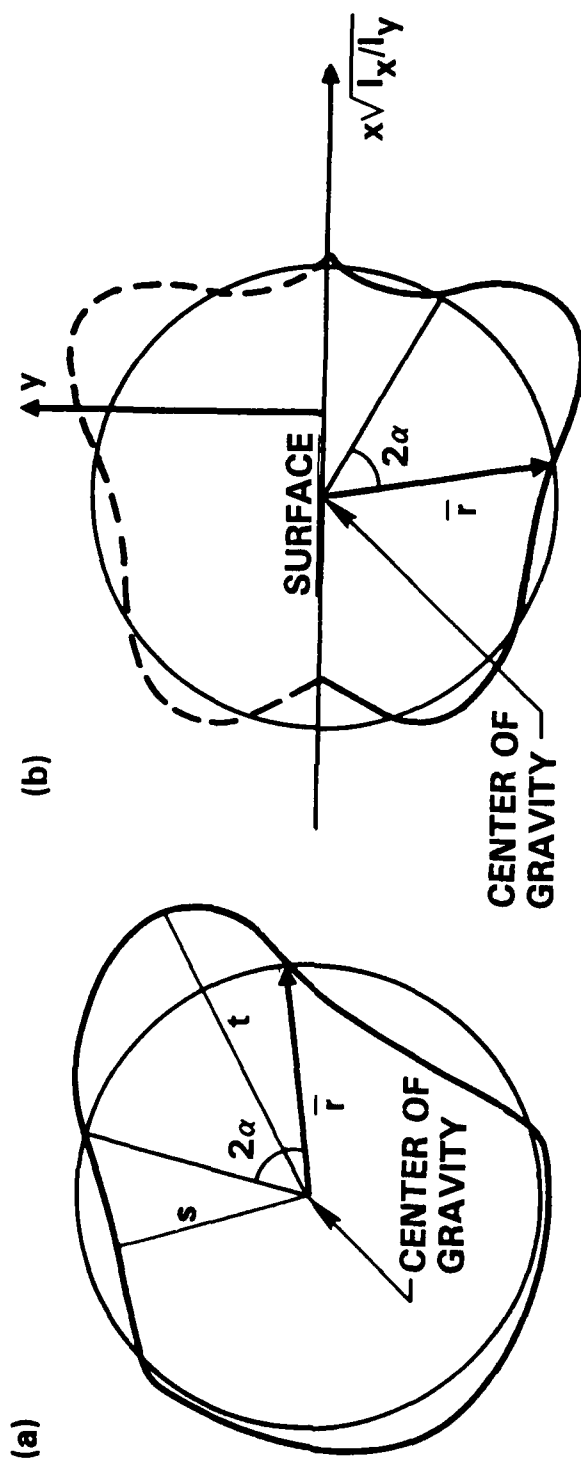
10. Leap-frogging caused by a local minimum in the crack radius. (a), (b), and (c) show the same portion of a crack front at successive discrete values of elapsed cycles. The direction of advance of the crack front is indicated by the arrows.
11. A simulation of the growth of a surface crack in Al 7075-T6. The position of the crack front is recorded at approximately equal intervals in crack size \sqrt{ac} , rather than in cycles.
12. Aspect ratios of small cracks in Al 7075-T6 as functions of the crack size \sqrt{ac} . The data (squares) are for cracks grown at a stress amplitude of 400 MPa. The continuous curves show the histories of $a/2c$ found in 10 Monte Carlo simulations.
13. The measure X^2 of the degree of irregularity of the crack front, defined as the average of deviations from the semiellipse possessing the same second moments. Each curve traces the history of X^2 for a single simulation as a function of the crack size \sqrt{ac} .



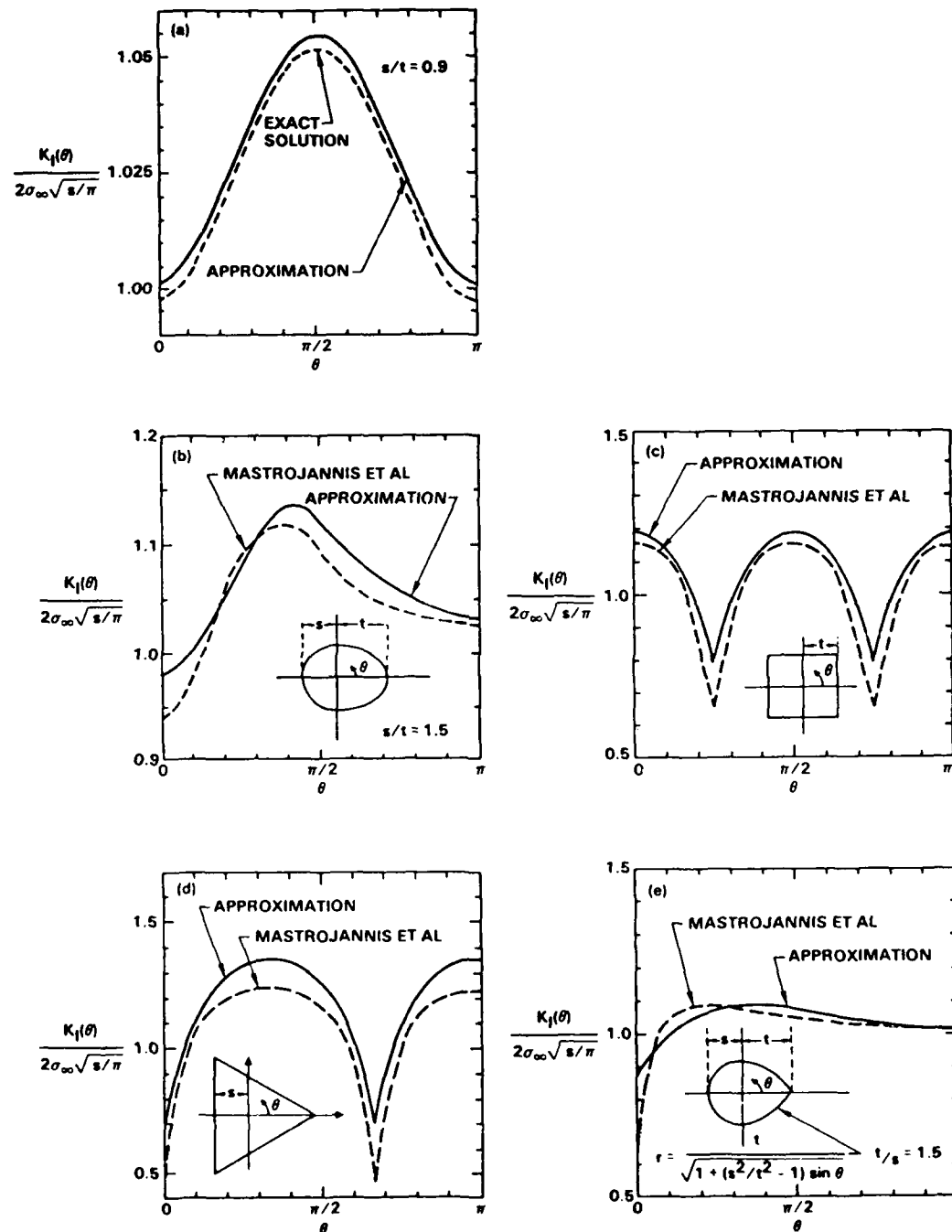
1. The geometries of (a) the protrusion and (b) the retarded segment used to estimate K_I at the extrema of an irregular plane embedded crack.



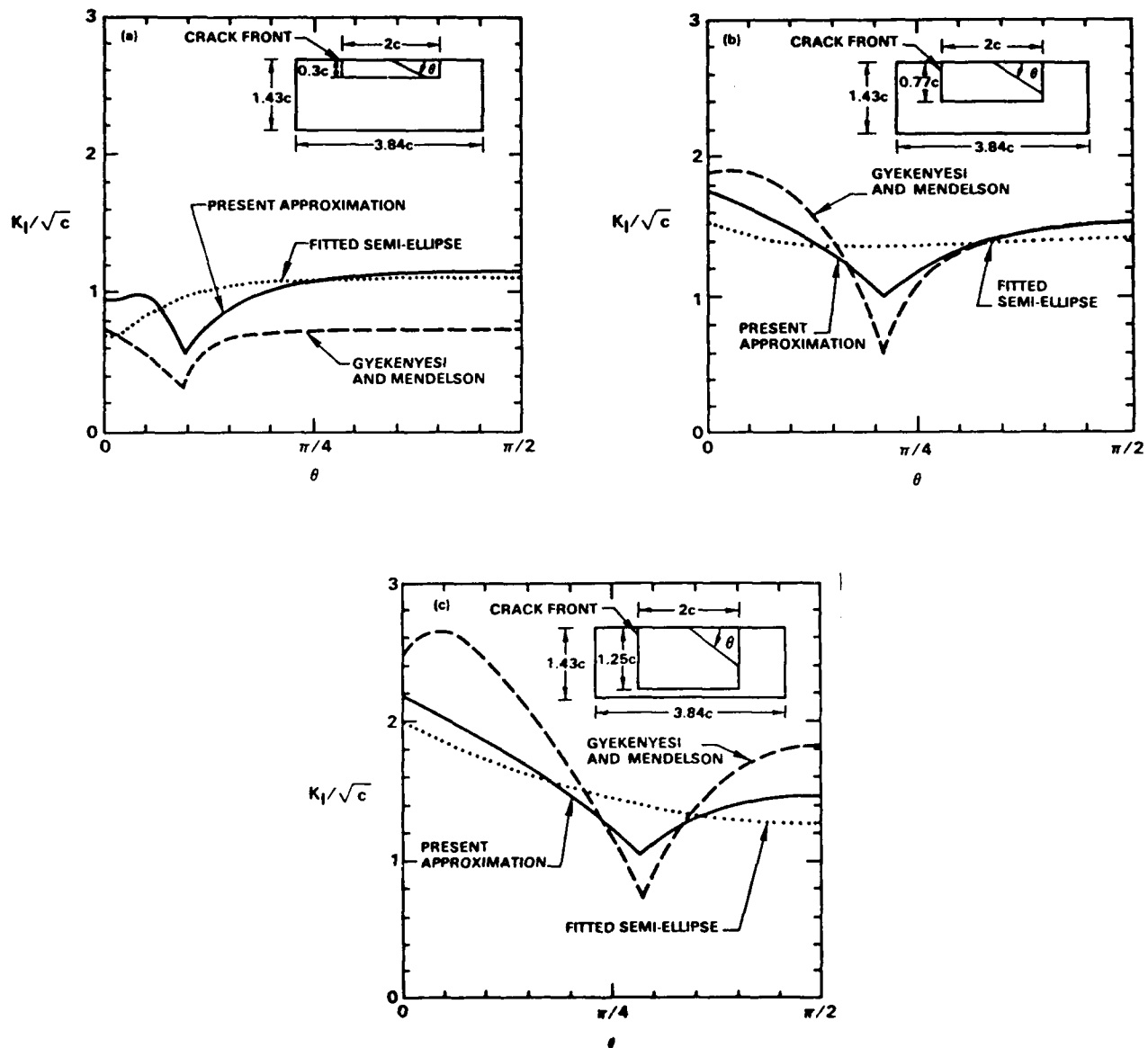
2. $K_I^P(\alpha)$ normalized with respect to K_I for a penny crack of radius s , as a function of s/t .



3. Illustrating the procedures used to define protrusions and retarded segments on an irregular crack for the purpose of invoking Eqs. (3), (7), and (8).

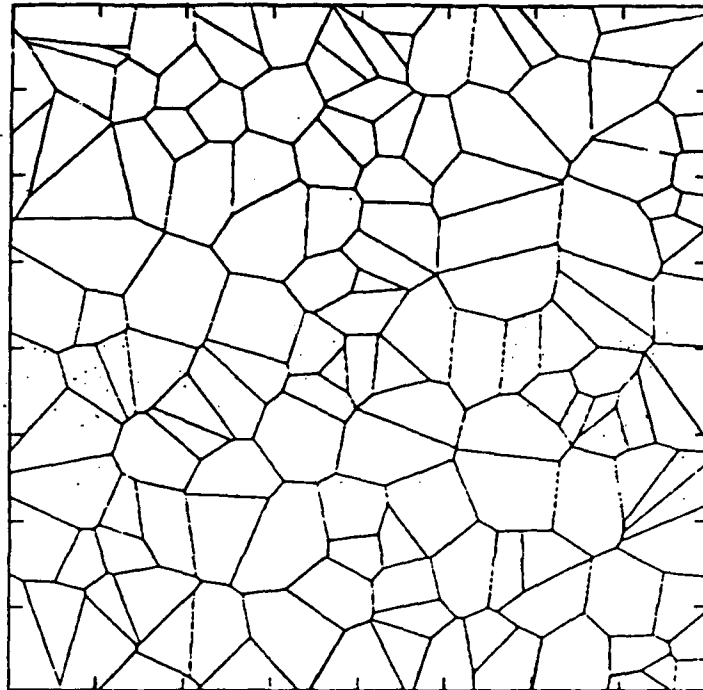


4. Testing the algorithm of Eqs. (3), (7), and (8) for embedded cracks against known solutions for embedded irregular cracks: (a) is for an ellipse with semi-axes as marked; the shapes of the cracks in (b)-(e) are shown as insets. The results of Mastrojannis et al were taken from Ref. 28.



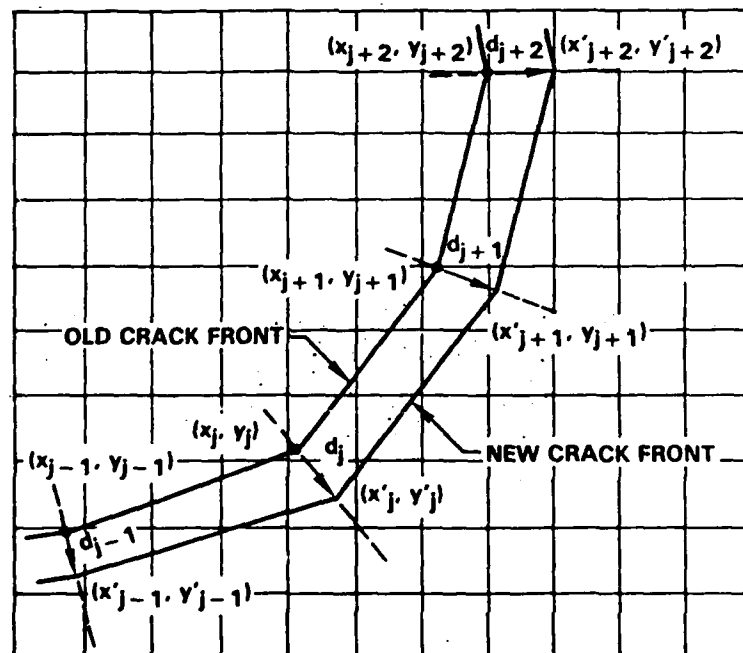
5. Testing the algorithm of Eqs. (3), (7), (8), and (9) for surface cracks against the calculations of Gyekenyesi and Mendelson [33] for rectangular cracks in finite rectangular bars. The insets show the dimensions of the cases considered. All values of K_I are normalized to \sqrt{c} , where $2c$ is the surface crack length. The curve marked 'fitted semiellipse' (dotted line) in each case shows the results of Eq. (9) for a semielliptical crack having the same moments of inertia as the rectangular crack.

SC39259

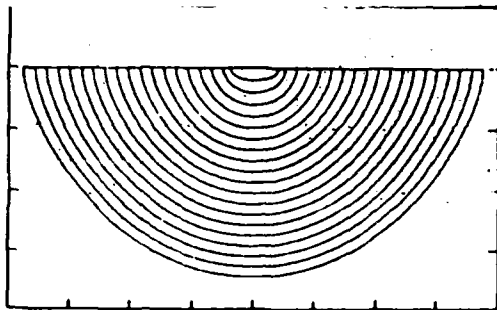


6. A typical random microstructure consisting of Voronoi polygons.

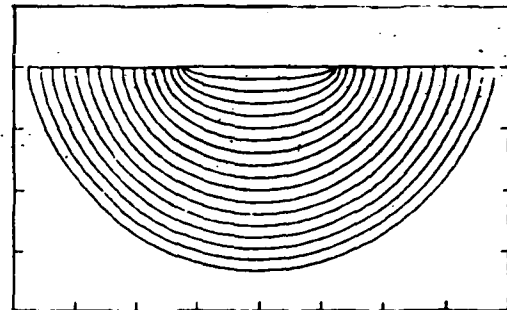
SC39262



7. Illustrating the algorithm for advancing the crack front. The square grid marks the discrete elements within each of which the microstructural parameters (e.g., size of the grain containing the element, or the distance of the element from the next grain boundary) are taken to be constant.

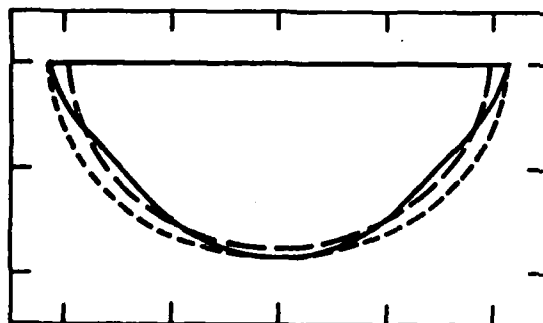


(a)

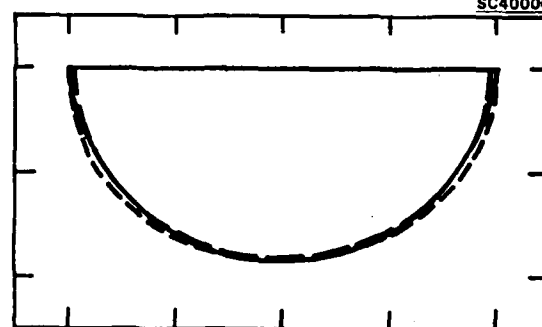


(b)

8. Propagation of surface cracks according to the Paris law in the absence of microstructural effects starting from a crack of aspect ratio (a) 0.25 and (b) 0.08. The parameter p in Eq. (10) has been assigned the value 2.



(a)

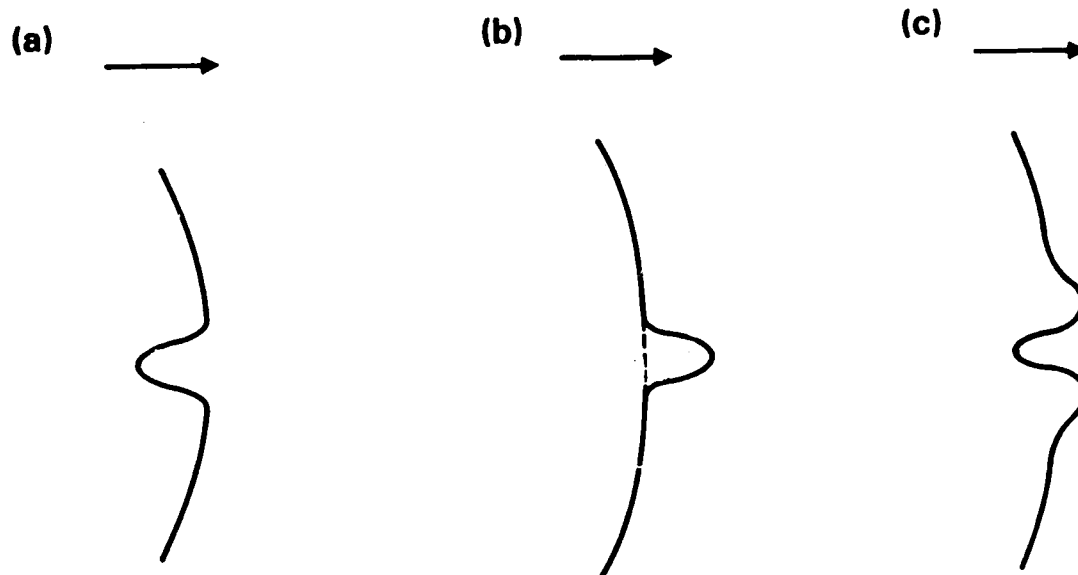


(b)

9. The equilibrium shapes of cracks propagating according to the Paris Law when (a) K_I is set at each point to the value calculated for a semiellipse whose semi-axes are calculated from the second moment of the crack; and (b) K_I is evaluated according to the algorithm of Eqs. (3), (7), (8), and (9).

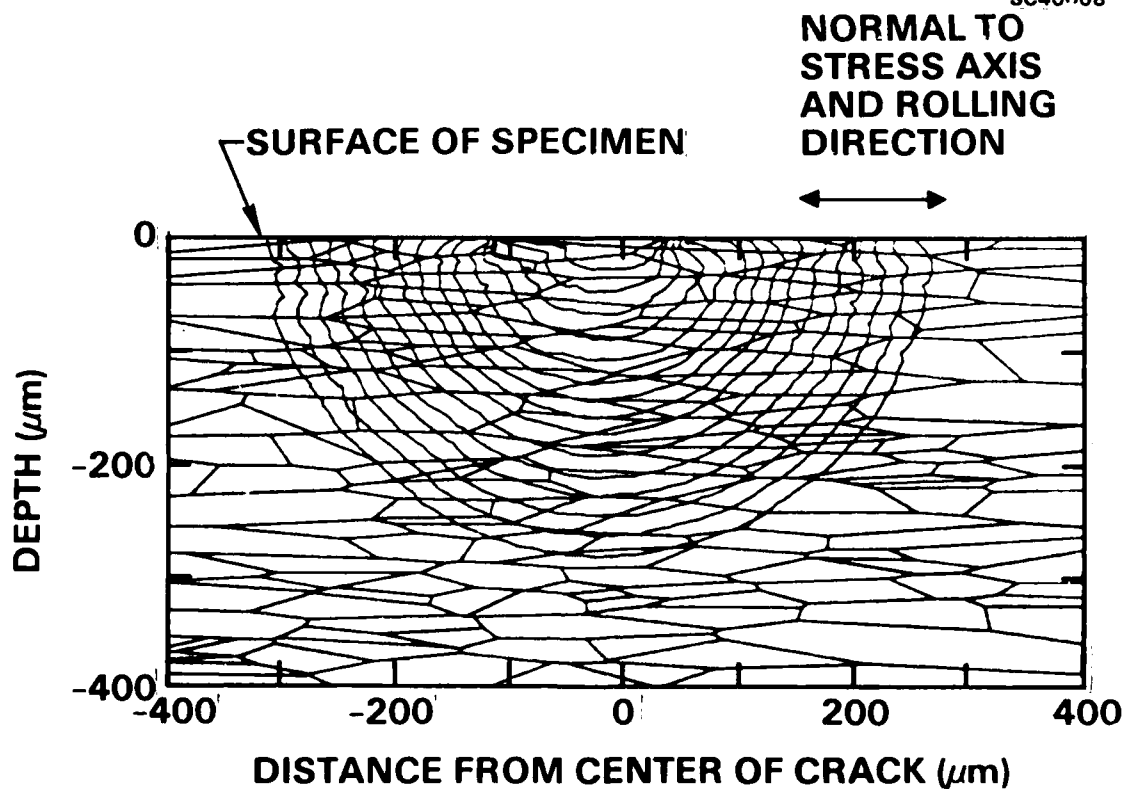
SC40006

SC39261

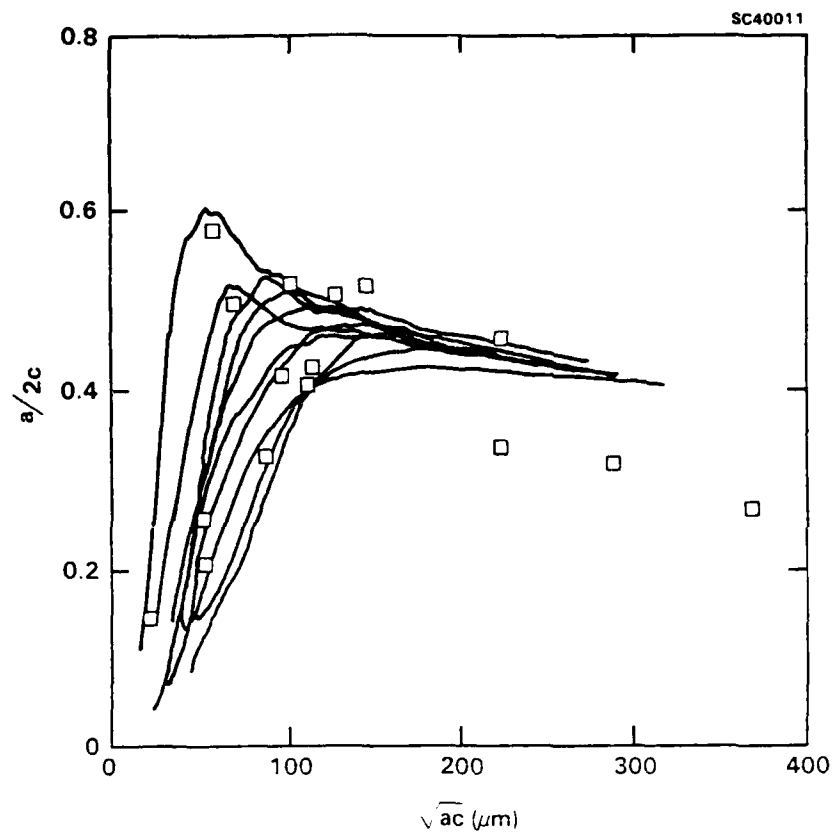


10. Leap-frogging caused by a local minimum in the crack radius. (a), (b), and (c) show the same portion of a crack front at successive discrete values of elapsed cycles. The direction of advance of the crack front is indicated by the arrows.

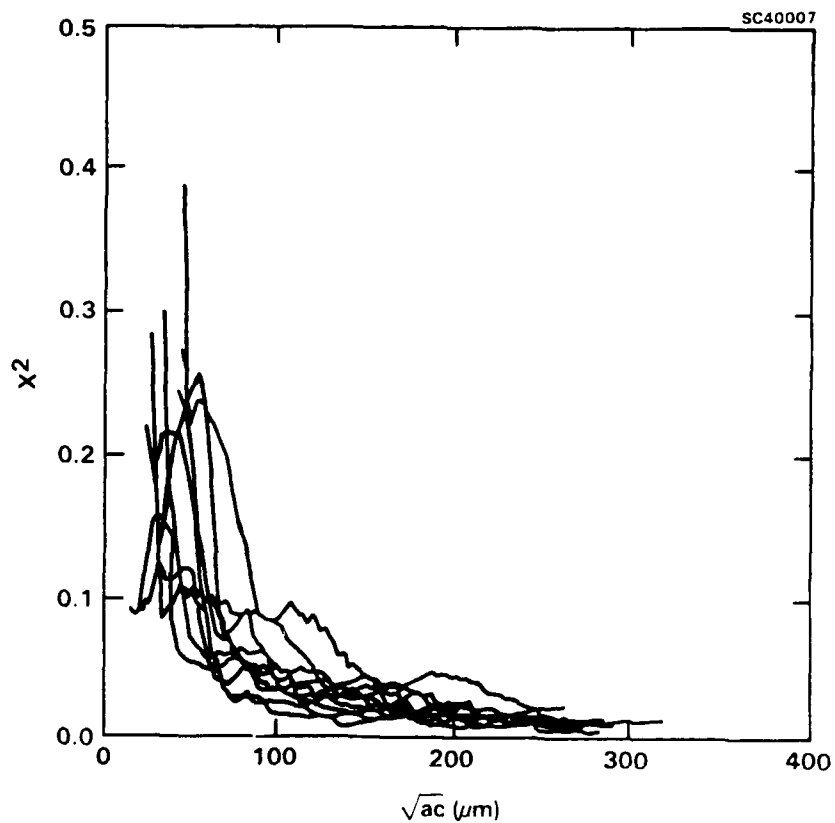
SC40008



11. A simulation of the growth of a surface crack in Al 7075-T6. The position of the crack front is recorded at approximately equal intervals in crack size \sqrt{aC} , rather than in cycles.



12. Aspect ratios of small cracks in Al 7075-T6 as functions of the crack size \sqrt{ac} . The data (squares) are for cracks grown at a stress amplitude of 400 MPa. The continuous curves show the histories of $a/2c$ found in 10 Monte Carlo simulations.



13. The measure X^2 of the degree of irregularity of the crack front, defined as the average of deviations from the semiellipse possessing the same second moments. Each curve traces the history of X^2 for a single simulation as a function of the crack size \sqrt{ac} .

INDUCTIONS FROM MONTE CARLO SIMULATIONS OF SMALL FATIGUE CRACKS

B.N. Cox

Rockwell International Science Center
1049 Camino Dos Rios
Thousand Oaks, CA 91360

ABSTRACT

The relationship between random microstructure and the statistics of small fatigue crack growth is illuminated by Monte Carlo simulations whose formulation has been described previously [1]. In this paper, more detailed analysis is presented of fluctuations in crack shape and the observed surface crack velocity, dc/dN , using empirical laws of growth proposed elsewhere for A1 2219-T851 and A1 7075-T6. Unusually large values of dc/dN are shown to follow retardation or arrest of the surface crack tips while the subsurface crack front has continued to advance. This relation implies that a physically based model of the statistics of dc/dN must account for irregular crack shape to predict the distribution of dc/dN and remaining lifetime accurately. The value of even rough measurements of surface crack depth in estimating remaining lifetime from nondestructive evaluation of a small crack is demonstrated. It is concluded that the statistics of dc/dN require at least two independent random variables for their description. It is also proposed that experimental observations of the degree of irregularity of cracks of various sizes provide the most direct means to date of comparing the mechanics of the growth of surface and subsurface segments of the crack front.

1. INTRODUCTION

In a previous paper [1], the formulation of Monte Carlo simulations of small fatigue crack growth was presented. The simulations explore the propagation under Mode I cyclic loading of small, plane, embedded or surface-breaking fatigue cracks through random microstructures. Unlike all prior statistical models of surface-breaking fatigue cracks, which study only the behavior of the visible surface tips of the crack, the simulations calculate the advance of the entire crack front. This allows explicit study of the dependence of the statistics of growth rates on fluctuations in crack shape. Various aspects of this dependence will be explored in this paper.

The fluctuations in shape of small cracks are generally caused by the random inhomogeneity of the microstructure they encounter. The fluctuations are moderated by the tendency of the crack driving force, specifically the Mode I stress intensity factor, K_I , to restore an irregular crack front to a smooth one. For small cracks, which is to say cracks that span only a few grains, the fluctuations in shape can be large [2-7]. Aspect ratios (depth to surface length) of surface-breaking small cracks can range from 0.1 to 0.7, and the crack front can depart dramatically from the smooth semi-ellipse that is often assumed [1]. In such cases, the surface velocity $2dc/dN$, where $2c$ is the surface crack length and N the number of elapsed cycles of fatigue loading, will show significant fluctuations that cannot be correlated with the microstructural features visible on the specimen's surface.

In this paper, various aspects of the relationships between fluctuations in crack shape, the micromechanics of crack growth, including grain

boundary blockage, and the statistics of dc/dN will be explored more fully. The underlying theme of the paper is to demonstrate the importance and usefulness of both calculating and measuring details of crack shape. In the unfortunate absence of this kind of experimental data, many of the arguments to be presented are didactic rather than definitive analyses of particular materials. One purpose of this paper is to encourage measurement of the detailed shapes of small cracks to 1) allow a clear test of whether the fluctuations in dc/dN under uniform cyclic loading can all be attributed to the randomness of the microstructure, and 2) take advantage of the potential for deducing the mechanics of microstructure-dominated crack growth from the statistics of crack shape, as demonstrated below.

2. SUMMARY OF THE SIMULATIONS

To describe small crack propagation in a given alloy, the Monte Carlo simulations require the specification of empirical or postulated laws defining the influence of local microstructural parameters on each segment of the crack front. These laws are generally based on microscopic observations of the growth of the surface tips of surface-breaking cracks and the surface manifestations of the surrounding microstructure. They may include representations of any or all of the phenomena believed to influence small crack growth, including grain boundary blockage [8-14]; closure induced by fracture surface roughness, plasticity, or oxide debris (e.g., [15] and references therein); out of plane deflections [16]; grain orientation; and the fatigue history of local mechanical properties [17-20]. Whether these laws are appropriate for describing the propagation of subsurface segments of the crack as well as its

surface tips is uncertain. In one case studied so far, namely small cracks in Al 7075-T6, it seems to be so [1], but in others it might not. The Monte Carlo simulations provide a useful test for this basic hypothesis. Differences in the laws of growth operating at and below the surface will cause consistent variations in random crack shapes. However, attention in this paper will not be focused on the question of differences in surface and subsurface mechanics. They will be assumed for argument's sake to be the same.

The cases of Al 2219-T851 and Al 7075-T6 will be taken here as the paradigm of small crack phenomena. Under fully reversed, uniform cyclic loading, the main effects influencing small crack growth in these alloys are crack closure and grain boundary arrest. The numerical treatment of propagation in the presence of crack closure has been described already in [1]. The modifications required for the consideration of grain boundary arrest are presented below. The treatment of crack initiation has also been discussed previously [1], but some elaborations that allow more faithful representation of the statistics of initiation are presented here in Appendix A. They are relegated to an appendix because they are not germane to the conclusions reached in this paper, which is concerned mainly with the statistics of propagation. The physical laws used to model closure and grain boundary arrest in Al 2219-T851 and Al 7075-T6 are as follows.

Crack closure modifies the rate of propagation of a surface crack tip across a grain [21] according to the empirical law used in [1]. As in [1], this law will be generalized here to apply to the entire crack front. Thus, the rate of advance of any point on the crack front under uniform cycling that produces the range ΔK_I in the mode I intensity factor is written

AD-A197 917

INTEGRATION OF STATISTICAL AND PHYSICAL MODELS OF SHORT

2/2

FATIGUE CRACK GRO. (U) ROCKWELL INTERNATIONAL THOUSAND

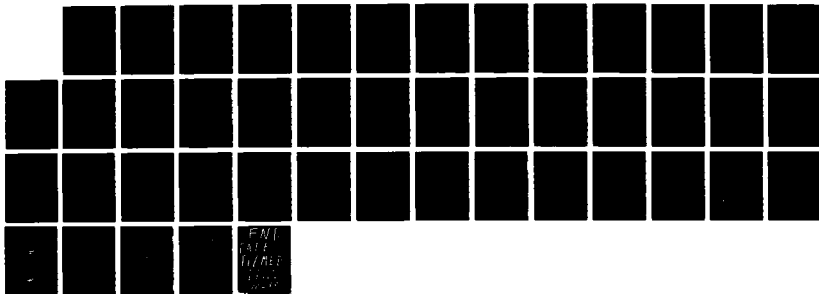
ONKS CA SCIENCE CENTER B N COX ET AL. JUN 88 SC5418.FR

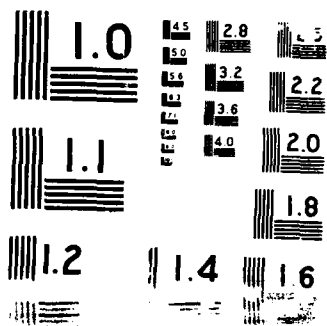
UNCLASSIFIED

AFOSR-TR-88-0690 F49620-85-C-0034

F/G 20/11

NL





$$\frac{d\omega}{dN} = A \Delta K_I^2 (1 - \alpha z / 2\bar{r})^2 H(1 - \alpha z / 2\bar{r}) \quad , \quad (1)$$

where the position variable ω is measured normal to the crack front; \bar{r} is the average crack radius calculated as $\sqrt{a\bar{c}}$, where $a = 2\sqrt{I_y}$ and $\bar{c} = 2\sqrt{I_x}$, and I_x and I_y are the moments of inertia of the crack and its mirror image about the specimen surface; z is the distance from the crack front to the next grain boundary; H is the Heaviside step function, whose presence signifies that closure can arrest a crack [21]; and A and α are material constants ($A = 7.7 \times 10^{-10} \text{ MPa}^{-2} \text{ cycle}^{-1}$ and $\alpha = 0.7$ for Al 2219-T851; $A = 10^{-9} \text{ MPa}^{-2} \text{ cycle}^{-1}$ and $\alpha = 0.5$ for Al 7075-T6; see Discussion for further comments on these values). Note that Eq. (1) describes the acceleration of a crack tip across a grain. In other alloys, crack tips are observed to decelerate as they traverse grains, but the reader will see that the qualitative conclusions reached in this paper ought to apply equally to such materials.

According to observations of surface crack tips, the duration of arrest of small cracks in Al 2219-T851 and Al 7075-T6 at grain boundaries depends on the applied stress, the surface crack length, and the size and perhaps the orientation of the grain ahead of the arrested crack tip (e.g., [9, 21, 22]). Measurements of striation patterns of cracks broken open after fatigue [23] and cracks revealed by destructive sectioning [12] have shown that subsurface segments of cracks can also be arrested at grain boundaries. While doubt persists over the physics of grain boundary arrest even in the much studied Al 2219-T851, detailed phenomenological laws have been deduced from experimental data to describe the dependence of the duration of the arrest on the controlling factors [9]. The applied stress and the orientation

of the next grain are effective through the resolved shear stress, τ , and the size of the next grain is represented by the maximum slip distance D . The duration of arrest is also modified by the existence of a cutoff crack length $2c_0$, above which arrest no longer occurs. In Al 2219-T851, experimental observations suggest that $2c_0$ is related to a critical value ΔK_0 of the local value of ΔK_I [9]. Thus, in fully reversed loading, for example, $2c_0 \propto \sigma_{\max}^2$, where σ_{\max} is the maximum stress amplitude. For Al 2219-T851, $\Delta K_0 \approx 13 \mu\text{m}^{1/2} \sigma_y$, where σ_y is the bulk cyclic yield stress [9]. Since it has been assumed here that these laws are equally valid for subsurface segments of the crack, the surface crack length has been replaced by twice the average radius of the crack, $2\bar{r}$.

The duration of arrest of a vertex is counted down by a parameter β , which has value zero when the vertex is first arrested and unity when it is about to resume propagation. The law for the rate of change of β is [9]

$$\frac{d\beta}{dN} = \gamma D \frac{\sqrt{2\bar{c}}}{1-\bar{c}/c_0} \left(\frac{\tau-\tau_0}{\sigma_y}\right)^2 H\left(\frac{\tau-\tau_0}{\sigma_y}\right) \quad \begin{array}{l} \bar{c} < c_0 \\ \infty \\ \bar{c} > c_0 \end{array} \quad (2)$$

where the slip distance D is approximated for simplicity by the square root of the area of the next grain and H is again the Heaviside step function. The resolved shear stress τ is close to $\sqrt{2}\sigma_{\max}$, since the high symmetry of Al ensures that one slip system will be at approximately 45° to the applied stress. The empirically determined parameter τ_0 is believed to represent an intrinsic back stress resisting the development of slip in the grain ahead of the crack tip [9]. It has the value $0.38\sigma_y$ in Al 2219-T851, where σ_y is the

bulk cyclic yield stress. The parameter γ is another empirically determined material constant, with the value $6.0 \times 10^{-5} \mu\text{m}^{3/2} \text{cycles}^{-1}$ for Al 2219-T851. The change in β is calculated for each blocked vertex at each iteration. If the new β exceeds unity, the status of the vertex concerned reverts to propagating.

The driving force ΔK_I has been estimated as in [1] at each point on the crack front, taking account of the crack's highly irregular shape. As described in [1], the crack front in a simulation is represented by a sequence of vertices separating small, straight line segments. The details of the random microstructure are stored for the duration of the simulation of one crack's history on a fine square grid. The microstructural environment of any vertex on the crack front can be found at any time by identifying the nearest point on that grid. One attribute of the grid point will be the grain in which it lies. The arrival of a vertex of the crack front at a grain boundary is signaled by a different grain being attributed to the nearest grid point from that on the last iteration. When that occurs, the vertex is labeled as being blocked, and the beginning of its term of arrest is noted. Thus, every vertex on the crack front is individually flagged as blocked or propagating. None, some, or all of the vertices may fall into either category at any time.

If at least one vertex is propagating at any time, the number of elapsed cycles in the next iteration is chosen to restrain the maximum advance of any vertex to a prescribed limit. This controls the step size in the numerical solution of the underlying, coupled first-order differential equations defining the propagation problem. If all vertices are blocked by grain boundaries, then β and $d\beta/dN$ are compared for all vertices, and the vertex

that will first resume propagation is identified. The number of cycles required for this is calculated from Eq. (2) and added to the running total of elapsed cycles. On the next iteration, the newly freed vertex will propagate again.

3. GRAIN BOUNDARY ARREST AND FLUCTUATIONS IN SHAPE

The general pattern of crack propagation observed in the simulations in the presence of grain boundary blockage is qualitatively similar to that found when crack closure, e.g., induced by plasticity, varies randomly around the crack front [1]. The crack front is made highly irregular as some segments are blocked by grain boundaries, while others continue to propagate. Since a blocked segment becomes retarded relative to the rest of the crack, K_I is amplified there, and when propagation resumes it is anomalously rapid.

The presence of the factor $\tau - \tau_0$ in Eq. (2) causes the fraction of time a crack or its various segments spends in arrest to increase dramatically as τ approaches τ_0 from above (if $\tau < \tau_0$, grain boundary arrest is permanent). Thus, the relative strength of grain boundary arrest increases with decreasing σ_{\max} . The increase in the irregularity of the crack front due to grain boundary arrest can therefore be demonstrated by comparing simulations for high and low values of σ_{\max} . Figure 1a shows the case $\sigma_{\max} = 0.7\sigma_y$ and Fig. 1b the case $\sigma_{\max} = 0.94\sigma_y$ in a simulation of a crack growing in Al 2219-T851 under fully reversed loading. The crack front is shown in each case at intervals marking approximately equal increments in the average crack radius. The intervals are unequal and irregular because the increment of crack growth on each iteration depends on stress-dependent details of the crack's shape.

Therefore, the sequences in Figs. 1a and 1b are not immediately equivalent, even though the same pseudo-random microstructure has been used in both cases, but one can see that the crack front is significantly more irregular in Fig. 1a than in Fig. 1b. Most of the irregularities are coincident with grain boundaries. The smallest ripples are caused by the discreteness of the grid on which the microstructure is recorded. The irregularity that persists at $\sigma_{\max} = 0.94\sigma_y$, when crack arrest at grain boundaries is very brief, can be shown to spring mainly from the random effects of the microstructure on crack closure during periods of propagation.

The irregularity of the crack front can be quantified in various ways. One convenient measure is

$$\langle X(\theta, \bar{r}) \rangle \equiv \frac{1}{n} \sum_{j=1}^n X_j(\theta, \bar{r}) \equiv \frac{1}{n} \sum_{j=1}^n |1 - r_j(\theta, \bar{r}) / \langle r_j(\theta, \bar{r}) \rangle| \quad , \quad (3)$$

where $r_j(\theta, \bar{r})$ is the radius of the j th crack front at angle θ when the crack's size is \bar{r} . The angle θ is defined in Fig. 2. The sum in Eq. (3) is over all simulations (cracks) in a Monte Carlo ensemble and the square brackets $\langle \dots \rangle$ denote an ensemble average. The term $\langle r_j(\theta, \bar{r}) \rangle$ represents the ensemble average of $r_j(\theta, \bar{r})$ over the same set of Monte Carlo simulations:

$$\langle r_j(\theta, \bar{r}) \rangle = \frac{1}{n} \sum_{j=1}^n r_j(\theta, \bar{r}) \quad . \quad (4)$$

(The definition Eq. (3) of irregularity is different to that presented in [1], where $\langle r_j(\theta, \bar{r}) \rangle$ was replaced by the radius at angle θ of the

semi-ellipse of best fit. Equation (3) is superior because it allows $\langle X(\theta, \bar{r}) \rangle$ to be evanescent as the crack grows very large and the influence of the random microstructure diminishes. Using the definition of [1], this does not happen. For large cracks, $\langle X(\theta, \bar{r}) \rangle$ as defined in [1] tends to a constant, which merely reflects the fixed departure of the equilibrium crack front from the semi-ellipse of best fit. The true shape of the equilibrium crack front is given by $\langle r_j(\theta, \bar{r}) \rangle$.)

The angle dependence of $\langle X(\theta, \bar{r}) \rangle$ is shown in Fig. 2a for simulations similar to those of Fig. 1 and at the stress level $\sigma_{\max} = 0.95\sigma_y$. The irregularity is seen to be largest at $\theta = 90^\circ$, which corresponds to those segments of the crack propagating down into the specimen. Since the grain structure is highly nonequiaxed with depth/width ratios of 0.15 for the average grain, the downward propagating crack front encounters crack boundaries with relatively high frequency. This causes greater fluctuations in $r_j(\theta, \bar{r})$ in this direction. The dominant trend of $\langle X(\theta, \bar{r}) \rangle$ with increasing crack size is that it decays approximately as the m th power of \bar{r} , with $m \approx 1.5$ for $\sigma_{\max} = 0.95\sigma_y$. The trends in $\langle X(\theta, \bar{r}) \rangle$ for small \bar{r} are affected strongly by the initiation model used in the simulations. Since all cracks began as semicircles with $2c = 20 \mu\text{m}$ in the simulations of Fig. 2, $\langle X(\theta, \bar{r}) \rangle$ is zero at $\bar{r} = 10 \mu\text{m}$. The position of the maximum in $\langle X(\theta, \bar{r}) \rangle$ for $\theta = 90^\circ$, which occurs at $\bar{r} \approx 30 \mu\text{m}$, indicates the range of influence of the choice of initiation model.

The stress dependence of the degree of irregularity, which has already been seen qualitatively in Fig. 1, is shown quantitatively in Fig. 2b. For this figure, the average $\langle X(\bar{r}) \rangle$ of $\langle X(\theta, \bar{r}) \rangle$ over all angles has been calculated for $\sigma_{\max} = 0.95\sigma_y$ (the same simulations as in Fig. 2a) and $\sigma_{\max} =$

$0.7\sigma_y$. For the latter stress level, only 66 simulations were executed. The stress dependence of $\langle X(\bar{r}) \rangle$ is just as expected, with the lower stress marked by much greater irregularity because of the stronger effect of grain boundary arrest. For $\sigma_{\max} = 0.7\sigma_y$, $\langle X(\bar{r}) \rangle$ falls off approximately as $\bar{r}^{-0.8}$.

The error bars in Fig. 2 indicate the root mean square deviation of $\langle X \rangle$ (dropping the arguments θ and \bar{r} from the notation), which is given by (e.g., [24])

$$\sigma_{\langle X \rangle}^2 = \sigma_X^2/n, \quad (5)$$

where n is the number of simulations. The errors $\sigma_{\langle X \rangle}$ are functions of the crack size \bar{r} in Fig. 2, because both σ_X^2 and n depend on \bar{r} . n depends on \bar{r} for large \bar{r} because the simulations ran for a given number of iterations, with the amount of growth on each iteration and therefore the maximum \bar{r} achieved being random.

Even though $\langle X \rangle$ is small, there is significant difference between the cases $\sigma_{\max} = 0.7\sigma_y$ and $\sigma_{\max} = 0.94\sigma_y$. The ripples on the crack front reflected in $X_j(\theta, \bar{r})$ measure only $\sim 10 \mu\text{m}$ on a $300 \mu\text{m}$ crack, and the practice of most experimentalists would be to ignore them and declare the crack a smooth semi-ellipse. Nevertheless, they are presumably measurable. Furthermore, it should not be necessary to make the measurements for 100 cracks. Since $\sigma_{\langle X \rangle} \propto n^{-1/2}$, it can be seen from Fig. 2 that the dependences on angle θ and stress shown there should be borne out by measurements on as few as ten cracks. Unfortunately, such measurements are not yet available.

4. SUBSURFACE ARREST AND THE SURFACE VELOCITY

Minima in the surface velocity, dc/dN , of small, surface-breaking cracks are not always coincident with the arrival of one of the surface crack tips at a grain boundary. Lankford [23] reported the near-arrest or arrest of surface crack tips in Al 7075-T6 far from grain boundaries. The cracks he observed had initiated at fractured surface inclusions, which were typically less than 10 μm across. They propagated until the surface length was 30-40 μm , whereupon they suffered a steep decline in velocity, with some becoming essentially nonpropagating. All this occurred far from the boundaries of the grain of initiation, which was $\sim 100 \mu\text{m}$ across.

Since the grains in that Al 7075-T6 specimen were flat and approximately 18 μm deep, the possibility naturally arises that the surface velocity dc/dN is reflecting the status of subsurface segments of the crack front. For a semicircular crack, the observed minima in dc/dN would coincide approximately with the arrival of the subsurface crack front at the first subsurface grain boundary. Since striation markings clearly indicated crack arrest at the subsurface boundary, one might speculate [23] that dc/dN would be reduced as the crack tended to maintain its semicircular aspect ratio.

The present Monte Carlo simulations demonstrate that this is unlikely to be the case. Figures 3a and 3b show simulated striations left by a crack that is arrested at a subsurface boundary in Al 7075-T6. The crack in Fig. 3a has recently been arrested. In Fig. 3b, the effects of arrest are manifest in the jog of each striation at the subsurface grain boundary, and the left surface crack tip has just reached a surface grain boundary. The record of

dc/dN for the same simulation appears in Fig. 3c, with the points A and B marking the positions corresponding to the last striation in each of Figs. 3a and 3b. There is obviously no minimum in dc/dN at point A, nor was that found to be the case in any of many similar simulations at various stress levels. There is, of course, a dramatic drop in dc/dN just before point B, when the left surface tip reaches a grain boundary.

It is easy to see why there is no minimum in dc/dN at point A in Fig. 3c from the mechanics embodied in the simulation. The transmission of information about the deepest point of the crack to the surface tips is via the dependence of K_I on the crack's shape. When the deepest point is arrested, the crack becomes shallower. The canonical expressions of Newman and Raju [25-27], which are part of the estimated K_I in the simulations [1], then yield smaller values of K_I at the surface tips. But this is a gradual decrease, and dc/dN is not significantly affected unless the fluctuation in subsurface velocity (i.e., the crack's arrest there) persists until $2c$ approximately doubles. Thus one has a general and mildly surprising induction from many Monte Carlo simulations: that there is only weak correlation between short-lived fluctuations in dc/dN and in the velocity of the deepest point on a surface-breaking crack, even for cracks spanning less than one grain. This extends and generalizes a conclusion reached previously for model-based analysis of the statistics of dc/dN for surface cracks spanning several grains in a Ti alloy [28].

When velocity fluctuations around the crack do persist long enough for the aspect ratio $a/2c$ to be severely distorted, fluctuations in dc/dN will be found to be correlated with fluctuations in $a/2c$. This point will be elaborated below.

The minima in dc/dN reported by Lankford require another explanation. Perhaps they mark a change in the mode of propagation of the surface tips of the crack, involving a discontinuous change in closure stresses or in the crack driving force, the latter perhaps because of a microscopic crack deflection.

5. QUALITATIVE NATURE OF THE STATISTICS OF dc/dN

The law of propagation of surface tips of which Eq. (1) is a generalization for all points on the crack front has one feature in common with most micromechanical models in the literature that describe the influence of microstructure. The effect of the microstructure in Eq. (1) is to reduce the velocity of the crack from that which it would have had in the absence of the factor $(1-\alpha z/2\bar{r})$. There is therefore an upper bound to dc/dN as it is prescribed by Eq. (1) for a given value of the applied K_I (or ΔK_I). This same feature is found in the popular theory that small cracks grow faster than long cracks at the same applied ΔK_I because plasticity-induced closure is absent or relatively small in small cracks (e.g., [15] and references therein). (This model is not to be confused with that underlying Eq. (1), which considers the restriction of crack tip opening displacements by back stresses associated with the constraint of the crack tip plastic field by grain boundaries [21].) An upper bound to dc/dN is also present in models of roughness-induced closure (e.g., [29-31]). Similarly, the effective crack driving force for a kinked, curved or deflected crack is lower than that for a plane crack [16,32].

Since most workers observe and model just the surface trace of a small, surface-breaking crack, the applied K_I is calculated from the surface

length $2c$ under the assumption that the crack is semi-elliptical with fixed aspect ratio. At constant stress, K_I is therefore a smooth, monotonically increasing function of $2c$, and so therefore is the upper bound to dc/dN in models like Eq. (1). The effect of these assumptions on the statistics of dc/dN is to make them unrealistic. This was demonstrated by the simulations in the following way.

5.1 Case A - Modeling the Surface Crack Tips Only

The customary analysis of the statistics of dc/dN was emulated by calculating the propagation rate dw/dN according to Eq. (1) and db/dN according to Eq. (2) for the surface tips only. The rest of the crack was assumed to be semicircular, and K_I for the surface tips was calculated according to the canonical expressions of Raju and Newman [25-27].

Each simulation generates a sequence $(2c_{i,j}, N_{i,j}, i = 1, 2, \dots)$ of surface crack lengths and elapsed cycles. For the simulation to be accurate, the sequence must be much denser than the equivalent experimental data. Therefore, in the interests of obtaining statistics as much like experimental statistics as possible, the sequence $(2c_{i,j}, N_{i,j}, i = 1, 2, \dots)$ for each crack was replaced by the sequence $(\hat{2c}_{i,j}, iN_0, i = 1, 2, \dots)$, where N_0 is an interval of elapsed cycles that might separate experimental measurements of crack length, and $\hat{2c}_{i,j}$ is the value of $2c$ after iN_0 cycles, found by linear interpolation over $(2c_{i,j}, N_{i,j}, i = 1, 2, \dots)$.

Two density functions for the surface velocities were then constructed from the sequences $(\hat{2c}_{i,j}, iN_0, i = 1, 2, \dots)$ for all cracks in an

ensemble. The first, $h_c(V)dV$, refers to the probability that a crack of surface length $2c$ will have normalized velocity

$$V \equiv \frac{dc/dN}{A\Delta K_I^2(c)} \quad (6)$$

lying between V and $V + dV$, where $\Delta K_I(c)$ is the nominal stress intensity factor for the semicircular crack of surface length $2c$. The denominator in Eq. (6) is just the upper bound to dc/dN at crack length $2c$ according to Eq. (1). The density $h_c(V)$ was approximated by

$$h_c(V) = \frac{\delta}{n\pi} \sum_{j=1}^n \frac{1}{\delta^2 + (V-V_j)^2}, \quad (7)$$

where the sum is over the n simulations in an ensemble, and V_j is the normalized velocity found for the j th simulation at crack length $2c$:

$$V_j = \frac{\hat{c}_{i+1,j} - \hat{c}_{i,j}}{N_0}, \quad (8)$$

where $2\hat{c}_{i,j} \leq 2c < 2\hat{c}_{i+1,j}$. The Lorentzian peak width δ was set to 0.02 in the cases reported below. In fact, when dealing with the normalized velocities V , it is convenient to consider the average \bar{h}_c of the densities h_c for several crack lengths $2c$. When the same procedure is carried out for limited experimental data, smoother density functions are obtained for such an average than would be obtained for one crack length. Of course, the density $h_c(V)$ of normalized velocities will be slightly different for different given crack lengths. However, when the average is limited to lengths in the small

crack regime, the points to be made in this section are qualitatively unaffected. The subscript c is retained in the notation \bar{h}_c to emphasize that it still represents the result of sampling dc/dN for cracks of certain specified lengths. For a sum over lengths 100, 120, 140, ..., 300 μm , the density $\bar{h}_c(V)$ is shown in Fig. 4a for the cases $\sigma_{\text{max}} = 0.7\sigma_y$ and $\sigma_{\text{max}} = 0.96\sigma_y$, with the interval N_0 set to 2000 cycles. (The median number of cycles for a crack to grow to $2c = 300 \mu\text{m}$ when only the surface tips were modeled explicitly was $\sim 90,000$ when $\sigma_{\text{max}} = 0.7\sigma_y$ and $\sim 30,000$ when $\sigma_{\text{max}} = 0.96\sigma_y$.) The upper bound to dc/dN is manifested in the fact that $\bar{h}_c(V) = 0$ for $V > 1$. (The slight tails of $h_c(V)$ that penetrate out of the interval $[0,1]$ are just the tails of the Lorentzian peaks in Eq. (7)).

The second density function considered for the surface velocities, denoted $h_N(V)dV$, refers to the probability that a crack will have normalized velocity V lying between V and $V+dV$ when N cycles have elapsed from the initiation event (i.e., from the beginning of the simulated propagation). In analogy to $h_c(V)$, $h_N(V)$ is estimated from a Monte Carlo ensemble as a sum of Lorentzian peaks, with V_j in the analogue of Eq. (7) now being the normalized velocity found for the j th simulation after N cycles. Once again, a smoother density function (more information) can be obtained by averaging the functions $h_N(V)$ for various values of N , with the resultant density function denoted $\bar{h}_N(V)$.

The density $\bar{h}_N(V)$ is shown for $\sigma_{\text{max}} = 0.7\sigma_y$ and $\sigma_{\text{max}} = 0.95\sigma_y$ in Fig. 4c, with the average of $h_N(V)$ in this case being over values of elapsed cycles that are multiples of 5000 up to 50,000. As for $\bar{h}_c(V)$, $\bar{h}_N(V)$ was estimated from the time-averaged sequences $(2\hat{c}_{ij}, iN_0, i = 1, 2, \dots)$ with $N_0 = 2000$

cycles. Like $\bar{h}_C(V)$, $\bar{h}_N(V)$ is confined to the interval $[0,1]$, apart from the small excursions of the tails of the Lorentzian peaks in the approximation analogous to Eq. (7).

The densities $\bar{h}_C(V)$ and $\bar{h}_N(V)$ show one important qualitative difference: $\bar{h}_C(V)$ is biased strongly towards higher values of V . Low values of V are weakly represented in $\bar{h}_C(V)$ because the crack does not grow much when V is small. In a plot of V vs c for a single crack (or simulation), low values of V are accordingly found to occur over relatively short intervals of c . If one samples V at a specified crack length $2c$, it is therefore disproportionately likely that a high value of V will be obtained. This effect is absent in \bar{h}_N . When sampled after a prescribed number of elapsed cycles, low values of V , including $V = 0$ (arrested crack), are well represented. Thus \bar{h}_N shows a significant peak at $V = 0$, corresponding to the arrest of both surface crack tips. When $\sigma_{\max} = 0.7\sigma_y$ and grain boundary arrest is more prevalent, there is even a small peak discernible at $V = 0.5$, corresponding to the arrest of just one surface crack tip. This distinction between \bar{h}_C and \bar{h}_N (or h_C and h_N) is important to bear in mind when analyzing experimental statistics of grain boundary blockage (see Discussion).

5.2 Case B - Modeling the Whole Crack Front

Now consider the density functions \bar{h}_C and \bar{h}_N found for the surface velocities dc/dN when the simulations trace the propagation of the whole crack front rather than the surface tips alone. The densities in this case (Figs. 4b and 4d) are different in several important ways.

First, the normalized velocity is no longer bounded by any upper limit. Both \bar{h}_c and \bar{h}_N show significantly many cracks propagating faster than the nominal upper bound of unity. These high values of velocity can all be traced in the present simulations to high values of ΔK_I at one or both of the surface crack tips. High values of ΔK_I occur at any point on the crack front that is retarded relative to the rest of the crack front [1]. Thus high values of dc/dN generally follow a period of arrest of either crack tip. When the surface tip finally breaks free from the grain boundary or other microstructural feature that arrested it, it is whiplashed by the subsurface crack front, which has grown ahead of it during its arrest.

The second noteworthy difference between Figs. 4b and 4d (whole crack front) and Figs. 4a and 4c (surface tips only) is in the probability of arrest of the surface tips. This is especially visible in \bar{h}_N , which has a much larger peak near $V = 0$ in Fig. 4c than in Fig. 4d. In other words, with all other modeling details equal, the surface crack tips are much less likely to be found in a state of arrest after given elapsed cycles when the whole crack front is simulated. This is because the duration of arrest is much less when the subsurface crack front is modeled. The subsurface crack front is normally found to grow ahead of an arrested surface tip, so that the average crack size \bar{r} continues to increase, reducing the time of arrest in accord with Eq. (2). This, of course, negates the validity of using values of the parameters γ , τ_0 and c_0 in Eq. (2) that have been deduced from measurements of surface crack tips alone, with ΔK_I calculated as for a semicircular crack [9]. It even raises doubts about the functional form of db/dN . In principle, a statistical analysis of surface velocity data based on modeling the entire crack

front should be used to determine laws such as Eq. (2). This has not been done in this paper, which is concerned only with trends and concepts. Even if the assumed functional form of db/dN was found to be in error, none of the conclusions reached here would be affected materially.

5.3 Experimental Densities

For qualitative comparison, densities \bar{h}_C and \bar{h}_N were constructed from unpublished raw data of M.R. James and W.L. Morris for Al 2219-T851. They are shown in Figs. 5a and 5b. Because of the sparseness of the data, even densities averaged over different values of crack length or elapsed cycles are imperfectly defined. However, it is quite clear that the densities in Fig. 5 are similar to those of Figs. 4b and 4d, exhibiting no indication of an upper bound to V .

The importance of the high velocity tail of \bar{h}_C or \bar{h}_N far exceeds its weight relative to the rest of the density function, because the fastest cracks are very likely to be the fatal ones. One must conclude that physically based models of remaining lifetime ought to include some representation of this intrinsically three-dimensional effect. The alternative is to apply a purely statistical analysis of surface velocity data, as exemplified by the approach of Bogdanoff and Kozin [33]. Such an approach does not provide the satisfaction of attributing statistical fluctuations to micromechanical origins, and on account of this, it does not share the same potential for accuracy.

6. CRACK SHAPE AND REMAINING FATIGUE LIFETIME

Correlations between crack shape, surface velocity dc/dN , and remaining fatigue lifetime were studied qualitatively for simulations identical in form to those reported in the preceding sections. Parameter values were chosen appropriate to A1 2219-T851. The mutual dependence of dc/dN and the aspect ratio $a/2c$, where a is the deepest point on the crack front, is shown in Fig. 6a for $\sigma_{\max} = 0.95\sigma_y$. Each point in Fig. 6a represents simultaneous values of the surface velocity \hat{dc}/dN (where the circumflex again indicates an average over pseudo-measurement intervals, but now of length 1000 cycles) and $a/2c$ for each crack in 97 simulations when $2c = 100 \mu\text{m}$. The correlation between \hat{dc}/dN and $a/2c$ is imperfect, as one expects, but there is a clear trend that \hat{dc}/dN increases with $a/2c$. This is highlighted by the solid line in Fig. 6a, which was obtained by linear regression analysis. The two dashed lines indicate the 95% confidence interval for the slope of the solid line. Note that the distributions of both \hat{dc}/dN and $a/2c$ in Fig. 6a are natural, in the sense that when $2c = 100 \mu\text{m}$, negligible memory is left of the initiation model, in which $2c$ was initially $40 \mu\text{m}$.

One might expect correlations between dc/dN and $a/2c$ to be the product of two competing factors. On the one hand, when $a/2c$ is large, K_I is enhanced at the surface crack tips, and so dc/dN is enhanced. On the other hand, according to the physical basis of the laws for dc/dN in A1 2219-T851 or A1 7075-T6, $a/2c$ probably became large because the surface crack tips were retarded. Given a large value of $a/2c$, one might expect to find sometimes that the surface tips are still retarded and exhibiting slow growth. Figure 6a reveals that the latter effect is not dominant.

The influence of crack shape on remaining lifetime was assessed by calculating the cycles N_r taken for each crack to grow from $2c = 100 \mu\text{m}$ to $2c = 300 \mu\text{m}$, the latter representing a fatal flaw. The fatal flaw could obviously be defined to be a bigger crack if desired, but since dc/dN is proportional to at least the first power of c , there would be no qualitative effect on the conclusions to be reached here.

Figure 6b shows N_r for each simulation in Fig. 6a as a function of the value of $a/2c$ when $2c = 100 \mu\text{m}$. One sees the expected trend that N_r decreases with $a/2c$, with the solid line in Fig. 6b again being the line of best fit. The narrowness of the 95% confidence interval for the slope of this line shows that variations in $a/2c$ are the source of most of the variations in N_r . The most likely slope indicates that N_r is most likely to be reduced by 30-40% when $a/2c = 0.8$ relative to N_r for the median $a/2c = 0.55$. In applications of a policy of damage tolerance based on periodic inspections of a part in service (retirement for cause), there is obviously great merit in estimating $a/2c$ as well as $2c$ at each inspection.

Much of the reduction in N_r with increasing $a/2c$ is attributable to the fact that dc/dN tends to be higher when $a/2c$ is higher. Thus there is also strong correlation between N_r and \hat{dc}/dN when $2c = 100 \mu\text{m}$ (Fig. 6c). However, there is a weaker effect in Fig. 6c than in Fig. 6b, which is presumably because \hat{dc}/dN is affected by local, near-surface fluctuations in shape, which are short-lived and have little influence on N_r for a growth increment of $200 \mu\text{m}$.

To illustrate the effects on N_r of departures of the crack's shape from semi-elliptical, the following special simulations were performed. Semi-elliptical cracks of surface length $2c = 100 \mu\text{m}$ were initiated with depths uniformly distributed from zero to $100 \mu\text{m}$ ($a/2c$ uniformly distributed between 0 and 1). Growth was then followed to $2c = 300 \mu\text{m}$. The correlation between the initial \hat{dc}/dN and the initial $a/2c$ (i.e., at $2c = 100 \mu\text{m}$) is shown in Fig. 6d. Figure 6d differs from Fig. 6a in that $a/2c$ now spans a greater range and the highest values of \hat{dc}/dN are absent, because there are no locally retarded surface tips, a typical feature in cases of high $a/2c$, that can be suddenly accelerated. Figures 6e and 6f show the correlations between N_r and the values of $a/2c$ and \hat{dc}/dN at $2c = 100 \mu\text{m}$. There are now many instances of cracks that existed at $2c = 100 \mu\text{m}$ not propagating to $2c = 300 \mu\text{m}$ or getting there very slowly, which are represented by the points lying either to the upper left of Figs. 6e and 6f or off the scale. This part of the distribution has no analogue in Figs. 6b and 6c, because in that case the cracks at $2c = 100 \mu\text{m}$ had already grown from $2c = 40 \mu\text{m}$: the nonpropagating or very slow cracks did not appear in the statistics of N_r . For the current purposes, the most significant part of the distribution in Figs. 6e and 6f is for $a/2c > 0.2$ or $\hat{dc}/dN > 0.02 \mu\text{m}/\text{cycle}$. There the trends are similar to those of Figs. 6b and 6c, but with the correlations between N_r and $a/2c$ or \hat{dc}/dN being weaker. This is clearly an effect of crack shape. If one estimated N_r using the measured distribution of $a/2c$ at $2c = 100 \mu\text{m}$ and K_I for the surface tips of a semi-elliptical crack, one would significantly underestimate the reduction of N_r for unusually deep cracks. An accurate estimate requires an account of the irregularity of the cracks, especially the relative retardation of the surface tips that often accompanies large values of $a/2c$.

The correlations of N_r with \hat{dc}/dN and $a/2c$ are also affected by the applied cyclic stress amplitude, σ_{\max} . Figures 6g, 6h, and 6i show the same information as in Figs. 6a, 6b, and 6c, but at $\sigma_{\max} = 0.7\sigma_y$. At the lower stress level, the cracks are much more irregular (Fig. 2b). The correlation between \hat{dc}/dN and $a/2c$ is less definite (Fig. 6g), because near-surface fluctuations in shape, which are not directly correlated with $a/2c$, are much larger. This is indicated by the wide 95% confidence interval for the slope of the line of best fit in Fig. 6g. The correlations between N_r and $a/2c$ or \hat{dc}/dN (Figs. 6h and 6i) are still comparable to those for $\sigma_{\max} = 0.95\sigma_y$, but the trend is mixed in with a much wider scatter in N_r .

7. DISCUSSION

7.1 On Statistics and Mechanics

The nonexistence of experimental data on the details of crack shape has frustrated the demonstration of the full power of the Monte Carlo simulations of [1]. It is hoped, however, that sufficient stimulus has been provided for such experimental measurements to be made. Various fundamental aspects of the mechanics of small cracks could be thereby elucidated. In particular, differences in surface and subsurface mechanics could be quantified. Models of the role of microstructure or environment could be tested by, for example, determining the irregularity measure X at different stress levels, in different microstructures, and in different environments. The effects of isolated overloads, an area of much doubt, could be measured in terms of ensuing, consistent variations in crack shape. If, for example, an

overload causes the greatest changes in the plastic zone in large grains, which are known to be more microplastic in Al alloys [17,18], then this should lead to distinctive variations in crack shape.

The Monte Carlo simulations have made a major contribution to deciding whether fluctuations in the crack properties such as the surface velocity dc/dN can be attributed to fluctuations in the microstructure. This is a prerequisite to physically based and potentially more accurate models of fatigue lifetime. However, further work on this question remains necessary. Data for many more cracks must be analyzed, and compared quantitatively with the output of simulations.

7.2 On Predicting Lifetime

The Monte Carlo simulations bear out a fundamental and very important fact of small fatigue crack growth: more than one independent variable is required to account successfully for the statistics of growth. It is not possible to construct an accurate model of fatigue crack growth as a stochastic process in one dimension, e.g., the surface crack length $2c$, its depth a , or its total area. If, for example, the crack length $2c$ is chosen as the first independent variable, then there remains significant information about the state of the crack contained independently in its shape. This information is sufficient, if calculated or measured, to change basic predictions such as of remaining lifetime by significant amounts. Of course, crack shape (e.g., $a/2c$) is not the only possible choice for the second variable. Since the crack shape is a manifestation of interactions of the crack with the microstructure, some direct measure of the microstructure itself at or near the

crack front might serve equally well. Such a physically based, two-dimensional, probabilistic model has already been formulated [34] and illustrated by a description of roughness-induced closure in a Ti alloy [28].

The necessity of a second independent variable can also be shown by studying the covariance of experimentally measured crack properties, usually the surface crack velocity, dc/dN , but also, for example, the degree of irregularity, X . A correlation length for fluctuations in dc/dN [34] or X [1] may be defined and evaluated by the analysis of experimental data [28,35]. When a physically based probabilistic model has been constructed, this process can also assist in identifying the mechanics of failure [28]. The correlation lengths are closely related to the spatial scale of the underlying random microstructural factors that cause fluctuations in growth.

The importance of correlation lengths and the necessity of formulating two-dimensional rather than one-dimensional stochastic models to describe crack growth can of course be demonstrated without attempting to understand the underlying physics. In particular, Bogdanoff and Kozin have reached this same conclusion by purely mathematical analysis of the statistics of crack growth [36]. It is interesting that their analysis was of long crack data: one is led to suspect that longer-range material inhomogeneity plays the same role for long cracks that grain structure plays for small cracks. Bogdanoff and Kozin's two-dimensional stochastic model [37], while having a different formulation, is functionally similar to our own model, which was proposed in the context of small cracks [34].

One of the most important goals of physical models of small crack growth is to calculate the shape of the short-life tail of the distribution of fatigue lifetimes. This regime of the distribution, which is of course the most important in any engineering application in which failure must be avoided, is especially vulnerable to miscalculation by nonphysical statistical analysis of fatigue crack growth data. It has been demonstrated here that qualitatively realistic distributions of dc/dN are produced by the Monte Carlo simulations. Although this has not yet been shown quantitatively, this suggests the possibility of accounting for the first time for fluctuations in dc/dN under uniform loading conditions in terms of fluctuations in microstructure. Such a demonstration would open the way for the first physically based, accurate calculation of the short-life tail of the lifetime distribution using the Monte Carlo simulations.

It has been shown that there is no upper bound to the surface velocity dc/dN during fatigue at constant cyclic stress amplitude, in contradiction of previous physically based models that treat only the motion of the surface crack tips. However, it may still be that there is a lower bound, at least in A1 2219-T851 and A1 7075-T6, to the cycles required for propagation over a given, large increment in $2c$. Values of the normalized velocity V exceed unity only when one or both surface crack tips is relatively retarded. V returns to values less than unity when the crack front is locally smooth again. The net effect over long intervals of growth is that the integral of V may remain bounded. Unfortunately, sufficient experimental data to test this hypothesis were not at hand at the time of writing.

7.3 On Using K_I and the Treatment of Plasticity for Small Cracks

The characterization of the crack driving force by the mode I stress intensity factor K_I is contentious for small cracks, especially those spanning only one or two grains. In many alloys, large-scale yielding around the tips of the smallest cracks calls into question the significance of a cracking driving force that is calculated according to elastic fracture mechanics. Unfortunately, there has been no clearcut experimental confirmation or refutation of the use of K_I to model the mechanics of growth. Discussion of this question has been confined to theoretical conjectures. However, it should be noted that nearly all of the simulations presented above are of cracks growing from $2c \sim 100 \mu\text{m}$ to $2c \sim 300 \mu\text{m}$. Over this interval the cracks span 2-5 grains on the surface and 3-10 grains in depth. It is very likely that the mechanics and statistics of cracks in this regime can be well represented by some ΔK_{eff} that incorporates plasticity-induced closure as a modification to ΔK_I . Note furthermore that laws of propagation such as Eq. (1) describe discontinuous crack mechanics. The plasticity represented implicitly therein is constrained by grain boundaries, and may bear no similarity to the deformation in the plastic zone of a long crack.

The analysis of Section 3, in which growth was studied within a single grain, is more problematic. However, the point made there was that the crack driving force for the surface crack tip, characterized in this work by the ΔK_{eff} implicit in Eq. (1), is slow to respond to the arrest of a subsurface segment of the crack. The crack continues to grow along the surface only weakly impeded, and $2c$ doubles before significant, gradual deceleration occurs. Even if the crack driving force was calculated as a J integral or

taken to be proportional to the crack opening displacement or the local plastic strain range, this result would very likely remain true.

In the model equations used in an illustrative way in this paper, plasticity-induced closure is described as depending on the local microstructure as well as the average crack radius. One might suspect that it should also depend on position around the crack front, since the constraints on plastic deformation at the free surface are quite different from those at the bottom of the crack. The simpler view was maintained in this paper for want of any experimental or theoretical statement of a superior law of growth. This failing should not be considered inherent to the simulations. On the contrary, the results of this paper are an explicit guide to the experimental verification and assessment of differences between surface and subsurface mechanics, including plasticity. One of the major points of this paper has been to show how measurements of the statistics of crack shape, when interpreted by Monte Carlo simulations based on various hypothetical laws, could resolve such questions. A prime feature of the simulations is that laws of growth can be substituted freely to enable such a study.

7.4 On the Reporting of Experiments

The substantial difference between the density of crack velocities for cracks of given length, h_c , and after a given number of elapsed fatigue cycles, h_N , has been demonstrated. That only the latter reveals clearly the statistics of crack arrest and deceleration by closure is commonly overlooked in the literature. Note especially that when dc/dN is presented as a function of nominal ΔK_I for data taken at constant stress amplitude, this is equivalent

to presenting dc/dN for given crack lengths. The distribution of data on a dc/dN vs ΔK_I plot will therefore follow a family of densities like h_c . According to the foregoing, such a presentation obscures important information about the probability of a crack being arrested after a given number of cycles. It would be a great service to those interested in statistical analysis if raw data of the form $(c_i, N_i, i = 1, 2, \dots)$ were also presented. The low velocity tail of densities like h_N could then be constructed with accuracy, and the mechanics of grain boundary arrest, crack closure, etc., illuminated.

8. CONCLUSIONS

1. The irregularity in shape of a small crack contains valuable information about the mechanics of small crack growth.
2. Minima in the surface velocity dc/dN cannot be correlated with arrest of the deepest part of the crack front at a subsurface grain boundary.
3. Instantaneous values of dc/dN , or values averaged over reasonably short measurement intervals, are strongly affected by crack irregularity. This could affect significantly the interpretation of experimental observations of surface crack growth in relation to the local micro-structure.
4. The consideration of detailed fluctuations in the shapes of small cracks changes qualitatively the statistics of the surface velocity dc/dN ,

which are then more consistent with experiment. This implies that an adequate probabilistic model of the statistics of dc/dN must be based on at least two independent variables, rather than one, e.g., the surface crack length $2c$ and the crack depth a , rather than $2c$ alone.

5. Estimates of the crack depth in an NDE inspection of small cracks can significantly affect the estimated remaining fatigue lifetime. A detailed account of crack shape and irregularity is required to calculate accurately the penalty associated with a relatively deep crack.
6. Presentation of experimental data in the form dc/dN vs ΔK_I obscures the statistics of slow and arrested cracks, frustrating statistical analysis of the mechanics of crack arrest and closure.

REFERENCES

- [1] B.N. Cox and W.L. Morris, Monte Carlo Simulations of the Growth of Small Fatigue Cracks, *Engng Fracture Mech.*, in press.
- [2] A. LeFrancois, P. Clement and A. Pineau, The Growth of Short Fatigue Cracks in an Aluminum Alloy in Relation with Crack Closure Effect, in *Proc. Int. Conf. on Fatigue of Engng Struct. and Mater.*, Sheffield, England, 15-19 September 1985.
- [3] P. Clements, J.P. Angeli and A. Pineau, Short Crack Behavior in Nodular Cast Iron, *Fatigue Engng Mater. Struct.* 7, 251-65 (1984).
- [4] K. Tokaji, T. Ogawa, Y. Harada and Z. Ando, Limitations of Linear Elastic Fracture Mechanics in Respect of Small Fatigue Cracks and Microstructure *Fatigue Fracture Engng Mater. Struct.* 9, 1-14 (1986).
- [5] T.A. Beer, Crack Shapes During Biaxial Fatigue, Report No. 106, Materials Engineering-Mechanical Behavior, College of Engineering, University of Illinois at Urbana-Champaign (1984).
- [6] L. Wagner and G. Lütjering, Microstructural Influence on Propagation Behavior of Short Cracks in an ($\alpha + \beta$) Ti Alloy, *Z. Metallkde.* 78, 369-75 (1987).
- [7] R.K. Bolingbroke and J.E. King, The Effect of Microstructure on the Surface Crack Length: Crack Depth Relationships for Short Cracks, in *Fatigue '87, Proc. 3rd Int. Conf. on Fatigue and Fatigue Thresholds*, Charlottesville, VA, 1987.
- [8] J. Lankford, Initiation and Early Growth of Fatigue Cracks in High Strength Steel, *Engng Fracture Mech.* 9, 617-24 (1977).
- [9] W.L. Morris, M.R. James and O. Buck, Growth Rate Models for Short Surface Cracks in Al 2219-T851, *Met. Trans.* 12A, 57-64 (1981).
- [10] A.K. Zurek, M.R. James and W.L. Morris, The Effect of Grain Size on Fatigue Growth of Short Cracks, *Met. Trans.* 14A, 1697-1705 (1983).
- [11] W.J. Pardee, (Ed.), Quantitative Nondestructive Evaluation (NDE) for Retirement-for-Cause. Final Report on DARPA Contract No. MDA903-80-C-0641, Rockwell International Science Center.
- [12] L. Wagner, J.K. Gregory, A. Gysler and G. Lütjering, Propagation Behavior of Short Cracks in Ti-8.6 Al Alloy, in *Proc. 2nd Int. Workshop on Small Fatigue Cracks*, Santa Barbara, CA (Ed. by R. Ritchie and J. Lankford), 1986.

- [13] K.J. Miller, H.J. Mohamed, M.W. Brown and E.R. de los Rios, Barriers to Short Fatigue Crack Propagation at Low Stress Amplitudes in a Banded Ferrite-Pearlite Structure, in *Proc. 2nd Int. Workshop on Small Fatigue Cracks*, Santa Barbara, CA (Ed. by R. Ritchie and J. Lankford), 1986.
- [14] E.R. de los Rios, Z. Tang and K.J. Miller, Short Crack Fatigue Behavior in a Medium Carbon Steel, *Fatigue Engng Mater. Struct.* 7, 97-108 (1984).
- [15] R.O. Ritchie, W. Yu, A.F. Blom and D.K. Holm, An Analysis of Crack Tip Shielding in Aluminum Alloy 2124: A Comparison of Large, Small, Through-Thickness and Surface Fatigue Cracks, *Fatigue Fracture Engng Mater. Struct.* 10, 343-62 (1987).
- [16] K.T. Faber and A.G. Evans, Crack Deflection Processes - I. Theory, *Acta Metall.* 31, 565-76 (1983).
- [17] W.L. Morris, B.N. Cox and M.R. James, Microplastic Surface Deformation of Al 2219-T851, *Acta Metall.* 35, 1055-65 (1987).
- [18] B.N. Cox, W.L. Morris and M.R. James, Two-Stage Microplastic Surface Deformation in Al 2219-T851, *Acta Metall.* 35, 1289-99 (1987).
- [19] W.L. Morris, M.R. James and B.N. Cox, Evolution of the Mechanical Properties of Individual Grains in Al 2219-T851 During Fatigue, in *Proc. Fatigue '87*, Charlottesville, VA (ed., R.O. Ritchie and E.A. Starke, Jr.) (1987), pp. I.93-I.102.
- M.R. James and W.L. Morris, The Effect of Microplastic Surface Deformation on the Growth of Small Cracks, in *Small Fatigue Cracks* (ed., R.O. Ritchie and J. Lankford) (TMS-AIME, Warrendale, PA, 1986), pp. 145-56.
- [21] W.L. Morris, The Noncontinuum Crack Tip Deformation Behavior of Surface Microcracks, *Met. Trans.* A11, 1117-23 (1980).
- [22] K.S. Chan and J. Lankford, A Crack Tip Strain Model for the Growth of Small Fatigue Cracks, *Scripta Met.* 17, 529-32 (1983).
- [23] J. Lankford, The Growth of Small Fatigue Cracks in 7075-T6 Aluminum, *Fatigue Engng Mater. and Struct.* 5, 233-48 (1982).
- [24] S.S. Wilkes, *Mathematical Statistics*, John Wiley and Sons, NY (1962), Chapter 8.
- [25] I.S. Raju and J.C. Newman, Jr., Stress-Intensity Factors for a Wide Range of Semi-Elliptical Surface Cracks in Finite-Thickness Plates, *Engng Fracture Mech.* 11, 817-29 (1979).
- [26] J.C. Newman, Jr. and I.S. Raju, An Empirical Stress-Intensity Factor Equation for the Surface Crack, *Engng Fracture Mech.* 15, 185-92 (1981).

- [27] J.C. Newman, Jr. and I.S. Raju, Stress-Intensity Factor Equations for Cracks in Three-Dimensional Finite Bodies Subjected to Tension and Bending Loads, NASA Technical Memo 85793, April 1984.
- [28] B.N. Cox and W.L. Morris, Model-Based Statistical Analysis of Short Fatigue Cracks Growth in Ti 6Al-2Sn-4Zr-6Mo, *Fatigue Fracture Engng Mater. Struct.* 10, 429-46 (1987).
- [29] S. Suresh, Crack Deflection: Implications for the Growth of Long and Short Fatigue Cracks, *Met. Trans.* 14A, 2375-85 (1983).
- [30] S. Suresh, Fatigue Crack Deflection and Fracture Surface Contact: Micro-mechanical Models, *Met. Trans.* 16A, 249-59 (1985).
- [31] M.R. James and W.L. Morris, Effect of Fracture Surface Roughness on Growth of Short Fatigue Cracks, *Met. Trans.* 14A, 153-5 (1983).
- [32] B. Cotterell and J.R. Rice, Slightly Curved or Kinked Cracks, *Int. J. Fracture* 16, 155-69 (1980).
- [33] J.L. Bogdanoff and F. Kozin, *Probabilistic Models of Cumulative Damage*, John Wiley & Sons, NY (1985).
- [34] B.N. Cox and W.L. Morris, A Probabilistic Model of Short Fatigue Crack Growth, *Fatigue Fracture Engng Mater. Struct.* 10, 419-28 (1987).
- [35] Y.K. Lin and J.N. Yang, On Statistical Moments of Fatigue Crack Propagation, *Engng Fracture Mech.* 18, 243-56 (1983).
- [36] J.L. Bogdanoff and F. Kozin, Probabilistic Models of Fatigue Crack Growth - II, *Engng Fracture Mech.* 20, 255-70 (1984).
- [37] J.L. Bogdanoff and F. Kozin, Probabilistic Models in Fatigue Crack Growth: Results and Speculations, *J.N. Engng and Design*, in press.
- [38] M.R. James and W.L. Morris, The Role of Microplastic Deformation in Fatigue Crack Initiation, in *Fatigue Mechanisms: Advances in Quantitative Measurement of Physical Damage*, ASTM STP 811, ed. J. Lankford, D.L. Davidson, W.L. Morris, and R.P. Wei (American Society for Testing and Materials, 1983), pp. 46-70.
- [39] W.L. Morris, M.R. James and B.N. Cox, Fatigue Crack Initiation Mechanics of Metal Aircraft Structures, Final Report on Naval Air Development Center Contract No. N62269-86-C-0261, 1988.

FIGURE CAPTIONS

- Fig. 1 The increase in irregularity of the crack front accompanying an increase in the duration of arrest at grain boundaries.
- Fig. 2 (a) The irregularity measure $\langle X(\theta, \bar{r}) \rangle$ for various angles θ , which is defined in the inset. (b) The irregularity measure $\langle X(\bar{r}) \rangle$ averaged over all angles θ for two stress levels.
- Fig. 3 A typical simulated history of a crack that suffers arrest at a subsurface grain boundary. The striations in (a) and (b) show the position of the crack front at generally unequal intervals of elapsed cycles. The surface velocity dc/dN is shown in (c) as a function of half the surface crack length, $2c$.
- Fig. 4 The probability density $\bar{h}_c(V)$ that a crack has normalized surface velocity V when its length is given; and $\bar{h}_N(V)$ that it has normalized velocity V after a given number of elapsed cycles. (a) and (c) show \bar{h}_c and \bar{h}_N when the propagation of the surface crack tips only is simulated, and (b) and (d) when that of the entire crack front is simulated.
- Fig. 5 Densities (a) $\bar{h}_c(V)$ and (b) $\bar{h}_N(V)$ for small cracks in Al 2219-T851 at the two cyclic stress amplitudes marked. The cracks ranged over $40 \mu\text{m} \leq 2c \leq 500 \mu\text{m}$.
- Fig. 6 (a) Correlation between the average velocity over 1000 cycles, \hat{dc}/dN , and the aspect ratio, $a/2c$, when $2c = 100 \mu\text{m}$ at $\sigma_{\text{max}} = 0.92\sigma_y$ in Al 2219-T851. Correlations between the cycles, N_r , to grow from

$2c = 100 \text{ } \mu\text{m}$ to $2c = 300 \text{ } \mu\text{m}$ and (b) $a/2c$ and (c) \hat{dC}/dN for the same simulations as in (a). (d), (e) and (f) are the same as (a), (b) and (c) but for cracks that are semi-elliptical when $2c = 100 \text{ } \mu\text{m}$. (g), (h) and (i) are the same as (a), (b) and (c) but for $\sigma_{\max} = 0.7\sigma_y$.

ACKNOWLEDGEMENTS

Research sponsored by the Air Force Office of Scientific Research (AFSC) under Contract No. F49620-85-C-0034. The United States Government is authorized to reproduce or distribute reprints for governmental purpose notwithstanding any copyright notation herein. The author is indebted to Drs. M.R. James and W.L. Morris for making available unpublished data. Drs. A. Blum, R.O. Ritchie, and A. Wang made helpful suggestions during preparation of the manuscript. Dr. Morris contributed much deeply appreciated guidance throughout the work.

APPENDIX A INITIATION IN UNUSUALLY LARGE GRAINS

Initiation of fatigue cracks in Al 2219-T851, whether by the fracture of intermetallic particles, the formation of persistent slip bands, or grain boundary failure, occurs first in surface grains whose width is between two and five times the average [38]. That is not to say that initiation occurs first in the largest grain: very large grains soften and harden again so quickly in fatigue that they sustain relatively little plastic damage [19,39]. Rather, crack initiation events after a certain number of cycles are distributed over large grains of many sizes, with the details of the distribution depending on the loading conditions and the alloy [39].

This state of affairs was represented in the Monte Carlo simulations as follows. An area A_1 of random Voronoi polygons representing the microstructure was generated by the Wigner-Seitz construction, as described in [1] (e.g., Fig. A-1). Then there was chosen a subdomain A_2 of that area (e.g., as marked in Fig. A-1) that was far enough from the boundaries of A_1 that all grains having at least one vertex in A_2 were complete and unaffected by boundary effects in the Wigner-Seitz construction. The largest such grain was then selected as the site for crack initiation (e.g., the shaded grain in Fig. A-1). The free specimen surface was created by bisecting the whole array of Voronoi polygons by a line passing through the selected grain's center of mass (point G in Fig. A-1). The initial crack was then located on the free surface at a point chosen randomly in the selected grain. The factor by which the average width of the selected grains in an ensemble of simulations exceeds the average width of all grains (measured through their centers of mass) obviously

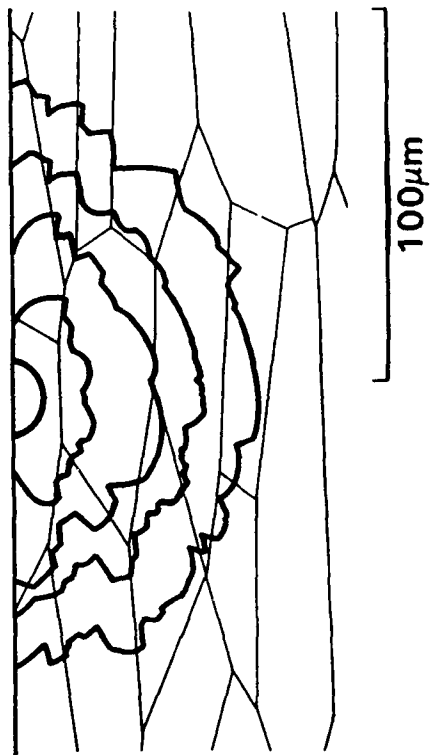
depends on the area of A_2 . This is illustrated in Fig. A-2. The distribution of the widths of the selected grains can be modified further by choosing the area of A_2 randomly: with a little playing round, any experimental distribution can be matched.

LIST OF FIGURES

- Fig. A-1 A nonequiaxed random microstructure, simulating a rolled sheet of Al 2219-T851, in which the largest grain (shaded) has been found in the subdomain A_2 of the total domain A_1 of calculated grains.
- Fig. A-2 The distribution of widths of all grains compared to the distributions of the widths of grains selected as initiation sites for various values of the side a_2 of the square subdomain A_2 , as marked.

SC44588

(b) $\sigma_{\max} = 0.94 \sigma_y$



(a) $\sigma_{\max} = 0.7 \sigma_y$

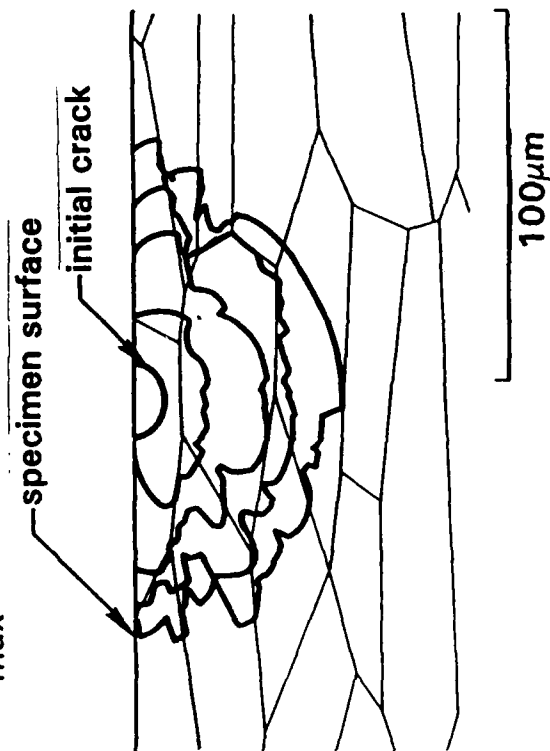


Fig. 1

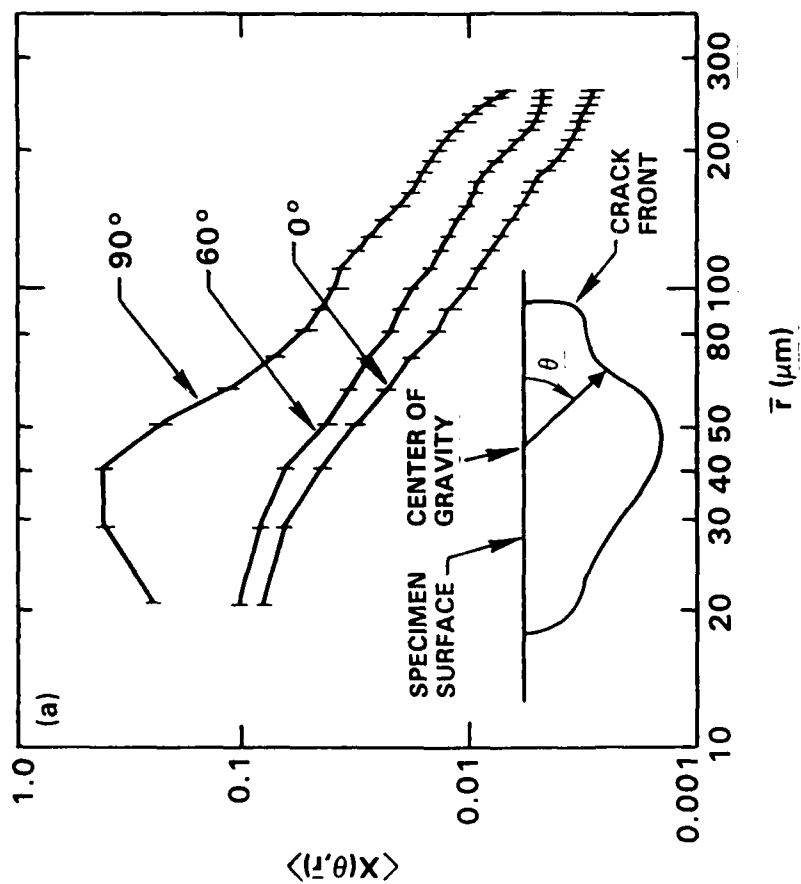
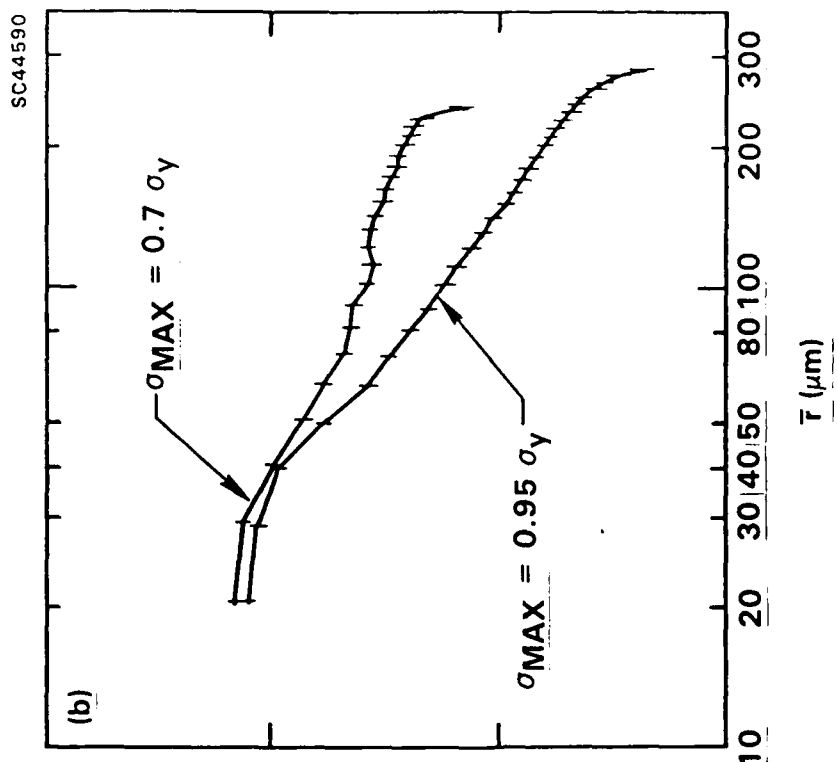


Fig. 2

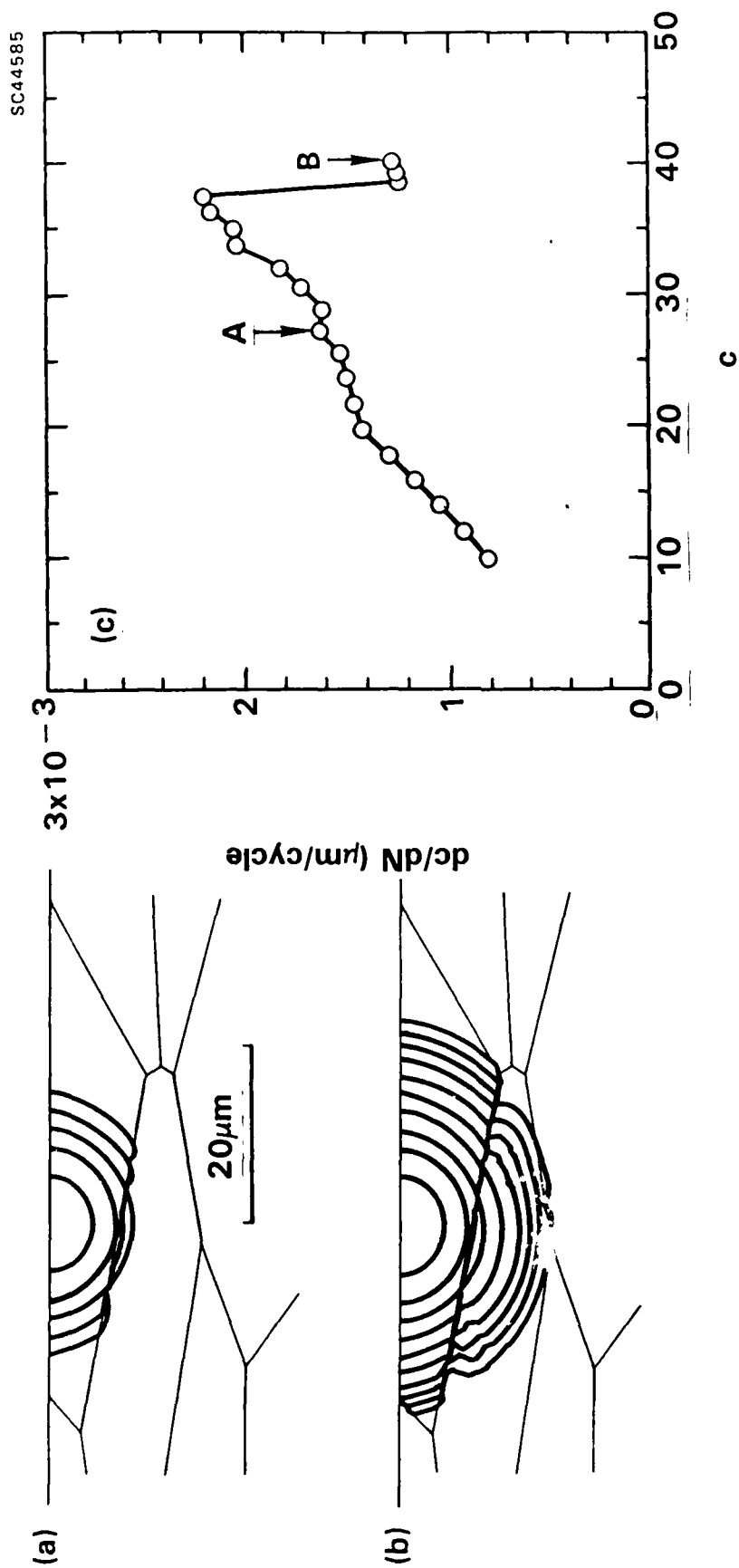
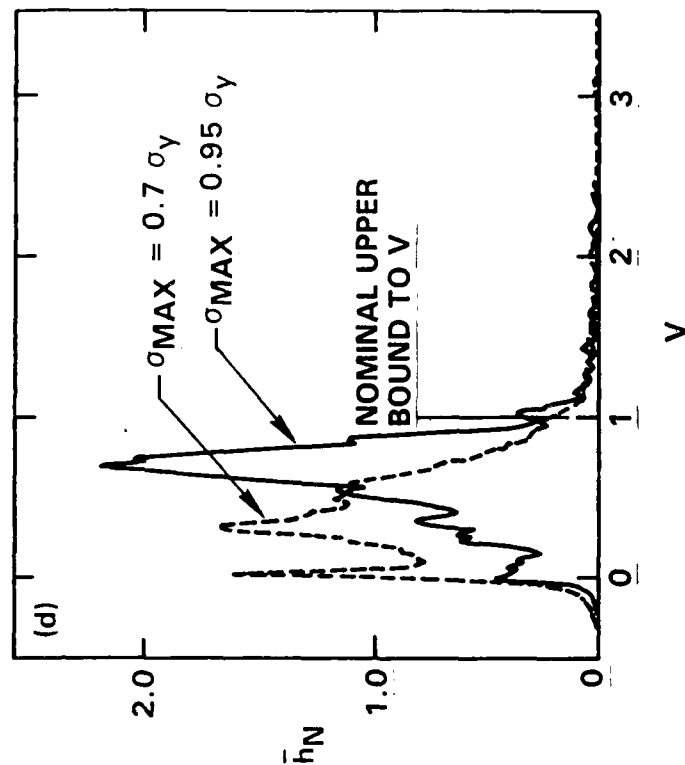
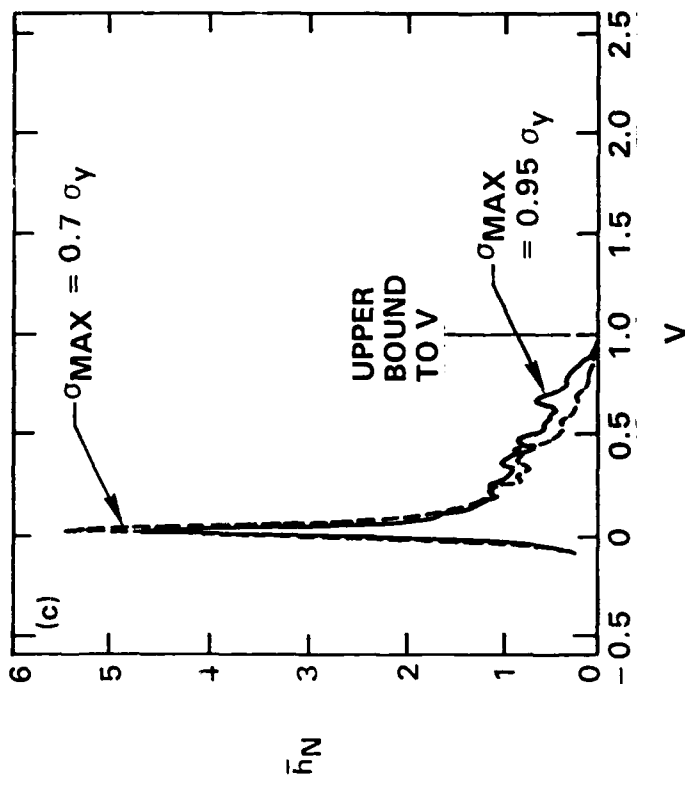
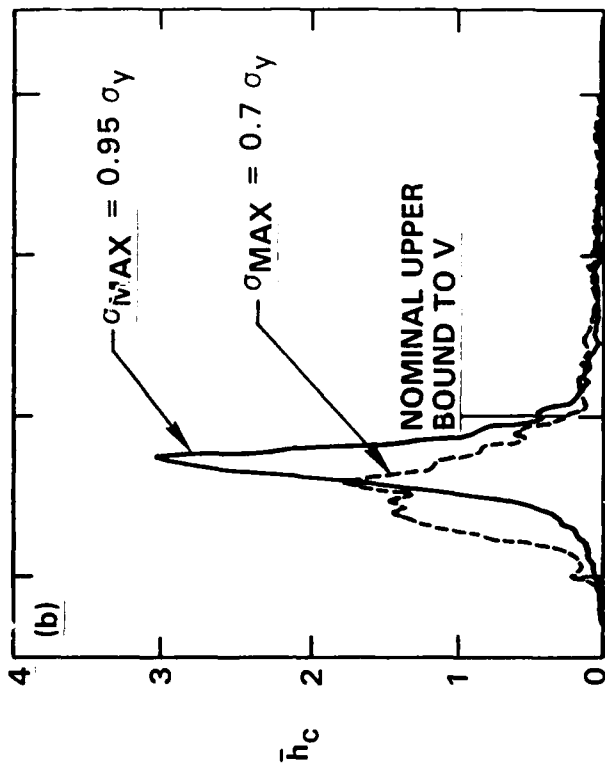
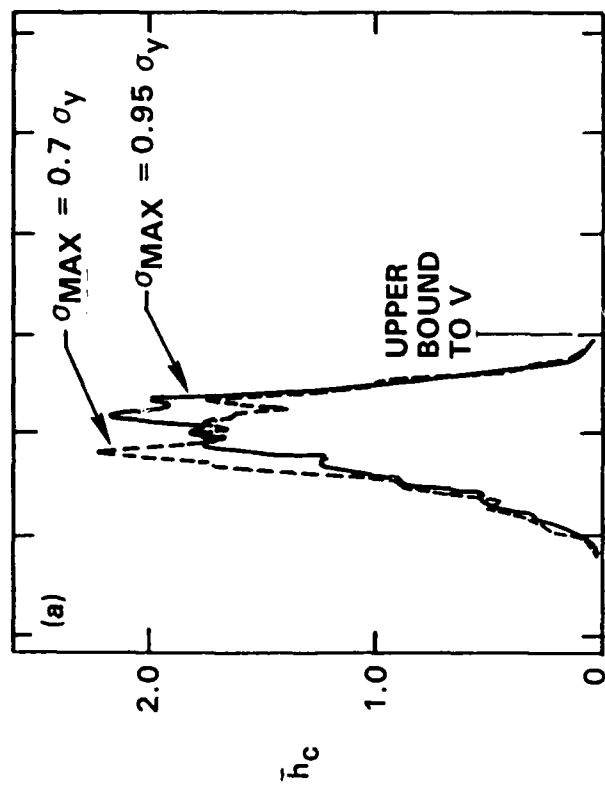


Fig. 8



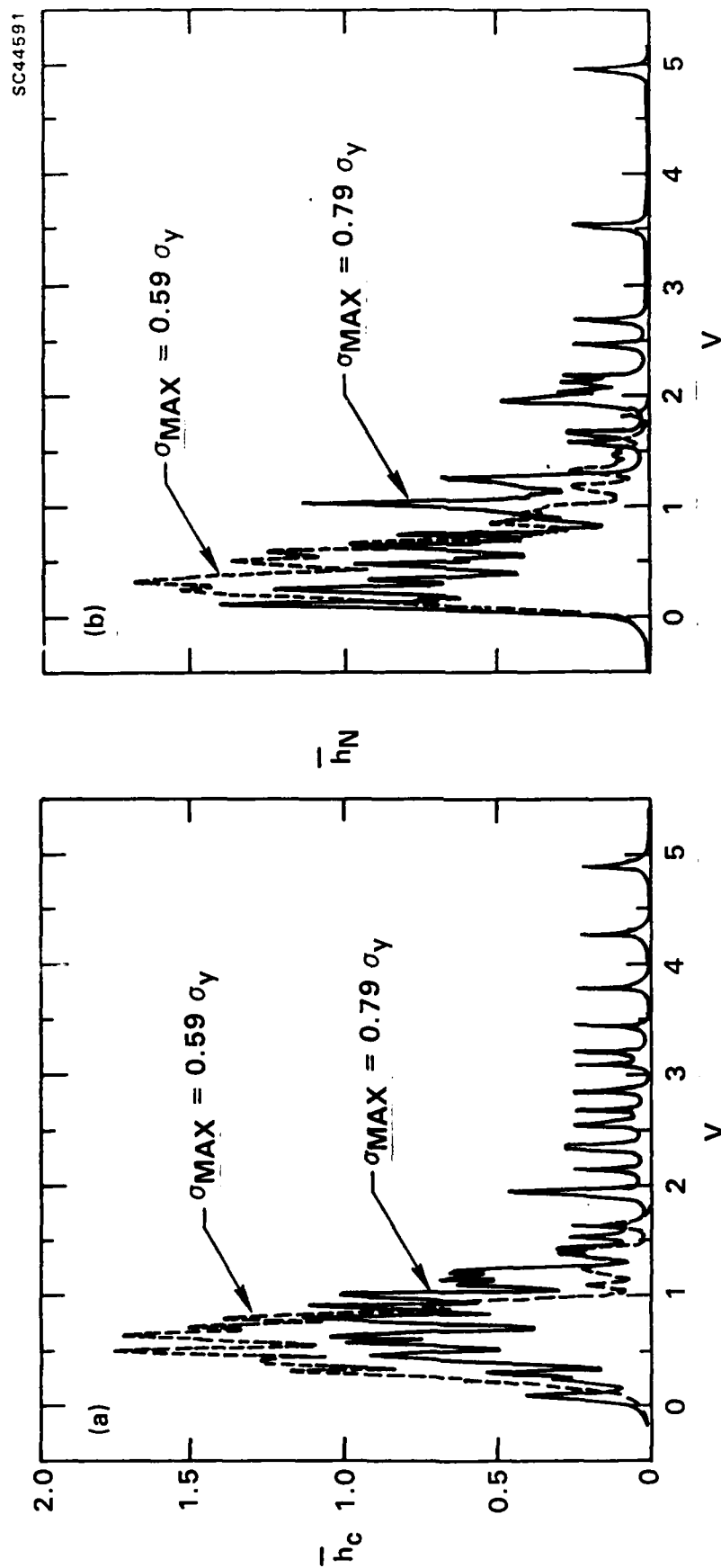


Fig. 2

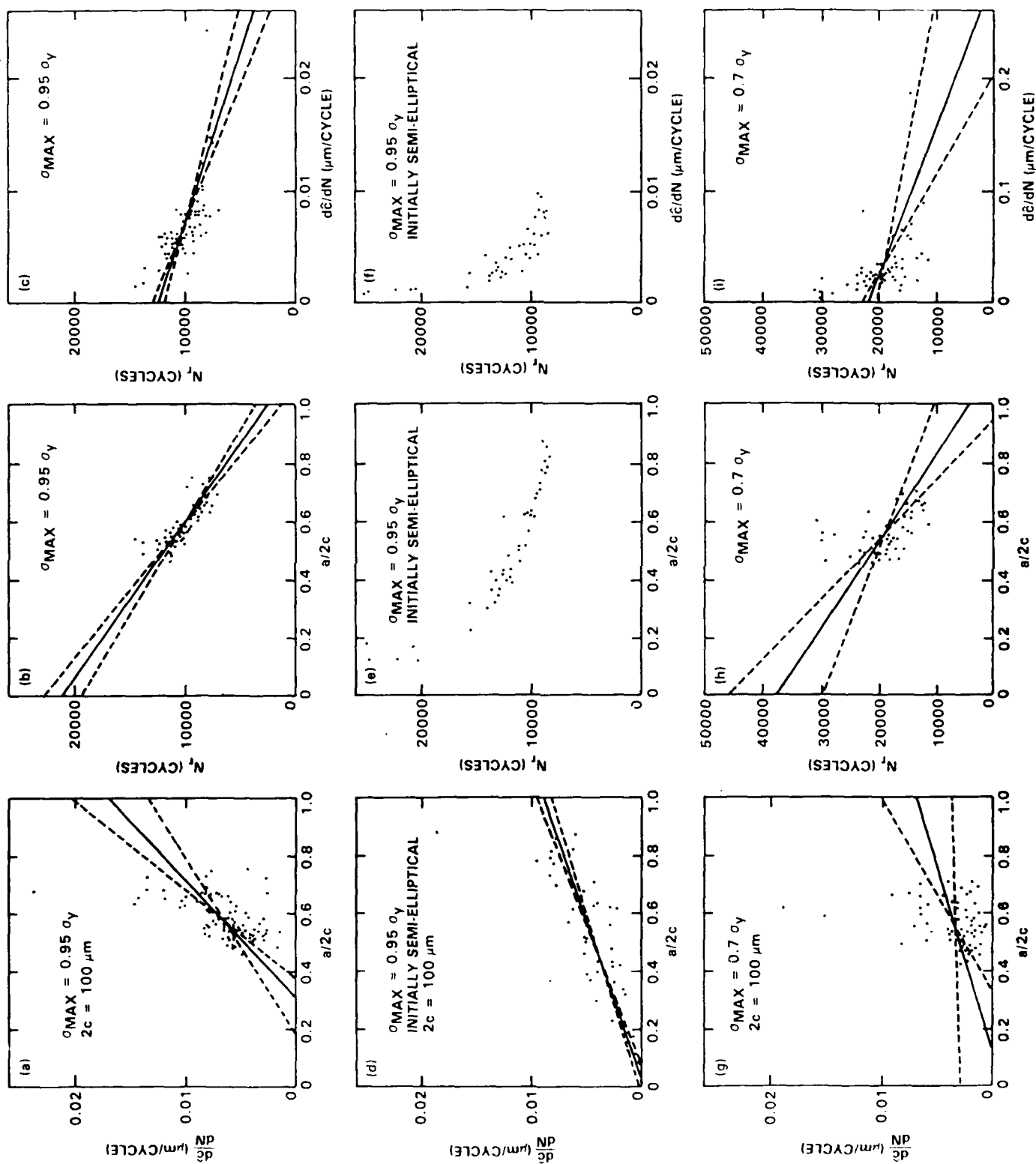


Fig. 5

SC44584

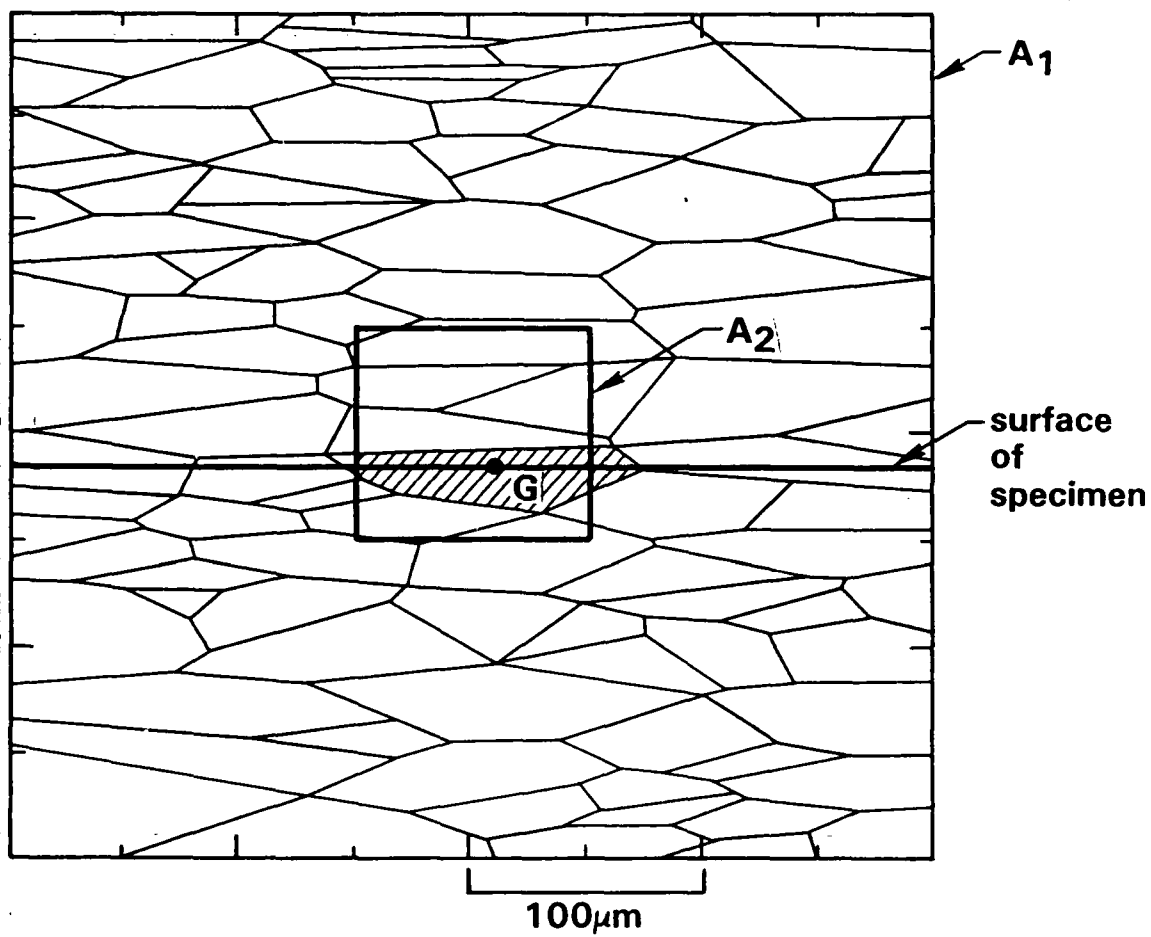


Fig. H-1

SC44589

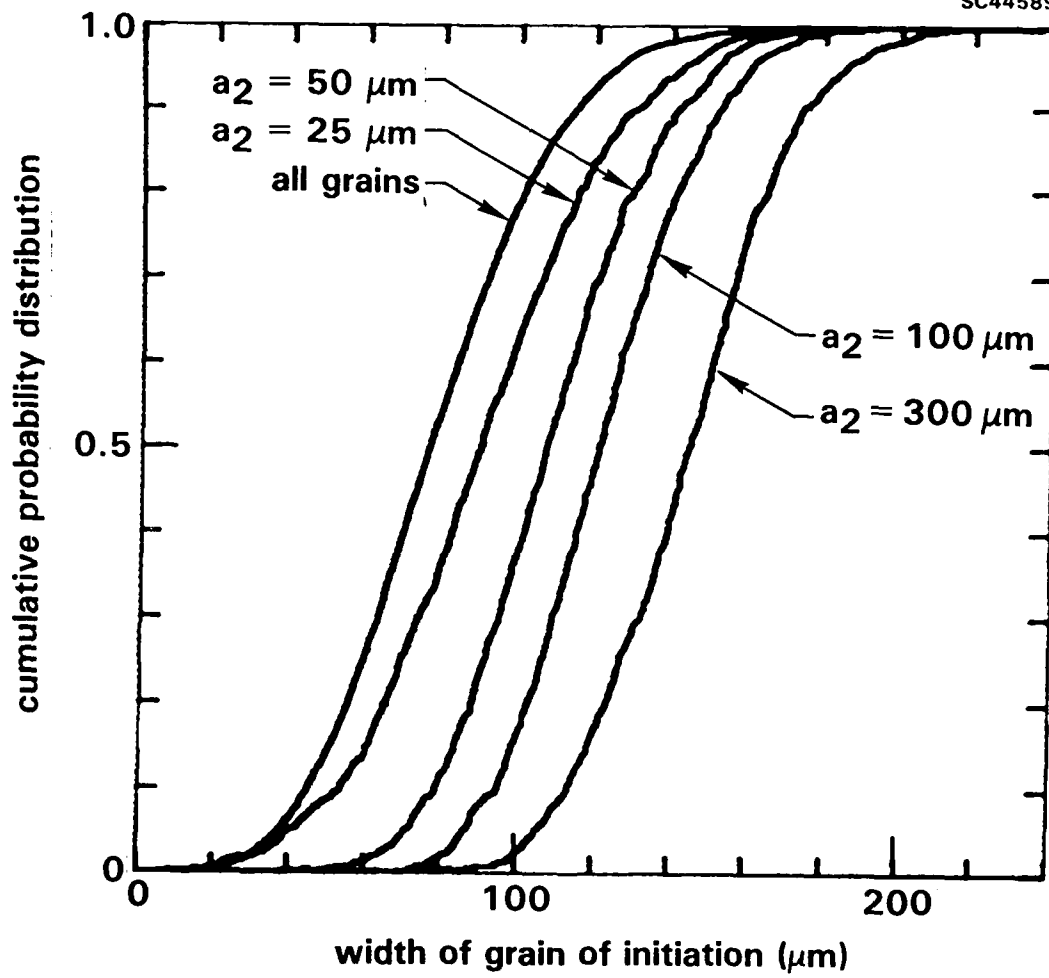


Fig. A-2

END

DATE

FILMED

DTIC

10-88